Université de Liège

Académie Wallonie-Europe

Université de Liège

Faculté des Sciences

Continuation and bifurcation analyses of a periodically forced slow-fast system

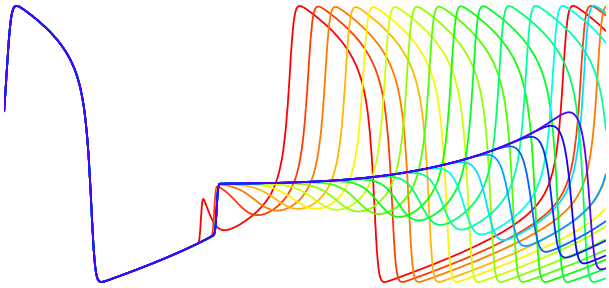

Thèse présentée par
Huguette CROISIER
en vue de l'obtention du grade
de **Docteur en Sciences**

Liège, mars 2009

Je tiens à remercier tout particulièrement Pierre Dauby, le promoteur de cette thèse, de m'avoir à la fois prodigué un encadrement constant et accordé une liberté considérable au cours de ces années de doctorat. Ses tout aussi importantes rigueur scientifique et ouverture d'esprit m'ont beaucoup appris ; son enthousiasme permanent et ses encouragements à propos m'ont été très précieux. Nos discussions stimulantes vont me manquer.

I am also grateful to Michael Guevara, without whom a part of this work that I consider important could not have seen the light of day. I thank him for his welcome and guidance during the six months I spent in Montreal. I am still amazed by the incredible number of incredibly pertinent references he sent me since we met electronically.

Je suis reconnaissante au F.R.I.A., à l'Université de Liège et aux contribuables pour le soutien financier qu'ils m'ont accordé pour réaliser ce doctorat. J'ai également bénéficié d'une bourse de la Communauté Française de Belgique lors de mon séjour scientifique à l'Université McGill. I am grateful to the Centre for Nonlinear Dynamics in Physiology and Medicine of McGill University for the scientific hospitality I benefited from during the six enriching months I spent there.

Mes remerciements vont également à toutes les personnes du deuxième étage du B5A qui contribuent à en faire un lieu où il est agréable de travailler.

Enfin, je remercie mon entourage, famille et amis, d'avoir partagé avec moi aussi bien les moments agréables que les épisodes plus difficiles qui ont jalonné ce doctorat.

Liège, le 26 mars 2009.
Huguette Croisier.

Résumé

Cette thèse consiste en l'étude d'un système lent-rapide forcé périodiquement, considéré successivement dans ses régimes excitable et auto-oscillant. Le système lent-rapide étudié est le modèle de FitzHugh-Nagumo et la stimulation périodique consiste en un train d'impulsions de forme gaussienne, dont la largeur est nettement inférieure à la durée du potentiel d'action. Ce système fournit un modèle qualitatif à la fois pour une cellule excitable et pour une cellule s'excitant spontanément lorsque cette cellule est soumise à une stimulation électrique périodique. Une telle configuration a été étudiée à maintes reprises en électrophysiologie cardiaque, du fait qu'elle constitue un modèle simplifié de la situation d'une cellule cardiaque dans le coeur intact et peut dès lors contribuer à une meilleure compréhension des phénomènes d'arythmies. Par des méthodes de continuation (logiciel AUTO), nous calculons des branches de solutions périodiques pour le système forcé périodiquement, en utilisant la période de stimulation comme paramètre de bifurcation. Nous étudions ensuite l'évolution du diagramme de bifurcations obtenu en fonction de l'amplitude de stimulation. Dans les deux régimes excitable et oscillant, nous observons l'existence d'une amplitude critique de stimulation, en-dessous de laquelle le comportement du système est "trivial": dans le cas excitable, le diagramme de bifurcations se réduit à une branche stable de période 1 subliminaire et dans le cas oscillant, tous les rythmes stables appartiennent à des boucles isolées (c'est-à-dire, à des branches de solutions fermées distinctes). En raison de la nature lente-rapide du système, les changements qui surviennent dans le diagramme de bifurcations lorsque l'amplitude de stimulation critique est franchie sont drastiques, alors que le diagramme de bifurcations se simplifie à nouveau de manière beaucoup plus douce au-delà d'une deuxième valeur caractéristique de l'amplitude. Dans le cas auto-oscillant, nous montrons que l'amplitude de stimulation critique est aussi l'amplitude à laquelle la courbe dite de "réajustement de phase" change de nature topologique. Nous expliquons l'origine de cette coïncidence en considérant une application discrète du cercle dérivée de la courbe de réajustement de phase ("l'application de réajustement de phase"), application qui constitue une bonne approximation du système d'équations différentielles original sous certaines conditions. Nous montrons que le diagramme de bifurcations d'une telle application du cercle où le paramètre de bifurcation n'intervient que de manière additive est toujours caractérisé par le fait que les solutions de période 1 appartiennent à des boucles isolées lorsque le degré topologique de l'application est égal à un, tandis que ces solutions de période 1 appartiennent à une seule et même branche lorsque l'application est de degré zéro.

Abstract

This thesis consists in the study of a periodically forced slow-fast system in both its excitable and oscillatory regimes. The slow-fast system under consideration is the FitzHugh-Nagumo model, and the periodic forcing consists of a train of Gaussian-shaped pulses, the width of which is much shorter than the action potential duration. This system is a qualitative model for both an excitable cell and a spontaneously beating cell submitted to periodic electrical stimulation. Such a configuration has often been studied in cardiac electrophysiology, due to the fact that it constitutes a simplified model of the situation of a cardiac cell in the intact heart, and might therefore contribute to the understanding of cardiac arrhythmias. Using continuation methods (AUTO software), we compute periodic-solution branches for the periodically forced system, taking the stimulation period as bifurcation parameter. We then study the evolution of the resulting bifurcation diagram as the stimulation amplitude is raised. In both the excitable and the oscillatory regimes, we find that a critical amplitude of stimulation exists below which the behaviour of the system is "trivial": in the excitable case, the bifurcation diagram is restricted to a stable subthreshold period-1 branch, and in the oscillatory case, all the stable periodic solutions belong to isolated loops (*i.e.*, to distinct closed solution branches). Due to the slow-fast nature of the system, the changes that take place in the bifurcation diagram as the critical amplitude is crossed are drastic, while the way the bifurcation diagram re-simplifies above some second amplitude is much more gentle. In the oscillatory case, we show that the critical amplitude is also the amplitude at which the topology of phase-resetting changes type. We explain the origin of this coincidence by considering a one-dimensional discrete map of the circle derived from the phase-resetting curve of the oscillator ("the phase-resetting map"), map which constitutes a good approximation of the original differential equations under certain conditions. We show that the bifurcation diagram of any such circle map, where the bifurcation parameter appears only in an additive fashion, is always characterized by the period-1 solutions belonging to isolated loops when the topological degree of the map is one, while these period-1 solutions belong to a unique branch when the topological degree of the map is zero.

Contents

Introduction

Slow-fast systems are nonlinear dynamical systems in which two or more processes take place on different time scales. Often, in such systems, a phenomenon that would normally go unseen, because it is intrinsically weaker than another competing phenomenon, can express itself temporarily in a rather spectacular way, because it turns on much more quickly than its opponent, before the dominant phenomenon takes over and forces the system back to the initial state. When such a slow-fast system possesses a stable equilibrium, at which the motion stops, it is called an *excitable system*[1]. The term "excitable" refers to the fact that a sufficient initial impulse must be given for the "excitation" process to take place; there exists an excitation threshold. On the other hand, when the system possesses no stable equilibrium but that the excitation process is self-sustained and repeats periodically, one speaks of a *relaxation oscillator* (as termed originally by van der Pol, see Sec. 1.1).

Slow-fast systems are ubiquitous in physics and biology. Examples are the stick-slip cycle of a bowed violin string (e.g., [Sch74, Jac90]); the see-saw with a water reservoir at one side (Fig. 1, and, e.g., [Gra87]); the saline oscillator (e.g., [Wal77]); the closing of plant leafs (e.g., [vdPvdM28]); the release of calcium from intracellular stores into the cytoplasm (e.g., [KS98]); the "firing" of neurons and also cardiac cells (e.g., [KS98]).

The original motivation for the work presented in this thesis lies in the last example. The firing, or electrical excitation, of cardiac cells is what triggers their muscular contraction and therefore, the heartbeats. Most of the cells in the heart are excitable, and get the necessary impulse to get excited through the periodic propagation of an electrical current from the sinus node, the natural pacemaker of the heart. Indeed, this group of cells located in the right atrium behaves electrically like a relaxation oscillator. Other regions of the heart also fire spontaneously, namely the atrio-ventricular node and the Purkinje fibres, but since they beat with a lower frequency than the sinus node, they remain enslaved by its stimulations in normal conditions. Hence, in first approximation, cardiac cells can be considered as periodically forced slow-fast systems, and the study of the response of a slow-fast system to a periodic stimulation of variable amplitude and period can be considered as a first step towards a better understanding of cardiac rhythms and arrhythmias. Of course, many cardiac arrhythmias are intrinsically spatial phenomena, but some types of arrhythmias (which can possibly degenerate into deadly spatial patterns such as fibrillation in the whole heart) also occur in isolated cardiac cells, or small groups of cardiac cells, submitted to periodic electrical stimulation. In particular, this is the case for "$M:N$ rhythms" ($M:N \neq 1:1$), in which the response of the cell to the stimulation remains periodic, but departs from the healthy $1:1$ pattern.

[1] In general, it is not sufficient for a two-time-scale system to possess a stable equilibrium to be an excitable system, as we explain in section 2.2.1, but in the following we refer to slow-fast dynamical systems only as being either excitable systems or relaxation oscillators.

Figure 1. *A typical slow-fast system [Gra87]. When the amount of water exceeds the weight at the other side, the see-saw flips. Then the reservoir is emptied and returns to its original position. If there is a steady flow of water, the phenomenon repeats periodically and one has a relaxation oscillator. Otherwise the system is excitable; the flip (and subsequent return to equilibrium) is triggered by pouring a sufficient amount of water into the reservoir.*

In this work, we have studied $M : N$ rhythms in the FitzHugh-Nagumo model, a simple differential-equation model of a slow-fast system, submitted to a periodic train of Gaussian-shaped pulses. We have considered successively the excitable and oscillatory regimes of the slow-fast system. Because the FitzHugh-Nagumo model is a qualitative model which does not describe specifically cardiac cells (it can equally well be used as a model for an excitable or spontaneously firing nerve cell), the comparisons we can make with experimental results on cardiac cells are limited to the qualitative realm. On the other hand, this feature is also precisely what allows us to consider our results as a quite general picture of the behaviour of a periodically forced slow-fast system. The width of the pulses in the periodic forcing is chosen small compared to the characteristic time of excitation of the slow-fast system, so that one stimulus can trigger at most one excitation, or *action potential*, of the system. This is the type of stimulation usually used in electrophysiological studies on cardiac cells.

The originality of the work is intimately linked to the fact that we have used continuation methods to study the evolution of the $M : N$ rhythms as a function of the stimulation amplitude and period, *i.e.*, to compute bifurcation diagrams for the $M : N$ rhythms. In contrast with time-integration of the equations as an initial value problem, which permits tracking stable solutions only, continuation allows following asymptotic solutions beyond the parameter value at which they become unstable. This gives rise to bifurcation diagrams where the unstable connections between the different stable solutions (or the absence of such connections) are revealed. These unstable portions of branches are important because they constrain how the bifurcation diagram can evolve following the variation of a second parameter. Continuation methods have been applied only rarely to periodically forced slow-fast systems. In particular, we are not aware of any prior continuation analysis of a slow-fast system submitted to pulsatile forcing such as the one we present in this thesis.

In the oscillatory regime, in addition to studying the periodic solutions of the ordinary differential equations, we have also studied the periodic orbits of a one-dimensional discrete map of the circle derived from the so-called "phase-resetting curve" of the oscil-

lator. The phase-resetting curve quantifies the effect of a single stimulus on the oscillator as a function of the phase along the cycle at which it is given. The corresponding "phase-resetting map" constitutes a good approximation of the full differential equations under certain conditions. Among other things, the comparison of the phase-resetting map to the ordinary differential equations has allowed us to relate two *a priori* distinct topological features, namely the "connectivity" of the period-1 solutions in the bifurcation diagram and the topological "type" (or "degree") of phase-resetting.

The manuscript is organized as follows. In Chap. 1, we review the evolution of the modelling of the heart electrical activity from the beginning of the 20th century until today. In particular, we describe the genesis of the Hodgkin-Huxley equations, which is the first mathematical model that succeeded in accounting for cellular electrical excitability. In Chap. 2, we introduce the model of slow-fast system studied in this work, the FitzHugh-Nagumo model, which is in some sense a simplified version of the Hodgkin-Huxley equations. We explain how such a simple two-dimensional ordinary differential equation is able to account for excitability or relaxation oscillations depending on the values of the parameters. We discuss the notion of threshold of excitation, and the associated problem of distinguishing between subthreshold and suprathreshold responses (action potentials). In Chap. 3, we present the numerical methods used in this work, *i.e.*, the continuation methods. In particular, we explain the advantages of "pseudo-arclength" continuation, and we describe the method we have used to study the periodic solutions of our periodically forced system with the AUTO continuation software. Chap. 4 provides a common introduction to the two chapters of results that follow. We introduce the periodic forcing to which we have submitted the FitzHugh-Nagumo model, and we put our work into perspective with prior electrophysiological studies on cardiac cells and prior theoretical works on periodically forced slow-fast systems. We also introduce, and discuss, the notion of $M : N$ rhythm. Chap. 5 is dedicated to the continuation and bifurcation analysis of periodic solutions in the periodically forced excitable FitzHugh-Nagumo system. Two values of the parameter ε controlling the timescale difference in the slow-fast system are considered successively. The evolution of the bifurcation diagram, where the stimulation period is the bifurcation parameter, is studied as the stimulation amplitude is gradually raised. This study is followed by a brief review of prior experimental and theoretical works on periodically forced excitable systems in which the phenomena we observe have also been reported. We then discuss in more detail two prior studies (one experimental and one theoretical) in which the influence of both the stimulation period and amplitude on the periodic responses of the excitable system has been studied, as in our work. The first part of Chap. 6 consists in a continuation and bifurcation analysis analogous to that carried out in Chap. 5, except that the FitzHugh-Nagumo model is studied this time in its relaxation oscillation regime. The second part of the chapter is dedicated to the study of a circle map derived from the phase-resetting response of the oscillator, the "phase-resetting map". We investigate the extent to which this circle map provides a good approximation of the original differential equations. This study allows us to underscore an important property of the bifurcation diagram of circle maps where the bifurcation parameter appears in an additive fashion only, namely, that the period-1 orbits belong to isolated "loops" when the topological degree of the map is one, while they belong to a unique branch when the topological degree is zero.

Chapter 1

Modelling excitability and relaxation oscillations in the heart

It is no exaggeration to say that the Hodgkin-Huxley model is the most important model in all of the physiological literature.

J. Keener and J. Sneyd (1998)

In this chapter, we review the main steps of the history of the modelling of the heart electrical activity over the last century. This is the occasion to make a first analysis of a system of differential equations (the Hodgkin-Huxley equations) which exhibits excitability or relaxation oscillations depending on the parameter values (a more thorough analysis of such equations is done in Chap. 2 with the BVP-FHN model). This also allows us to give an idea of the nature and amount of the physiological processes which come into play to produce this characteristic electrical behaviour in cardiac cells, and of the complexity of the models which are used nowadays to describe these physiological processes. We examine in this chapter the modelling of the heart electrical activity from the temporal point of view only; the modelling of the propagation of the electrical impulse in the cardiac muscle is a very interesting and important subject as well, but it is beyond the scope of this thesis. Several sections in this chapter are based on [KS98].

1.1 The van der Pol oscillator

In 1926, van der Pol showed that the equation

$$\frac{d^2v}{dt^2} - \mu(1 - v^2)\frac{dv}{dt} + v = 0 \tag{1.1}$$

exhibits self-sustained oscillations[1] and that, for large values of the parameter μ, these oscillations depart considerably from a sinusoid, with $v(t)$ characterized by the alternation of fast and slow phases (Fig. 1.1) [vdP26]. He called these oscillations "relaxation

[1]The existence of such self-sustained oscillations appears intuitively obvious if Eq. (1.1) is interpreted as Newton's law for an harmonic oscillator subject to nonlinear friction. Indeed, when $|v| < 1$, there

oscillations" because, for $\mu^2 \gg 1$, the period of oscillation is proportional to μ (see Sec. 2.2.3), and that, in the electrical circuit he built to realize Eq. (1.1), μ was the time constant, or relaxation time, of the circuit [vdP26, Kan07].

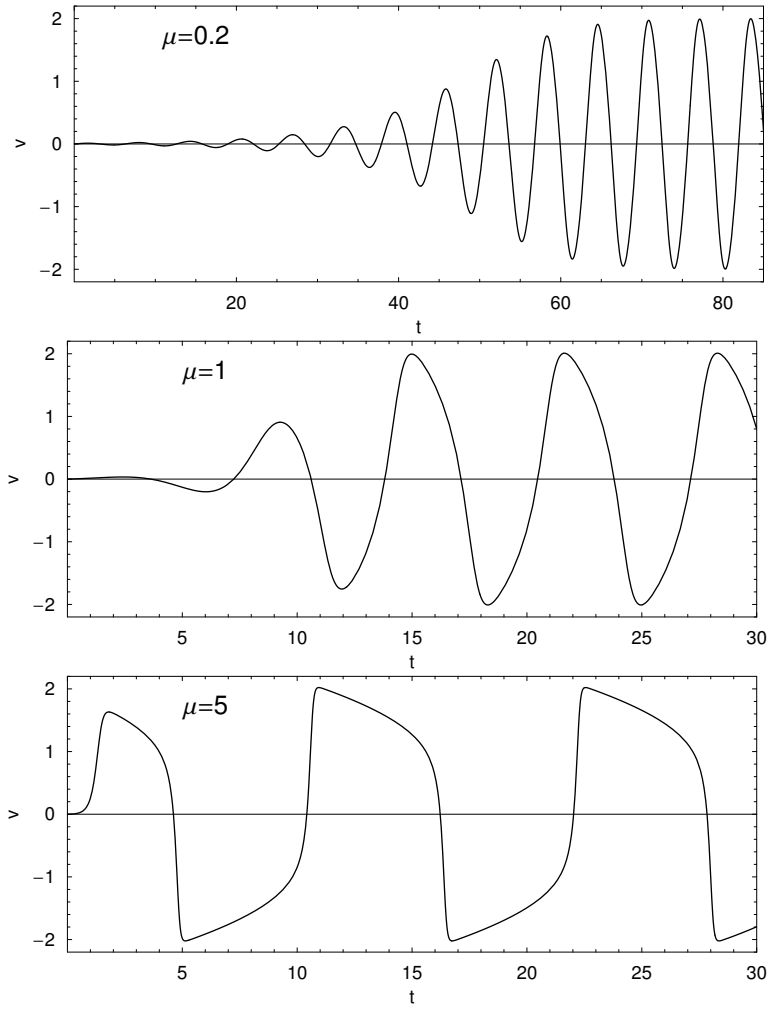

Figure 1.1. *Temporal evolution of the potential v in the van der Pol (VDP) model for different values of μ, using the same initial conditions $(v(0), \frac{dv}{dt}(0)) = (0, 0.01)$. A gradual departure from the sine waveform is observed as μ is increased. In the same time, the number of oscillations needed to reach the asymptotic waveform decreases.*

Although there were no experimental data at the cellular level available at the time to corroborate his view, van der Pol hypothesized the heartbeat to be a relaxation oscillation. In 1928, he and van der Mark proposed an electrical model of the heart where the sinus node (the natural pacemaker of the heart), the atria and the ventricules are described as three relaxation oscillators of different frequencies, interconnected by two unidirectional couplings [vdPvdM28]. In healthy circumstances, there is a one-to-one (1:1) synchronisation between these three regions of the heart, with the sinus node

is inverse friction, so that the amplitude of the oscillation grows, while when $|v| > 1$, dissipation tends to reduce the amplitude of the oscillation. Hence, it appears plausible that there exists a compromise amplitude at which a stable periodic oscillation exists. That compromise amplitude is that at which the amount of energy dissipated during one period equals the amount of energy gained during the same period of time.

imposing its frequency on the other two regions. By reducing the coupling strength between the atria and the ventricules, they could reproduce qualitatively the pathology known as "heart block", in which the ventricules fire less often than the atria, giving rise to skipped heartbeats. Their model is however unrealistic in several respects; for instance, the actual atria and ventricules do not behave like relaxation oscillators, but consist of excitable cells (*cf.* Sec. 1.3.1).

1.2 The Hodgkin-Huxley model

It was Hodgkin and Huxley who first succeeded to build a mathematical model of cellular excitability from the measurements of individual ionic currents at the cell level. Their model, published in 1952 [HH52], was originally developed for the giant axon of the squid, a nerve fibre, but their approach was subsequently extended to a wide variety of other excitable cells, including cardiac cells. They were awarded the 1963 Nobel Prize in physiology and medicine for their work, which stands out as one of the most successful combinations of experiment and theory in the field of biology.

Hodgkin and Huxley wanted to understand the mechanism of the *action potential* (AP), the electrical excitation undergone by an excitable cell when it is submitted to a sufficient electrical perturbation. When the transmembrane potential (the potential difference between the intracellular and the extracellular medium of the cell) is brought above some threshold value, it raises quickly to an excited value which is almost independent of the perturbation applied. The transmembrane potential returns spontaneously to its equilibrium value some time later. On the other hand, if the perturbation is not sufficient for the potential to overcome the threshold, no amplification is observed and the cell returns quickly to the rest state. The generation and propagation of APs is crucial to biological signal transmission.

When Hodgkin and Huxley started to work together at the end of the 1930s, it was known that the membrane of biological cells separates different ionic concentrations inside and outside the cell, thus acting as a capacitor, and it was strongly suspected that the membrane "permeability" to ions was changing during an AP, giving rise to variations of the transmembrane potential. This electrical behaviour of the cell membrane is schematized in Fig. 1.2, and the corresponding equation for the transmembrane potential writes

$$C_m \frac{dV}{dt} + I_{ion} = 0 \tag{1.2}$$

where C_m is the capacitance of the membrane. Outward ionic currents are by convention positive.

The first description of the squid giant axon in 1936 had just made it possible to measure transmembrane potentials, as the large diameter of the axon (~ 1 mm) permits the insertion of an axial electrode (~ 100 μm in diameter) into the axon (e.g., [Gue03]). Experimental evidence for changes in membrane conductance came in the 1940s, and with it the conviction that these changes were not identical for all ions, in contrast to what was believed since the beginning of the century. Indeed, Hodgkin and Huxley realized that only different changes in permeabilities for different ions could account for the voltage time course observed during an AP, as the voltage would approach the Nernst potential[2] for the ion to which the membrane was predominantly permeable, and this dominance could change with time. It was a key step in their work.

[2]Given a semi-permeable membrane separating two initially electrically neutral solutions containing

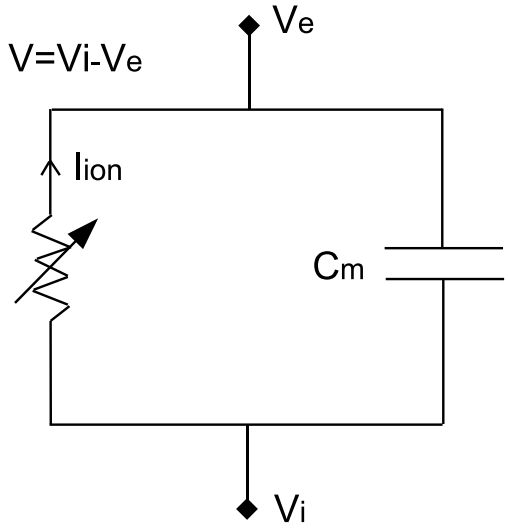

Figure 1.2. *Electrical circuit model of the cell membrane.*

They also gathered evidence that the sodium and potassium ions were the most important species implied in the generation of the AP, so that they wrote the total ionic current as

$$I_{ion} = I_{Na} + I_K + I_L$$

where I_L is a "leakage" current gathering the (presumably small) contribution of all other species. They wrote the individual ionic currents as

$$I_S(V,t) = g_S(V,t)(V - V_S),$$

where S is the ion species and V_S the corresponding Nernst potential. This is a generalization of Ohm's law since the ionic conductances $g_S(V,t)$ are expected to be non-constant. In order to determine the behaviour of the conductances $g_S(V,t)$ as a function of the voltage V, Hodgkin and Huxley used a technique called *voltage clamp*: they fixed the membrane potential at a given value by a rapid step from one voltage to another, and then measured the current that must be supplied in order to hold the voltage constant. Since the supplied current must equal the transmembrane current, this technique provides a way to measure the total ionic current that flows at a constant, known, voltage. Provided one has a method for distinguishing between the different ionic components

one ion S in different concentrations $[S]_i$ and $[S]_e$, the Nernst potential V_S of that ion is the potential difference across the membrane at which there would be no electrical current flowing if the ion S was the only one the membrane was permeable to:

$$V_S = \frac{RT}{zF} \ln\left(\frac{[S]_e}{[S]_i}\right)$$

where R is the universal gas constant, T is the absolute temperature, F is Faraday's constant, k is Boltzmann's constant, and z is the charge on the ion S. The existence of this electrical potential results from the competition between diffusion, which tends to equalize the concentrations $[S]_i$ and $[S]_e$ (or, more exactly, the chemical potentials of S on the two sides of the membrane), and the electric field resulting from the passage of charges through the membrane, and which opposes to the further building of charge imbalance.

in the total current[3] , one can then deduce from the voltage clamp the evolution of the conductances as functions of time only. Indeed, Hodgkin and Huxley observed that the value of the conductances are not functions of the voltage solely ; following a voltage step, they do not switch immediately to another value, but evolve in time towards this asymptotic value in a fashion that is characteristic of the species and of the fact that the voltage has been stepped up or down (see Fig. 1.3). Both the asymptotic value of the conductance and the characteristic time of the evolution depend on the value to which the voltage has been stepped.

To model this behaviour, instead of writing differential equations directly for the conductances, Hodgkin and Huxley found it easier to express the conductances as products of auxiliary *gating variables* $y(v,t)$, varying between 0 and 1, each of these variables obeying a linear differential equation of the form

$$\frac{dy}{dt} = \frac{y_\infty(v) - y}{\tau_y(v)}, \tag{1.3}$$

where $v = V - V_{eq}$ is the difference between the transmembrane potential V and the resting potential V_{eq} ($V_{eq} \simeq -65$ mV in the squid giant axon). The solution of this equation is

$$y(t) = y_\infty(v) - [y_\infty(v) - y(0)]e^{-t/\tau_y(v)}. \tag{1.4}$$

Eq. (1.3) is also often written in the literature as

$$\frac{dy}{dt} = \alpha_y(v)(1-y) - \beta_y(v)y \tag{1.5}$$

and one has the relationships

$$\begin{aligned} \tau_y(v) &= \frac{1}{\alpha_y(v) + \beta_y(v)}, \\ y_\infty(v) &= \frac{\alpha_y(v)}{\alpha_y(v) + \beta_y(v)}. \end{aligned}$$

Using such gating variables, the potassium conductance g_K, which follows a sigmoidal increase following a step increase in voltage, and an exponential decay following a step decrease in voltage (Fig. 1.3, bottom panel), was found by Hodgkin and Huxley to be well described by

$$g_K = \bar{g}_K n^4 \tag{1.6}$$

where $\bar{g}_K$ is the maximum potassium conductance and

$$\frac{dn}{dt} = \frac{n_\infty(v) - n}{\tau_n(v)}.$$

Therefore, for each value of v, the values of the two parameters n_∞ and τ_n were determined by fitting the fourth power of Eq. (1.4) to the measured conductance. When

[3]To do this, Hodgkin and Huxley compared the time evolutions, following a voltage step-up, of the total ionic current with normal extracellular sodium concentration and with almost zero extracellular sodium. Assuming that the initial inward current which is observed to develop following a voltage step-up is carried almost exclusively by sodium ions, and that the outward current observed to develop later is carried almost exclusively by potassium ions, they could deduce from the time evolution of the total ionic current that of the sodium and the potassium ionic components separately (see [KS98] for details).

Figure 1.3. *Evolution of Na^+ and K^+ conductances following a step increase in voltage (solid curves) and following a step decrease in voltage (dashed curves) in the squid giant axon (see ref. in Fig. 3.13 of [KS98]).*

the procedure had been repeated for a large enough number of values of v, Hodgkin and Huxley fitted smooth curves through the data points in order to obtain continuous descriptions of n_∞ and τ_n as functions of v (Fig. 1.4)[4]. The sodium conductance g_{Na} was itself observed to follow a more complex evolution for a step increase in voltage, since it first increases and then decreases later on, at the same fixed voltage (Fig. 1.3, middle panel). This behaviour was accounted for by writing

$$g_{Na} = \bar{g}_{Na} m^3 h \tag{1.7}$$

where $\bar{g}_{Na}$ is the maximum sodium conductance and

$$\begin{aligned} \frac{dm}{dt} &= \frac{m_\infty(v) - m}{\tau_m(v)} \\ \frac{dh}{dt} &= \frac{h_\infty(v) - h}{\tau_h(v)} \end{aligned}$$

The variables $n(t)$ and $m(t)$ are called *activation* variables because their asymptotic values $n_\infty(v)$ and $m_\infty(v)$ are increasing functions of the potential v (Fig. 1.4, left panel), so that their effect is to turn on, or *activate*, the corresponding currents when the voltage is raised high enough. On the other hand, $h(t)$ is called an *inactivation* variable because $h_\infty(v)$ is a decreasing function of v (Fig. 1.4, left panel), so that the effect of h is to turn off the sodium current at high values of the potential.

[4]These functions have no physiological significance, but it is convenient to have such analytical descriptions of $n_\infty(v)$ and $\tau_n(v)$.

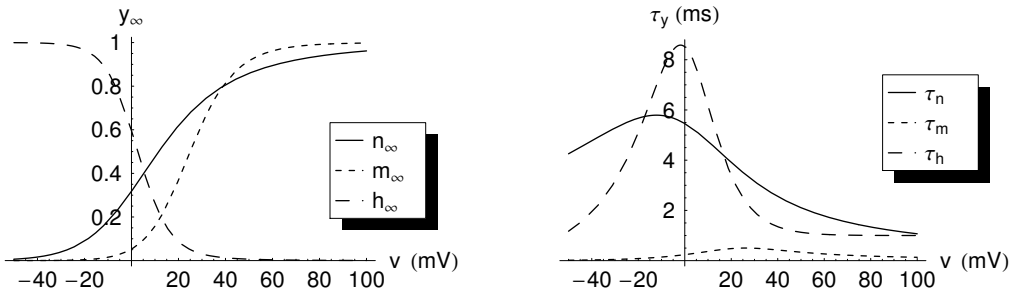

Figure 1.4. *Asymptotic values (left) and characteristic times (right) of the gating variables as a function of the potential $v = V - V_{eq}$ in the Hodgkin-Huxley model.*

The complete Hodgkin-Huxley (HH) equations write

$$C_m \frac{dv}{dt} = -\bar{g}_{Na} m^3 h (v - v_{Na}) - \bar{g}_K n^4 (v - v_K) - \bar{g}_L (v - v_L) \tag{1.8}$$

$$\frac{dn}{dt} = \frac{n_\infty(v) - n}{\tau_n(v)} \tag{1.9}$$

$$\frac{dm}{dt} = \frac{m_\infty(v) - m}{\tau_m(v)} \tag{1.10}$$

$$\frac{dh}{dt} = \frac{h_\infty(v) - h}{\tau_h(v)} \tag{1.11}$$

where $C_m = 1\mu\text{F/cm}^2$ is the membrane capacitance, $\bar{g}_{Na} = 120$ mS/cm^2, $\bar{g}_K = 36$ mS/cm^2, $\bar{g}_L = 0.3$ mS/cm^2 are the maximum ionic conductances, and $v_{Na} = 115$ mV, $v_K = -12$ mV, $v_L = 10.6$ mV are the Nernst potentials relative to the resting potential. The graphs of the functions $y_\infty(v)$ and $\tau_y(v)$ functions are given in Fig. 1.4. Their analytical expressions (via those of $\alpha_y(v)$ and $\beta_y(v)$), can be found, e.g., in [KS98]. The model possesses a unique steady-state at

$$\begin{aligned} v &= V - V_{eq} = 0 \text{ mV} \\ n &= n_\infty(v) = 0.318 \\ m &= m_\infty(v) = 0.053 \\ h &= h_\infty(v) = 0.596 \end{aligned}$$

Let us now explain why the HH model is able to account for the occurrence of action potentials. At the resting potential, because of the respective values of the Nernst potentials, the potassium current is an outward current, the sodium current is an inward current, and the (small) leakage current is also inward. The equilibrium results from the balance of these three currents. These ionic ionic currents are such that if a *small* external current is applied to the system for a brief period of time, the equilibrium is rapidly restored – the excitation threshold is not overcome. If the sodium and potassium conductances were constants, the potential would also go back quickly to it resting value when a *large* current is applied, but these conductances are not constant. In particular, the fact that the time needed by the sodium activation variable m to reach its asymptotic value $m_\infty(v)$ is much smaller (Fig. 1.4, right panel) than both the time needed by the sodium inactivation variable h and the time needed by the potassium

activation variable n to reach their asymptotic value, implies that for a large enough applied positive current (*i.e.*, when the excitation threshold is overcome), the potential will first rise quickly towards the sodium Nernst potential, due to the large inward flow of sodium current, unbalanced by an equivalent outward current. Only after some delay will the inactivation variable h fall to zero, turning off the sodium current and stopping the raise of the potential. In the same time, the activation variable n increases, so that the outward potassium current is turned on, and gradually drives the potential back to its resting value. Such an evolution of the potential corresponds to an AP (Fig. 1.5). The fact that the HH model is able to account for the occurrence of APs is thus intimately linked with the fact that it possesses variables with notably different time scales.

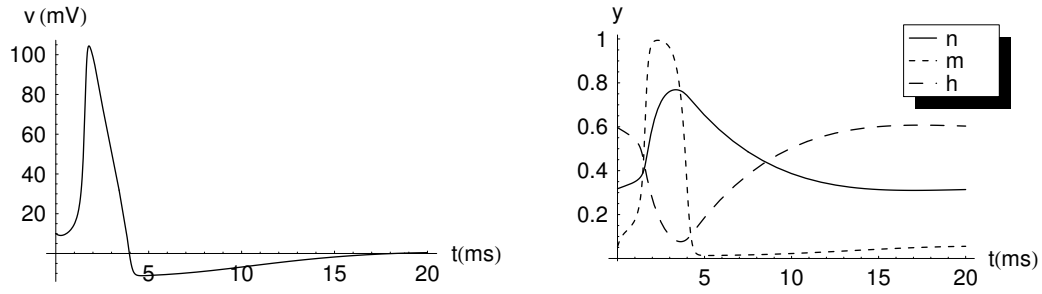

Figure 1.5. *Evolution of the variables in the HH model for the initial conditions* $v(0) = 10mV$, $n(0) = n_\infty(v = 0)$, $m(0) = m_\infty(v = 0)$ *and* $h(0) = h_\infty(v = 0)$. *An action potential is generated.*

The HH model also accounts for the fact that there exists, in excitable cells, a *refractory period*, *i.e.*, a period during which a second AP cannot be elicited following a first one. Indeed, the inactivation variable h has to relax back to a non zero value before the sodium current can be turned on again. Finally, note that the HH model can also exhibit relaxations oscillations when submitted to an external constant current of appropriate strength (see, e.g., the first bifurcation diagram in [XCKA08]) .

1.3 Ionic models of cardiac cells

After Hodgkin and Huxley's success with the squid giant axon, a great amount of work was done to apply their approach to other types of cells producing APs, in particular cardiac cells. In cardiac cells as in neurons, the upstroke (rising phase) of the action potential is caused by the fast entry of sodium ions, and the repolarization (decrease of the electrical potential back to the resting value) is mostly due to the exit of potassium ions. The main difference lies in the presence of an inward calcium current which, in myocardial cells (cardiac muscle cells), is responsible for triggering the contraction mechanism of the cell.

1.3.1 Types of cardiac cells

There are five main types of cardiac cells. The sinoatrial (SA) nodal cells, or sinus node cells, which are located in the upper part of the right atrium (Fig. 1.6), behave like electrical relaxation oscillators, in that they fire spontaneously and periodically. They play the role of the natural pacemaker of the heart. Their AP resembles that of

neurons in shape, because they have little calcium current, but occurs on a different time scale: its duration is of the order of 100ms while it is on the order of 1ms for the squid giant axon. Both the atrial and ventricular cells, are excitable myocardial cells. Their excitation is (periodically) triggered by the electrical current propagating from the SA node. Their AP has a different shape than that of SA node cells, due to the presence of a large inward calcium current that counteracts the outward potassium current and gives rise to a "plateau" phase between the upstroke and repolarization phases (Fig. 1.6). The electrical connection between the atria and the ventricules is restricted to the atrioventricular (AV) node, a region where the electrical conduction is slowed down. This insures the existence of a delay between the contraction of the atria and that of the ventricules, so that the latter are filled with blood when their contraction occurs. The AV node fires spontaneously like the SA node, but in normal circumstances it is enslaved by the SA node, and takes the role of the pacemaker only if the SA node fails. From the AV node, the electrical impulse enters the bundle of His, which separates into two branches to become the network of Purkinje fibres in the ventricules (Fig. 1.6). The role of the Purkinje fibres is to speed up the spreading of the electrical signal into the ventricules, so that the contraction of the ventricular muscle occurs in an approximately coordinated manner. Purkinje fibres are also spontaneously firing cells, and can take over if both other pacemakers fail. As myocardial cells, they are endowed with a substantial calcium current, and their AP is characterized by a plateau phase (Fig. 1.6).

Figure 1.6. *AP shape for the different types of heart cells [MP95].*

Although there are only a few main types of cardiac cells, there can be substantial variation within one type. For example, in the ventricules, epicardial, midmyocardial, and endocardial cells have noticeable differences in AP duration (APD)[5]. There is also great variation between species (e.g., the APD in guinea pig and canine ventricular myocytes is about 300ms while it is only about 13ms in rat ventricular myocytes [BSB$^+$04]).

[5]In this work, we refer to the APD simply as the approximate time during which the cell remains electrically excited. A rigorous (but also arbitrary) definition would identify the APD with the time during which the electrical potential remains above some precise value, but we do not need such a definition here.

1.3.2 First models

The first model accounting for the AP of a cardiac cell was the Noble 1962 model for Purkinje fibres [Nob62]. The primary purpose of the model was to show that the AP of a heart cell could be captured by a model of Hodgkin-Huxley type (*i.e.*, where the ionic currents are written in terms of gating variables obeying differential equations of type (1.3)). Although the Noble 1962 model takes into account the fact that there is more than one type of potassium current[6] in Purkinje fibres (and in cardiac cells in general), it is physiologically incorrect because there is no ionic current identified with calcium ions – the inward sodium current is given the dual role of generating the upstroke and maintaining the plateau (see, e.g., [KS98] for the equations). Indeed, the model was built before the voltage-clamp technique was successfully applied to cardiac cells (1964), and calcium currents discovered. The McAllister-Noble-Tsien (MNT) 1975 model for Purkinje fibres [MNT75] palliates this deficiency, and also includes additional components for the potassium currents that had also been discovered via voltage-clamp experiments [Nob02].

The next step was taken by Beeler and Reuter in 1977 [BR77], who found necessary to include an equation for the evolution of the intracellular calcium concentration in their model to account for the AP morphology in ventricular myocytes. Indeed, in myocardial cells, the entry of calcium ions triggers the release of additional calcium ions from an inner compartment called the sarcoplasmic reticulum (SR). This raises substantially the intracellular calcium concentration, so that the influence of this concentration change on the calcium ionic flow cannot be neglected (while the changes in other ionic concentrations can, in first approximation, be neglected). It is this calcium-induced calcium release (CICR) which triggers the mechanism of cellular contraction in myocytes. Models which, following Beuler and Reuter, include equations for the evolution of ionic concentrations are termed "second-generation" models.

1.3.3 Ionic pumps

For the repetitive generation of APs to be possible (and, more generally, for a cell to function properly), it is not sufficient that the transmembrane potential returns to its initial value at the end of an AP. It is also necessary that the initial concentration of each ion species inside and outside the cell, as well as the initial ionic concentrations in the SR, are restored. This restoration is ensured by *ionic pump* currents, which, in contrast to the ionic currents mentioned as up now, are not spontaneous currents[7], but require energy expanditure from the cell (e.g., through ATP consumption) to function.

Some ionic pumps are also termed "exchangers" because they use the energy inherent in the concentration gradient of one ion type (instead of ATP) to pump another ion type against its concentration gradient [KS98]. The first model to include the effect of ionic pumps on the cardiac AP, together with the effect of ionic concentration changes other than calcium, was the DiFrancesco-Noble 1985 model for Purkinje fibres [DN85]. It also

[6] As we discuss below, ions actually cross the cell membrane through channels, which are ion-selective pores. But there can be more than one type of channels allowing a given species through, each type being characterized by its own conductance profile (the number of ions that can flow per unit time at a given voltage).

[7] In the sense of thermodynamics: spontaneous processes are processes which increase the entropy of the universe. In the present context, this corresponds to an ion flowing in the direction of the gradient of the corresponding electrochemical potential.

includes an explicit model of CICR from the SR, *i.e.* it couples the differential equation for the intracellular calcium concentration to differential equations for the calcium concentration in the SR.

1.3.4 Ion channels

Although it is considered to be obvious today that ions cross the cell membrane through ion channels, which are protein-lined pores that can open or close via conformational changes following voltage changes[8], it has not always been so. The other main hypothesis was that ions pass through the membrane by bounding to a mobile protein carrier which is soluble in lipids (this is actually the way some large molecules enter the cell, as is illustrated in Fig. 1.7). Both means can *a priori* be ion-selective, and Hodgkin and Huxley's study did not really favor one of the two permeation mechanisms (e.g., [Hux02, MS02]). Hille, who contributed greatly to show that the ion-channel hypothesis was the correct one, reports in [HAM99] that during the annual meetings of the Biophysical Society between 1965 and 1973, when these ideas were regularly debated, prominent scientists would routinely rise to request that anyone who chose to use the word "channel" avow first that it bears absolutely no mechanistic implications(!). Hille, as well as Armstrong, accumulated lots of indirect experimental evidence in favor of the ion-channel hypothesis by studying ionic currents with voltage clamp and drugs that selectively block ionic conductances (see [HAM99] and refs. therein). The development of the patch-clamp technique by Neher and Sakmann in the late seventies, technique for which they received the Nobel prize in Physiology and Medicine in 1991, allowed further progress in the study of ionic currents. Indeed, they discovered that by using "suction" microelectrodes with a tip diameter of about 1 μm, they could obtain a very good seal between the microelectrode tip and a "patch" of cell membrane. This was not possible with the "sharp" microelectrodes (about 0.1 μm in diameter) used until then to study ionic currents in small cells such as cardiac cells (the squid giant axon was itself studied with electrodes about 100 μm in diameter). With the patch left intact in place ("cell-attached" recording; see, e.g., Fig. 4.27 in [MP95]), they could then study the ionic current flowing through a few membrane channels only, and even get single-channel recordings. With the patch ruptured ("whole-cell" recording; see, e.g., Fig. 4.27 in [MP95]), they could, in small cells, achieve much better voltage clamps than what was possible in the past. Indeed, because the resistance of suction microelectrodes is much less than that of sharp microelectrodes (due to the larger diameter), much more current can be delivered into the cell, allowing to keep the voltage constant even when large and fast ionic currents (such as the sodium current) are flowing. In the 1980s and 1990s, the development of cloning and mutagenesis allowed to infer still more properties of ion channels. However, it was only in 1998 that a direct "visualization" of an ion-channel structure became possible with MacKinnon's work using X-ray crystallography (see [HAM99] and refs. therein). MacKinnon received the 2003 Nobel Prize in Chemistry.

1.3.5 Markov models for ion channel kinetics

As experimental evidence accumulated for the fact that ion channels are proteins that change conformation in response to voltage changes or ligand binding, with some con-

[8] There exists also ion channels that change conformation in response to the binding of a ligand rather than in response to a change in potential.

Figure 1.7. *Schematic diagram of the cell membrane containing a protein carrier and a protein-lined ionic channel (see ref. in Fig. 2.2 of [KS98]).*

formations only corresponding to an open state for the channel, *Markov models* were proposed to model the transitions between the different conformations of the channel. A Markov model is a finite set of discrete states, in which the probability of transition from one state to another depends only on the current state, not on previous ones. For instance, in the markovian paradigm, a channel which could take only two states, open (O) and closed (C), would be modeled by the first-order reaction

$$C \underset{\beta(V)}{\overset{\alpha(V)}{\rightleftharpoons}} O \tag{1.12}$$

where $\alpha(V)$ and $\beta(V)$ are the conversion rates from one state to the other. If p_O and p_C denote respectively the proportion of channels in the open state and in the closed state, one has

$$\frac{dp_O}{dt} = \alpha(V)p_C - \beta(V)p_O = \alpha(V)(1 - p_O) - \beta(V)p_O \tag{1.13}$$

since $p_O + p_C = 1$.

Many channels are actually made of multiple subunits, each of which must be in a particular conformation to allow the passage of ions. For example, cardiac potassium channels are known to possess four identical subunits, each one containing a voltage sensor, and all four sensors must be in the activated position for the channel to open [RS06]. A simple model for these channels is to assume that each subunit can only be in two states, following a kinetics of the form (1.12), with the same reaction rates α and β for all subunits, and that the evolution of the different subunits is independent. In this case, denoting by C_i the state in which i subunits are closed, one can write the reaction scheme as

$$C_4 \underset{\beta}{\overset{4\alpha}{\rightleftharpoons}} C_3 \underset{2\beta}{\overset{3\alpha}{\rightleftharpoons}} C_2 \underset{3\beta}{\overset{2\alpha}{\rightleftharpoons}} C_1 \underset{4\beta}{\overset{\alpha}{\rightleftharpoons}} C_0$$

since, for instance, when 3 subunits are in the closed state (C_3), there are 3 possibilities for opening an additional channel (hence the transition rate 3α to C_2) but only one possibility for closing an additional one (hence the transition rate β to C_4). The proportion

of channels in the open state p_0 is then governed by the following equation system:

$$\begin{aligned}
\frac{dp_0}{dt} &= -4\beta p_0 + \alpha p_1 \\
\frac{dp_1}{dt} &= 4\beta p_0 - (\alpha + 3\beta)p_1 + 2\alpha p_2 \\
\frac{dp_2}{dt} &= 3\beta p_1 - (2\alpha + 2\beta)p_2 + 3\alpha p_3 \\
\frac{dp_3}{dt} &= 2\beta p_2 - (3\alpha + \beta)p_3 + 4\alpha p_4 \\
1 &= p_0 + p_1 + p_2 + p_3 + p_4
\end{aligned} \tag{1.14}$$

where p_i is the proportion of channels in state C_i. The corresponding ionic current is given by

$$I_K(V,t) = p_0(V,t) g_K(V)(V - V_K) \tag{1.15}$$

where $g_K(V)$ is the potassium conductance at potential V when all channels are open, and V_K the potassium Nernst potential. Expression (1.15), together with (1.14), is meant to replace the corresponding Hodgkin-Huxley formulation in terms of gating variables in the models of the cardiac AP where this type of potassium current plays a role.

1.3.6 A recent cardiac model

Fig. 1.8 shows a schematic of a recent cardiac model, the "Luo-Rudy dynamic" (LRd) ventricular cell model (see [RS06] and refs. therein), that includes all the features we have discussed above. It exhibits several types of spontaneous ionic currents, some of which are time-independent ("background" currents, abbreviated as $I_{S,b}$, where S is the ion species), while the others (time-dependent currents) are described either by Markov models (the boxed currents in Fig. 1.8) or by Hodgkin-Huxley type formulations. It possesses ionic pump ($I_{p(Ca)}$ and I_{NaK}) and exchanger (I_{NaCa}) currents. It includes evolution equations for the ionic concentrations, and in particular it includes a model of CICR from the SR with two subcompartments, a network SR (NSR) and a junctional SR (JSR).

1.3.7 Invariant manifold reductions for Markov models

The advantage of Markov models over Hodgkin-Huxley formulation of ionic currents is that the different states in a Markov model have (or are supposed to have[9]) a physiological signification, in terms of conformations of the channel, and that some genetic manipulations and diseases can be related to changes in specific rate constants in the Markov models [BSB$^+$04]. On the other hand, Hodgkin-Huxley gating variables have no physiological meaning – they are only a convenient way of fitting the voltage-clamp data using equations of type (1.3).

However, it has recently been shown that many Markov models possess a globally attracting invariant manifold, the dimension of which is often substantially smaller than the full equation system [Kee08]. The consequence is that simulations of ion channel

[9]Several Markov models used to describe ionic currents in recent cardiac models include states the existence of which has not (yet) been corroborated experimentally, but the presence of which is needed to reproduce within the markovian paradigm the behaviour of the ionic current (e.g., the Markov model of I_{Kr} used in [BSB$^+$04]).

Figure 1.8. *A schematic of the Luo-Rudy dynamic (LRd) ventricular cell model [RS06]. Troponin, calmodulin, and calsequestrin are calcium "buffers",* i.e., *large proteins to which calcium ions bind in the cytoplasm and in the SR. The shaded currents are ionic currents which are included only under pathological conditions or for testing particular effects.*

kinetics can be greatly simplified without approximation, because the dynamics of the system are restricted to the stable invariant manifold once the transients have decayed. In particular, the Markov model (1.14) has been shown to admit as globally attracting invariant manifold the binomial distribution

$$p_{i_C} = \frac{N!}{i_C!(N-i_C)!}(1-n)^{i_C} n^{N-i_C} \tag{1.16}$$

where i_C is the number of subunits in the closed conformation, $N = 4$ (total number of subunits), and n is the probability of one subunit being in the open conformation. That probability is given by

$$\frac{dn}{dt} = \alpha(V)(1-n) - \beta(V)n \tag{1.17}$$

since all the subunits are assumed to change conformation according to the reaction scheme (1.12). Eq. (1.16) tells us in particular that the proportion of channels in the open state is[10] $p_0 = n^4$. This means that the Hodgkin-Huxley formulation of potassium conductance (1.6), which is one-dimensional since it involves the sole gating variable n, is equivalent to the four-dimensional Markov model (1.14) once the transients have decayed. Hence, there is no advantage (on the contrary) in replacing the HH formulation for this channel by the detailed Markov model, even if one is interested in the proportion of channels in each state, since these proportions can be deduced from (1.16).

More generally, the Markov model for a channel with N independent, identical subunits, each of which can be in M different states, possesses as globally attracting invariant

[10] One can get some insight into (1.16) by checking that $p_0 = n^4$ with n obeing (1.17) is a solution of (1.14) if and only if $p_1 = 4(1-n)n^3$, $p_2 = 6(1-n)^2n^2$, $p_3 = 4(1-n)^3n$, and $p_4 = (1-n)^4$. One can also verify that this solution is a stable invariant manifold by considering the perturbed solution

$$p_{i_C} = \frac{N!}{i_C!(N-i_C)!}(1-n)^{i_C} n^{N-i_C} + \delta_{i_C}.$$

Indeed, one finds that the perturbations δ_{i_C} obey a linear system of equations $\dot{\delta}_{i_C} = \sum_j M_{i_C j}\delta_j$, with the eigenvalues of the matrix M having all negative real parts, so that the δ_{i_C} go exponentially to zero.

manifold the multinomial distribution [Kee08]:

$$p_{i_1,i_2,...,i_M} = \frac{N!}{i_1!i_2!...i_N!} p_1^{i_1} p_2^{i_2} ... p_M^{i_M} \tag{1.18}$$

where i_k is the number of subunits in state k and p_k is the probability for a subunit to be in state k. If β_{ij} denotes the transition rate between state i and state j for a subunit, then

$$\frac{dp_i}{dt} = -\sum_j \beta_{ij} p_i + \sum_j \beta_{ji} p_j. \tag{1.19}$$

This is a (M–1)-dimensional invariant manifold, because only $M-1$ differential equations in (1.19) are independent ($\sum_j p_j = 1$). On the other hand, the dimension of the full Markov model is

$$D = \Gamma_M^N - 1 = C_{M+N-1}^N - 1 = \frac{(M+N-1)!}{(M-1)!N!} - 1.$$

To give a concrete example, a model of cardiac potassium channels more realistic than (1.12) incorporates a second closed state for the subunits (see, e.g., [RS06]), so that the corresponding Markov model for the channel has $D = 14$ dimensions, while its globally attracting invariant manifold is only two-dimensional. This result is thus very powerful.

Another useful property of the invariant manifolds of Markov models is a multiplicative structure. If a N-subunit channel counts K subunits of one type a, and $N-K$ subunits of another type b, all subunits being independent, the globally attracting invariant manifold of the Markov model for the N-subunit channel will be given by the product of two multinomial distributions ; the globally attracting invariant manifold of the Markov model for an hypothetical channel exhibiting K identical subunits of type a, and the globally attracting invariant manifold of the Markov model for an hypothetical channel exhibiting $N-K$ identical subunits of type b [Kee08].

For instance, consider a four-subunit channel, with three subunits of type m and one subunit of type h, each of which can be in two states:

$$C_j \underset{\beta_j(V)}{\overset{\alpha_j(V)}{\rightleftharpoons}} O_j, \quad j = m, h. \tag{1.20}$$

If m (resp. h) represents the probability that a subunit of type m (resp. h) is in the open conformation, we have

$$\frac{dq}{dt} = \alpha_q(V)(1-q) - \beta_q(V)q, \quad q = m, h. \tag{1.21}$$

The channel can take eight possible states S_{ij}, where S_{ij} is the state in which there are i open m subunits and j open h subunits. The globally attracting invariant manifold of this Markov model is given by

$$p_{ij} = p_i(m;3)p_j(h;1) \tag{1.22}$$

where p_{ij} is the proportion of channels in state S_{ij} and $p_k(q;N)$ is the binomial distribution

$$p_k(q;N) = \frac{N!}{k!(N-k)!} q^k (1-q)^{N-k} \tag{1.23}$$

The proportion of channels in the open state is then given by $p_{31} = m^3 h$, which is the expression used by Hodgkin and Huxley to model the squid axon sodium conductance (1.7). Hence, in this case as well, there is no point in replacing the HH formulation by the full Markov model.

In conclusion, when using a Markov model of ion channel kinetics, it is worth checking whether the model admits a globally attracting invariant manifold of smaller dimension before running any numerical simulation, since using the reduced model can save substantial computational time.

Chapter 2

The FitzHugh-Nagumo model

The usefulness of an equation to an experimental physiologist (like the usefulness of his amplifier) depends on his understanding of how it works.

R. FitzHugh (1960)

In 1961, FitzHugh showed that the essence of the Hodgkin-Huxley model, as far accounting for excitability is concerned, is contained in a two-dimensional (2D) reduction of it, for which phase-plane analysis, and thus "visual" understanding, is possible. He also showed that this 2D reduction is qualitatively equivalent to the Bonhoeffer-van der Pol (BVP) model, a model FitzHugh built by modifying the van der Pol oscillator so that it can be turned into an excitable system by changing the value of a single parameter [Fit61]. His approach is inspired by the Bonhoeffer model of an iron wire in concentrated nitric acid [Bon48], which does exhibit excitability or relaxation oscillations depending on the intensity of the constant electrical current it is submitted to. However, FitzHugh's model is simpler ; in fact, it is the simplest smooth differential model of excitability[1]. The BVP model is nowadays very often referred to as the FitzHugh-Nagumo (FHN) model, Nagumo being the first person who has built (in 1962) an electrical circuit corresponding to FitzHugh equations [NAY62].

In this chapter, we first describe the 2D reduction of the HH equations done by FitzHugh. We then introduce the BVP-FHN model, and illustrate its qualitative similarities with the reduced HH model. We then explain how such a simple 2D model is able to account for cellular excitability. A discussion of the (delicate) notion of threshold manifold follows. We then underscore a few properties of the BVP-FHN model in the oscillatory regime[2], and end up the chapter by introducing the form under which we have studied the BVP-FHN equations in this thesis.

[1] Piece-wise linear models also exist which are even simpler, but their vector field is not differentiable.

[2] Throughout the manuscript, the expressions "oscillatory regime" and 'relaxation oscillation regime" should be considered to be equivalent.

2.1 2D reduction of the Hodgkin-Huxley model

FitzHugh's approach is based on the fact that the variables v and m in the HH model have much faster kinetics than the variables h and n. He decided to reduce the HH model to a 2D slow-fast model by replacing each pair of variables by a single one. For the slow variables h and n, FitzHugh noticed that over the course of an AP, $h(t) + n(t) \simeq 0.8$ (their approximately antisymmetrical evolution is apparent in Fig. 1.5, right panel), so that one can, e.g., eliminate h by setting $h = 0.8 - n$ in the equation for the potential v. For the fast variables v and m, one can set $m = m_\infty(v)$ (although this is not what FitzHugh did originally), which is equivalent to assuming that m adapts instantaneously to changes of the potential v. The HH model then reduces to

$$\begin{cases} C_m \dfrac{dv}{dt} = -\bar{g}_{Na} m_\infty^3(v)(0.8 - n)(v - v_{Na}) - \bar{g}_K n^4 (v - v_K) - \bar{g}_L (v - v_L) \\ \dfrac{dn}{dt} = \dfrac{n_\infty(v) - n}{\tau_n(v)} \end{cases} \tag{2.1}$$

An example of an AP (or *suprathreshold* response) in the reduced HH model, as well as an example of a *subthreshold* response, are shown in Fig. 2.1 (compare with Fig. 1.5), and the corresponding trajectories in the phase plane are shown in Fig. 2.2. The fact that the AP trajectory hugs the v-nullcline (the curve defined by $\dot{v} = \frac{dv}{dt} = 0$) in two regions of the phase plane is a consequence of the existence of two time scales in the system, as we explain in the next section.

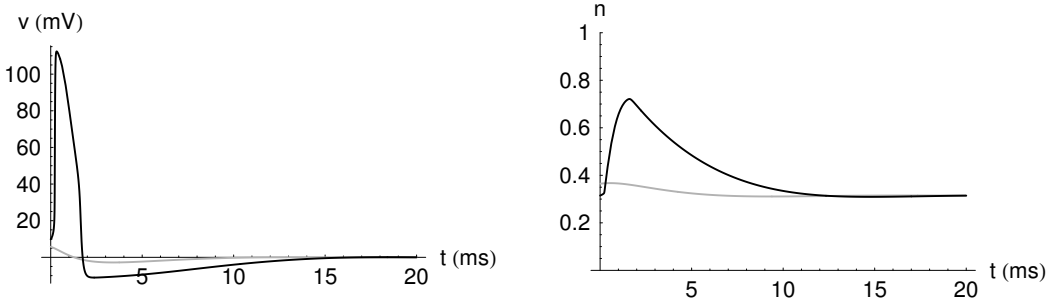

Figure 2.1. *Temporal evolutions obtained in the reduced HH model with the initial conditions* $v(0) = 10mV$, $n(0) = n_\infty(v = 0)$, *giving rise to an AP (in black), and* $v(0) = 6mV$, $n(0) = n_\infty(v = 0) + 0.05$, *giving rise to a subthreshold response (in grey).*

2.2 The BVP-FHN model

The van der Pol model (1.1) can be rewritten using the *Liénard* transformation $w = v - v^3/3 - \dot{v}/\mu$ as

$$\begin{cases} \dfrac{dv}{dt} = \mu(v - \dfrac{v^3}{3} - w) \\ \dfrac{dw}{dt} = \dfrac{v}{\mu} \end{cases} . \tag{2.2}$$

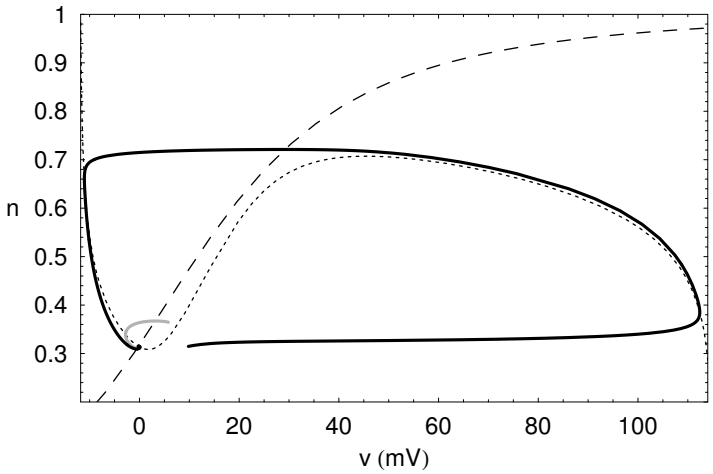

Figure 2.2. *Phase-plane trajectories corresponding to the time evolutions shown in Fig. 2.1 (reduced HH model). The dotted curve is the v-nullcline* $\frac{dv}{dt} = 0$*, the dashed curve is the n-nullcline* $\frac{dn}{dt} = 0$*).*

FitzHugh obtained the BVP model by generalizing these equations to:

$$\begin{cases} \dfrac{dv}{dt} = \mu(v - \dfrac{v^3}{3} - w) \\ \dfrac{dw}{dt} = \dfrac{1}{\mu}(v - cw - d) \end{cases} \tag{2.3}$$

with the condition

$$0 < c < 1, \tag{2.4}$$

that guarantees that the model exhibits a single fixed point (equilibrium point). Indeed, the possible fixed points of the system lie at the intersections of the nullclines, which are defined by

$$\begin{cases} \dfrac{dv}{dt} = 0 \\ \dfrac{dw}{dt} = 0 \end{cases} \Leftrightarrow \begin{cases} w = v - \dfrac{v^3}{3} \\ w = \dfrac{v - d}{c} \end{cases}$$

Requiring $0 < c < 1$ guarantees that the slope $1/c$ of the w-nullcline is larger than the maximum positive slope, equal to 1, of the v-nullcline, so that the nullclines intersect only once[3]. The stability of the fixed point (v_{eq}, w_{eq}) is determined via the computation of the Jacobian:

$$J(v_{eq}, w_{eq}) = \begin{pmatrix} \mu(1 - v_{eq}^2) & -\mu \\ \dfrac{1}{\mu} & -\dfrac{c}{\mu} \end{pmatrix}.$$

The fixed point is stable if

$$\begin{cases} \mathrm{tr}(J) < 0 \\ \mathrm{dtm}(J) > 0 \end{cases},$$

[3]The condition $0 < c < 1$ is sufficient, but not necessary, for the nullclines to intersect only once. This condition is however useful a second time in what follows.

that is, if

$$\begin{cases} 1 - v_{eq}^2 < \dfrac{c}{\mu^2} \\ \dfrac{1}{c} > 1 - v_{eq}^2 \end{cases}.$$

The second condition is always satisfied as a consequence of (2.4). The first condition is always satisfied for $1 - v_{eq}^2 < 0$, which corresponds to the fixed point being located on one of the "external branches" of the v-nullcline (the two "knees" of the v-nullcline are located at $v = \pm 1$, see, e.g., Fig. 2.4). Moreover, for $\mu^2 \gg 1$, the first condition is almost equivalent to $1 - v_{eq}^2 < 0$, so that the fixed point is unstable when it is located on the middle branch of the v-nullcline except when it lies very close to one of the two knees.

2.2.1 Excitable regime

An example of a subthreshold response and an example of an AP obtained for parameter values in the excitable regime of the BVP model are shown in Fig. 2.3 (evolutions in time) and Fig. 2.4 (phase-plane trajectories). Comparing these figures with Figs. 2.1 and 2.2 reveals, as announced above, striking qualitative similarities between the excitable BVP model and the reduced HH model, if the variable v in the BVP model is identified with the electrical potential as in the HH model[4].

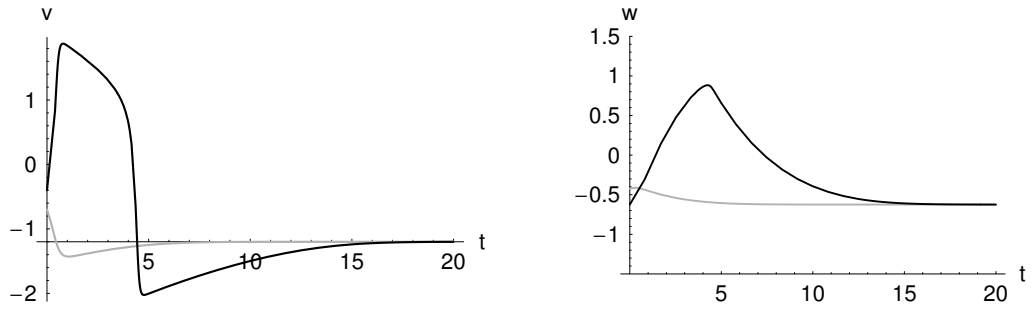

Figure 2.3. *Temporal evolutions in the BVP model for the parameter values* $\mu = 5$, $c = 0.8$, $d = -0.7$. *The black curves (AP) are obtained for the initial conditions* $v(0) = v_{eq} + 0.8$, $w(0) = w_{eq}$ *while the grey curves (subthreshold response) are obtained for* $v(0) = v_{eq} + 0.5$, $w(0) = w_{eq} + 0.2$ *where* $(v_{eq}, w_{eq}) = (-1.12, -0.624)$ *are the coordinates of the stable fixed point.*

Let us now analyse what are the essential features shared by these two models that allow the existence of excitability in two dimensions. We have already underscored in section 1.2 that the presence of two time scales is an essential feature for producing excitability. Let us see what $\mu^2 \gg 1$ implies for the trajectories in the phase plane in the excitable BVP model.

Suppose that the state-point is located at the stable fixed point (v_{eq}, w_{eq}) or close to it, and that a perturbation shifts its location to the point (v_p, w_p), for instance to the point (a) or (b) in Fig. 2.4. We assume $w_{lk} < w_p < w_{rk}$, where w_{lk} and w_{rk} are the ordinates respectively of the left and right knees of the v-nullcline ($w_{lk} = -2/3$ and

[4]In Fig. 2.4, the fixed point is located on the left branch of the v-nullcline. The BVP model is also excitable when the fixed point is located on the right branch, but then the potential v decreases, instead of increasing, during an excitation, which is not physiologically relevant.

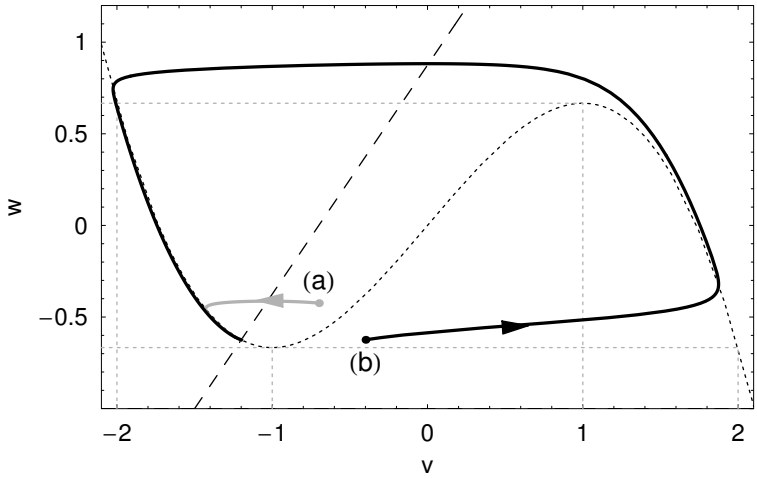

Figure 2.4. *Phase-plane trajectories corresponding to the temporal evolutions shown in Fig. 2.3 (BVP model). The dotted black curve is the v-nullcline* $\frac{dv}{dt} = 0$*, the dashed curve is the w-nullcline* $\frac{dw}{dt} = 0$*. The dotted grey lines highlight the coordinates of the two knees of the v-nullcline, as well as of the two points which have the same ordinate as the two knees on the opposite branch of the v-nullcline.*

$w_{rk} = 2/3$). Because $\mu^2 \gg 1$, we can make the approximation $\dot{w} = 0$ as long as the state-point is not too close to the v-nullcline, which is the case for the initial conditions (a) and (b) in Fig. 2.4. Then, (2.3) reduces to equation (the "fast subsystem", *cf.* Appendix A):

$$\frac{dv}{dt} = \mu(v - \frac{v^3}{3} - w_p).$$

Since $w_{lk} < w_p < w_{rk}$, this equation possesses three fixed points (the three intersections of the v-nullcline with the horizontal line $w = w_p$). Let us denote these fixed points, from left to right, v_l, v_u and v_r. It is easy to check that the two fixed points v_l and v_r are stable, while the fixed point v_u is unstable and plays the role of a separatrix between the bassins of attraction of the two stable fixed points. Thus, if $v_p < v_u$, v heads left towards v_l, while if $v_p > v_u$, v heads right towards v_r. In the fast subsystem, this is the end of the story. In the full system (2.3) however, after the initial, approximately horizontal, trajectory towards the left or right branch of the v-nullcline, it becomes incorrect to neglect $\dot{w}$ in comparison with $\dot{v}$ since the state-point is close to the v-nullcline.

If $v_p < v_u$ (as at point (a) in Fig. 2.4), the state-point is at that moment close to the left branch, where $\dot{w} < 0$, so that it starts moving downward. The evolution takes place very close to the left branch since each time the state-point gets away from it, the fast dynamics takes over again and brings the state-point back in the vicinity of the left branch. The motion along the left branch is very slow compared to the motion towards it since it is determined by $\dot{w}$ ($\dot{v}$ being zero), which is small. The motion along the left branch stops when the state-point reaches the stable fixed point (v_{eq}, w_{eq}).

If $v_p > v_u$ (as at point (b) in Fig. 2.4), the state-point is close to the right branch, and starts moving slowly upward along it since $\dot{w} > 0$ in that region of the phase plane. Because the right branch contains no stable fixed point, the state-point continues upward until it reaches the right knee $(v_{rk}, w_{rk}) = (1, 2/3)$. At this point, the fast subsystem has only one stable fixed point left, the point of ordinate w_{rk} located on the left branch, *i.e.*, $(-2, 2/3)$. Thus, the fast dynamics forces the state-point to head quickly towards the

point $(-2, 2/3)$. When the state-point reaches the left branch, the evolution becomes similar to what happens for $v_p < v_u$; the state-point moves slowly downward along the branch until it hits the stable fixed point, at which point the motion ends.

In conclusion, the middle branch of the v-nullcline plays approximately the role of a threshold between two qualitatively different behaviours; a subthreshold response, in which the state-point comes back rather quickly to the stable fixed point via the left branch, and a suprathreshold response (AP), in which there is first a large excursion away from the fixed point, involving a portion of trajectory along the right branch of the v-nullcline, before the eventual return to the stable fixed point takes place along the left branch. It is also interesting to note that the BVP model accounts for the existence of a refractory period in excitable cells. Indeed, with a perturbation parallel to the v-axis (which is the only meaningful type of perturbation from a physiological point of view), it is impossible to elicit a second AP when the state-point lies on the quasi-horizontal higher portion of the trajectory (there is *absolute refractoriness* in that region), and, when the state-point is on the left branch, it is more difficult to elicit a second AP for an ordinate close to that of the right knee than for an ordinate close to that of the fixed point (there is *relative refractoriness* in that region).

What makes the excitable behaviour possible in the BVP model is, in addition to the existence of two time scales in the system, the fact that the fast variable v possesses a N-shaped nullcline, which implies that the equation for v exhibits bistability in a bounded range of w values, while it exhibits a single stable solution outside this range. In addition, the w-nullcline is such that it intersects the v-nullcline only once, and that $\dot{w}$ has appropriate opposite signs on the two external branches of the v-nullcline. The simplest differentiable function that has a N-shape is a cubic polynomial, and the simplest differentiable function that yields the required properties for the w-nullcline is a straight line. That is why the BVP model is the simplest smooth differential model of excitability that can be constructed.

2.2.2 Threshold manifold

We have mentioned above that the middle branch of the v-nullcline can be considered as an approximation to a threshold curve which allows distinguishing between subthreshold and suprathreshold responses. We give in this section some more detail about this. In order to divide the phase plane into two qualitatively different regions, a curve has to be an *invariant manifold*. This means that any trajectory starting on the curve will remain on the curve for all times, and, as a consequence, all the trajectories starting on one side of the invariant curve will remain on the same side for all times. If such an invariant manifold is to play the role of a threshold, it should in addition repel trajectories, since it is expected to provide a qualitative distinction between two types of behaviours. The middle branch of the v-nullcline, which is an invariant manifold repelling trajectories to the left and to the right in the limit $\mu \to \infty$, is not an invariant manifold for finite μ. However, as can be seen from Fig. 2.5 (left panel), for a sufficiently large value of μ, there exists a family of trajectories (*i.e.*, a family of invariant manifolds) which are very close to the middle branch and close to each other, and which clearly repel the neighbouring trajectories to the left and to the right, at least when these trajectories are initiated away from the right knee[5]. This is actually a result from geometric singular

[5]The same is actually true of the left and right branches of the v-nullcline, except that the corresponding families of invariant manifolds *attract* neighbouring trajectories instead of repelling them, *cf.*

perturbation theory (see Appendix A). All of these trajectories play equally well the role of the threshold manifold away from the right knee, so that an arbitrary hypothesis about the behaviour of the threshold away from the middle branch is needed if one wishes to define unequivocally this manifold. For example, one might require that it is the trajectory in the left panel of Fig. 2.5 which takes the largest time to come within a certain distance of the fixed point, or which passes closest to the right knee (in both cases, a metric should be defined to evaluate the distance). No matter which choice is made however, it will remain true that the threshold manifold plays its role in a weaker manner in the vicinity of the right knee than lower in the phase plane. Indeed, the divergence of trajectories fades in the region of the right knee, as was already noticed by FitzHugh [Fit61]. As a consequence, the qualitative difference between subthreshold and suprathreshold responses elicited from equidistant initial conditions will be smaller in the region of the phase plane close to the right knee than lower in the phase plane, as is illustrated in Fig. 2.5. In both panels of that figure, the same distance Δv_0 separates the v coordinates $v(0)$ of the leftmost and rightmost initial conditions (the value of $w(0)$ is the same for all trajectories in a given panel), but the two extreme points give rise to much more different trajectories in the left panel than in the right one. The fading of the divergence of the trajectories from the threshold in the region of the right knee is also apparent through the small number of trajectories in the right panel compared to the number of trajectories in the left panel. Indeed, the trajectories in Fig. 2.5 are computed using the AUTO continuation software [DCF$^+$98], using the same integration time for all trajectories, and using the same, constant, continuation stepsize in both panels. Because AUTO uses the "pseudo-arclength" continuation method (see Chap. 3), in which the continuation stepsize is a distance in the full space of the parameter *plus* state variables (the parameter being here $v(0)$), requiring a constant stepsize guarantees that the successive trajectories will appear quite[6] regularly spaced in the phase plane[7]. Hence, the fact that, given an identical continuation stepsize, much more trajectories are needed in the left panel than in the right panel to span the Δv_0 interval, reflects the fact the trajectories in the left panel vary much more rapidly than those in the right panel as the value of $v(0)$ is varied.

In summary, while determining if a response is subthreshold or suprathreshold is straightforward for most initial conditions in the region of the phase plane just above the left knee[8], because of the strong divergence of the trajectories from the threshold in

Appendix A.

[6]What is constant from one trajectory to the next is actually the value of

$$\Delta s = \int_0^{IT} (x_i(t) - x_{i-1}(t))^{\sim} \dot{x}_i(t)\, dt + (\lambda_i - \lambda_{i-1})\dot{\lambda}_i$$

where x_i denotes the trajectory corresponding to the parameter value λ_i (which is here the value of $v(0)$), $(\dot{x}_i, \dot{\lambda}_i)$ is the tangent to the solution branch, and IT is the integration time (see also Chap. 3).

[7]It would be much more difficult to generate a set of trajectories as nicely spaced as those in the left panel of Fig. 2.5 by direct numerical integration (time-integration of the equations as an initial value problem). In fact, it might even be impossible because it might require using values of $v(0)$ that are separated by a distance smaller than what double numerical precision allows (given the extreme sensitivity to initial conditions in that region of the phase plane). This problem does not arise with AUTO precisely because the continuation step is taken in the full parameter-plus-state-variable space, not simply in the parameter ($v(0)$) space. A similar application of pseudo-arclength continuation is described in Sec. 6.2.2.1.

[8]Again, one should realize that the majority of the trajectories shown in the left panel of Fig. 2.5 are typically missed by direct numerical integration, and that only the outmost, unambiguously subthreshold

that region, it is no longer the case for initial conditions close to the right knee, and a precise knowledge of how the threshold extends in that region (requiring an arbitrary assumption) is needed to classify the trajectories. We will come back on this observation in Chap. 5 since it allows understanding some characteristics of the bifurcation diagrams of the periodically forced FHN model.

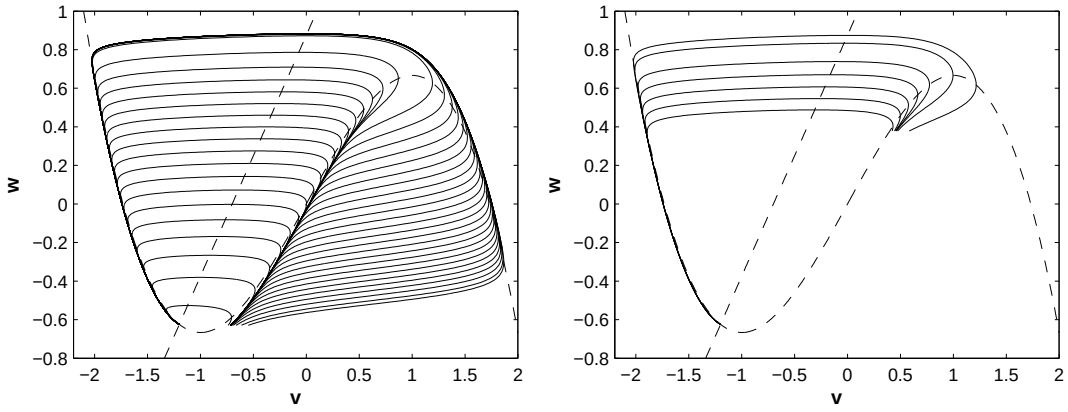

Figure 2.5. *Trajectories obtained by continuation with AUTO for the BVP-FHN model* (2.3) *with* $\mu = 5$, $c = 0.8$, *and* $d = -0.7$. *The continuation parameter is the* v *coordinate* $v(0)$ *of the initial condition* $(v(0), w(0))$, *the value of* $w(0)$ *being fixed to* $w(0) = -0.6293$ *in the left panel and to* $w(0) = 0.3787$ *in the right panel. In both panels, the leftmost and rightmost initial conditions are distant of* $\Delta v_0 = 0.25$, *and the integration time is set to* $IT = 50$.

2.2.3 Oscillatory regime

From the reasoning in Sec. 2.2.1, it is not difficult to understand that, for $\mu^2 \gg 1$, the BVP model possesses a limit cycle for the parameter values such that the fixed point of (2.3) is located on the middle branch of the v-nullcline. Indeed, in that case, nothing prevents the state-point from following the left branch all the way down to the left knee, at which point it is forced to jump to the right branch. Since there is no fixed point on the right branch either, the same behaviour (except that it is oriented upward) is observed on the right branch, and the motion never ends.

Because $\mu^2 \gg 1$, the time spent outside of the v-nullcline is almost negligible and the period of the relaxation oscillation T_0 is well approximated by the time spent on the two external branches of the v-nullcline:

$$T_0 \simeq \left(\int_{t_{l1}}^{t_{l2}} + \int_{t_{r1}}^{t_{r2}} \right) dt$$

where t_{l1} (resp. t_{r1}) is the time at which the state-point reaches the left (resp. right) branch and t_{l2} (resp. t_{r2}) the time at which the state-point leaves the left (resp. right) branch, so that

$$T_0 \simeq \left(\int_{-2}^{-1} + \int_{2}^{1} \right) \frac{1}{\dot{v}} \, dv$$

since the state-point is assumed to leave a given branch when it reaches the corresponding knee, and that its trajectory towards the opposite branch is assumed to be horizontal (see

or suprathreshold, trajectories would in general be encountered.

the dotted grey lines in Fig. 2.4). On the v-nullcline, $w = v - v^3/3$, so that $\dot{w} = (1-v^2)\dot{v}$ and

$$T_0 \simeq \mu \left(\int_{-2}^{-1} + \int_{2}^{1} \right) \frac{(1-v^2)}{(1-c)v + c\frac{v^3}{3} - d}\, dv.$$

In the case of the VDP oscillator ($c = d = 0$), this gives

$$T_0 \simeq 2\mu \left[\ln v - \frac{v^2}{2} \right]_2^1 dv = \mu(3 - \ln 4) \simeq 1.614\mu.$$

In the excitable case, where the fixed point is located on the left branch of the v-nullcline, the threshold manifold is located on the right of the middle branch of the v-nullcline, and the divergence of trajectories from the threshold fades in the vicinity of the right knee (Fig. 2.5, left panel). Figure 2.6 shows that in the oscillatory case, where the fixed point is located on the middle branch of the v-nullcline, the threshold manifold is located on the right of the middle branch above the fixed point, and on its left below the fixed point. In addition, the divergence of trajectories from the threshold curve fades in the vicinity of both knees.

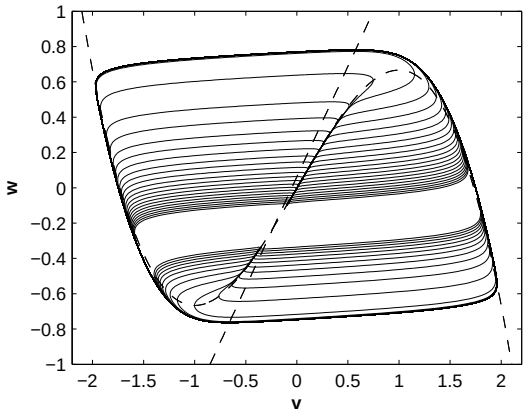

Figure 2.6. *Trajectories obtained from two continuation runs with AUTO for the BVP-FHN model* (2.3) *with* $\mu = 5$, $c = 0.8$, *and* $d = -0.05$ *(oscillatory regime). As in Fig. 2.5, the initial conditions are chosen close to the middle branch of the* v*-nullcline, and the continuation parameter is the* v *coordinate* $v(0)$ *of the initial condition. Two values of the* w *coordinate* $w(0)$ *are considered in turn. The lack of trajectories in the vicinity of the fixed point reflects the difficulty of performing the continuation with initial conditions very close to the fixed point, due to the slowness of the dynamics in that region.*

2.3 The BVP-FHN model studied in this thesis

In this work, we use the BVP-FHN model under the following form:

$$\begin{cases} \dfrac{dv}{dt} = Av(1-v)(v-v_s) - w \\ \dfrac{dw}{dt} = \varepsilon(v - cw - d) \end{cases}, \tag{2.5}$$

where $A = 1$, $v_s = 0.2$, and $c = 0.4$. It has the property that the fixed point is located at the origin, and is stable, when $d = 0$, which is the value of d we have used to study

the excitable case. We switched to $d = 0.2$ for studying the oscillatory case, which corresponds to having an unstable fixed point at $(v, w) = (0.2, 0)$ surrounded by a stable limit cycle of period $T_0 = 165.191$. The left panel of Fig. 2.7 compares the temporal evolution of the potential v for $d = 0$ to that for $d = 0.2$ over a time interval equal to $2T_0$, and with ε set to 0.005 (one of the two values of ε we have used in this work). One can see that the AP duration is of the same order of magnitude in both cases. The right panel of Fig. 2.7 shows the corresponding trajectories in the phase plane.

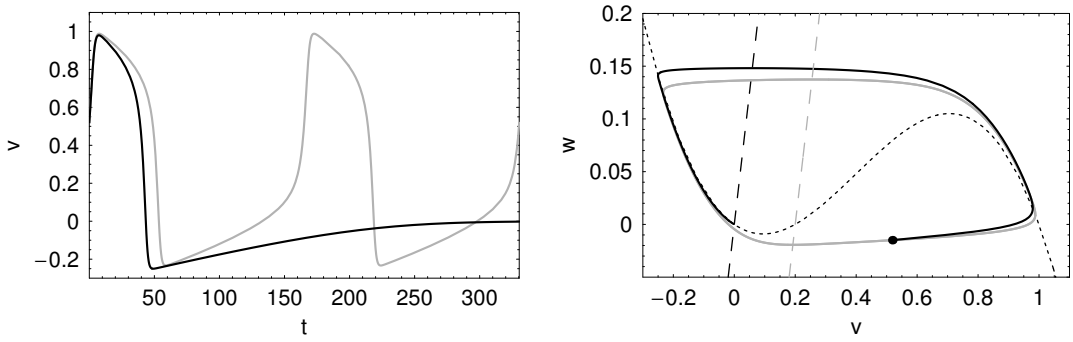

Figure 2.7. *Left: Temporal evolution of the potential v in the FHN model* (2.5) *with $\varepsilon = 0.005$ for $d = 0$ (excitable case, black curve) and $d = 0.2$ (oscillatory case, grey curve). The time interval is $[0, 2T_0]$ and the initial conditions are identical; $v(0) = 0.518559$ and $w(0) = -0.0149507$ (black dot in the right panel). These initial conditions correspond to a point on the limit cycle for $d = 0.2$. Right: Trajectories in the phase plane corresponding to the temporal evolutions shown in the left panel. The dotted curve is the v-nullcline, the dashed black curve is the w-nullcline for $d = 0$, and the dashed grey curve is the w-nullcline for $d = 0.2$.*

Chapter 3

Continuation methods

Je cherche un souffle, un son,
Une étincelle et sa continuation.

G. Roussel (2003)

In nonlinear dynamics, one is often interested in the evolution of asymptotic solutions as a parameter is varied. This information is then summarized in a *bifurcation diagram*, which is a plot giving the value of an (arbitrary) quantity identifying the solutions of interest as a function of the parameter value. It contains *bifurcation points*, which are points at which some of the solutions change stability, are born, or disappear. Numerical methods are generally needed to build such bifurcation diagrams because nonlinear systems usually do not admit closed-form solutions. Among these numerical methods, continuation is a favored tool because, in contrast with time integration of the equations as an initial value problem (which, in the following, we refer to as "direct numerical integration" for short), it allows following asymptotic solutions beyond the parameter value at which they become unstable. The knowledge of the unstable portions of solution branches is important because it reveals the structure of the bifurcation diagram (whether, and how, the different stable solutions are connected), and this structure constrains how the bifurcation diagram can evolve following the variation of a second parameter. Moreover, continuation can sometimes be computationally more efficient than direct numerical integration because it does not require integrating the equations until all transients have decayed. Finally, continuation, in its "pseudo-arclength" implementation (see Sec. 3.4) can allow the computation of solutions which cannot be obtained easily by direct numerical integration because they vary extremely rapidly as the parameter is varied[1].

In the following, we give a summary of the principles of continuation which are in relation to our work, using [Doe00, BCD$^+$02] as main sources. We give however very little detail about the practical implementation and the numerical cost of the different procedures, and we refer for instance to [Sey88, DKK91a, DKK91b] for more information.

[1]This has nothing to do with stability. In fact, the notion of stability may even not be defined for the solutions in question, see, e.g., the application in Sec. 6.2.2.1.

Several continuation packages are available on the web, with different types of applications (see the list on `http://www.dynamicalsystems.org/sw/sw/`). The best known ones for the application to ODE are AUTO [DCF$^+$98] and MATCONT [DGK03]. In this work, we have used AUTO, which is very versatile. In particular, it allows the continuation of solutions of very general boundary-value problems, and this is the framework in which we have studied our periodically forced system, as we explain in Sec. 3.9.2. Moreover, the source code is freely available, so that we could make the few modifications of the original subroutines that were necessary to study bifurcations of periodic solutions in the context of general boundary-value problems (see again Sec. 3.9.2).

3.1 Fixed points and numerical root finding

Consider the system of ordinary differential equations (ODE)

$$\dot{x} = f(x, \lambda) \tag{3.1}$$

where $x \in \mathbb{R}^n$ is the vector of variables, $\lambda \in \mathbb{R}$ is the parameter, and $f : \mathbb{R}^{n+1} \to \mathbb{R}^n$ is the vector field.

The fixed points of the system obey

$$f(x, \lambda) = 0. \tag{3.2}$$

Hence, for a given value of λ, any fixed point of (3.1), independently of its stability, can be found by solving a system of algebraic equations, whereas time integration of (3.1) until transients have decayed can only lead to a stable fixed point. However, because (3.2) is usually a nonlinear system of equations, a numerical root finding method must be used. The most famous one is probably the Newton-Raphson method. It relies on the Taylor expansion of f as a function of x:

$$f(x^{(i)} + \Delta x^{(i)}, \lambda) = f(x^{(i)}, \lambda) + f_x(x^{(i)}, \lambda)\, \Delta x^{(i)} + \mathcal{O}\left(\Delta x^{(i)} \cdot \Delta x^{(i)}\right)$$

where $f_x(x^{(i)}, \lambda)$ is the Jacobian matrix of f evaluated at $x = x^{(i)}$, and $x^{(i)}$ is the ith approximation of the solution in the iteration procedure. Neglecting terms of order $\Delta x \cdot \Delta x$ and higher, and requiring $f(x^{(i)} + \Delta x^{(i)}, \lambda) = 0$, gives a set of linear equations for the vector of corrections $\Delta x^{(i)}$ which makes $x^{(i+1)}$ closer to a zero of f than $x^{(i)}$:

$$\begin{aligned} &f_x(x^{(i)}, \lambda)\, \Delta x^{(i)} = -f(x^{(i)}, \lambda), \\ &x^{(i+1)} = x^{(i)} + \Delta x^{(i)}. \end{aligned} \qquad i = 0, 1, 2, ...$$

The process is iterated from the first estimate $x^{(0)}$ of the solution until convergence. However, for the iterative method to converge (and this is true no matter the iterative method used to solve the nonlinear set of equations, not only for the Newton-Raphson method), it is crucial that $x^{(0)}$ is a good first guess of the solution looked for. In particular, if f has multiple zeros for a given value of λ (*i.e.*, if (3.1) has multiple fixed points for a given value of λ), the iterative procedure must be run for each of these zeros, with each time a good first guess of the zero looked for. Moreover, one can never be certain that all the zeros of f have been found – this is not a limitation of the numerical method, but is an inherent property of nonlinear systems. Assuming that a zero of f has been found for a given value of λ, however, the following results tell us when, and how, the evolution of this zero as λ is varied can be followed.

3.2 Existence and uniqueness of solution branches

Let $X \equiv (x, \lambda)$. Then (3.2) can be written

$$f(X) = 0. \tag{3.3}$$

A solution $X_0 \equiv (x_0, \lambda_0)$ of (3.3) is called a *regular solution* if the Jacobian matrix $f_X^0 \equiv f_X(X_0)$ has maximal rank, *i.e.*, if $\mathrm{Rank}(f_X^0) = n$. This means that the $n \times (n+1)$ matrix $f_X^0 \equiv (f_x^0 | f_\lambda^0)$ has n linearly independent rows or, equivalently, has n (out of $n+1$) linearly independent columns. The following important theorem applies to regular solutions.

If $X_0 \equiv (x_0, \lambda_0)$ is a regular solution of (3.3), then, near X_0, there exists a unique one-dimensional continuum of solutions $X(s)$ with $X(0) = X_0$. Such a continuum of solutions is referred to as a *solution branch*.

This results can be understood as follows. If $\mathrm{Rank}(f_X^0) = n$, then either the $n \times n$ Jacobian matrix f_x^0 is nonsingular, and by the implicit function theorem the solution is locally a function of λ, or else one can interchange columns in f_X^0 to see that the solution can locally be parametrized by one of the components of x. In the second case, the solution branch exhibits a vertical tangent[2] at X_0 in the bifurcation diagram (where λ is assumed to be plotted along the horizontal axis). An example of such a point is a *simple fold*[3], or *limit point*, or *turning point*, at which the solution branch makes a "U-turn"[4]. Note that the above result, in that it makes use of the implicit function theorem, relies on the function f being sufficiently smooth (see, e.g., [Doe97]).

3.3 Parameter continuation

The above result implies that if (x_0, λ_0) is a regular point of the solution branch $f(x, \lambda) = 0$ such that f_x^0 is nonsingular, then, for $\Delta\lambda_0$ sufficiently small, there exists a unique x_1 such that

$$f(x_1, \lambda_1) = 0, \tag{3.4}$$

where $\lambda_1 = \lambda_0 + \Delta\lambda_0$. The point x_0 can be used as a first estimate of x_1. A better first estimate, if the tangent vector $\dot{x}_0 = \frac{dx}{d\lambda}\big|_{\lambda_0}$ is also known, is the "tangent predictor":

$$x_1^{(0)} = x_0 + \Delta\lambda_0 \, \dot{x}_0.$$

Solving (3.4) with $\lambda_1 = \lambda_0 + \Delta\lambda_0$ is known as *parameter continuation*, because the next point (x_1, λ_1) along the solution branch is searched as the point which is at a parameter distance $\Delta\lambda_0$ from the current point, i.e., λ_1 is fixed (*cf.* Fig. 3.1). The Newton-Raphson method applied to solving (3.4) writes:

$$\begin{aligned} &f_x(x_1^{(i)}, \lambda_1)\, \Delta x_1^{(i)} = -f(x_1^{(i)}, \lambda_1) \\ &x_1^{(i+1)} = x_1^{(i)} + \Delta x_1^{(i)} \end{aligned} \qquad i = 0, 1, 2, ... \tag{3.5}$$

[2] Assuming that the solutions are represented in the bifurcation diagram by a scalar quantity – a more general statement would be that the tangent to the solution branch is contained in an hyperplane orthogonal to the λ-axis.

[3] Folds are also saddle-node bifurcations for (3.1), but the terminology "fold" is more general in that it refers to a geometrical property of the branch, which is independent of the fact that the solutions of (3.3) represent fixed points of an ODE or not.

[4] An inflection point of the solution branch is another example of a regular point at which the branch exhibits a vertical tangent.

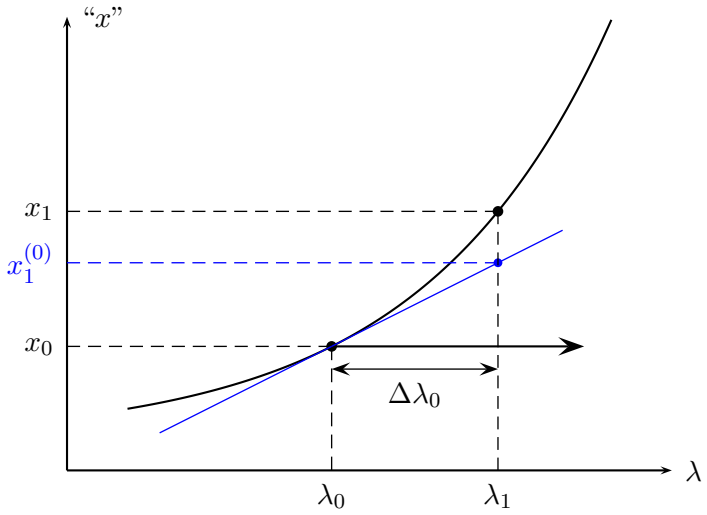

Figure 3.1. *Illustration of the parameter continuation method. The arrow indicates the continuation direction. The blue dot represents the tangent predictor.*

Upon convergence, the new tangent vector $\dot{x}_1$, which will be used to construct the first guess $x_2^{(0)}$ of x_2 such that $f(x_2, \lambda_2) = 0$, is obtained by solving

$$f_x(x_1, \lambda_1)\, \dot{x}_1 = -f_\lambda(x_1, \lambda_1).$$

This system of equations follows from differentiating $f(x(\lambda), \lambda) = 0$ with respect to λ at $\lambda = \lambda_1$.

3.4 Pseudo-arclength continuation

The parameter continuation method described above fails at folds. Here is an intuitive explanation why, and why the pseudo-arclength continuation method described below works [Sey88]. Imagine a bead threaded along the solution branch, with a string attached to the bead at one end and free to be pulled at the other end. Parameter continuation consists in trying to make the bead progress along the branch by pulling the string in the direction of the parameter-axis, while pseudo-arclength continuation consists in doing the same by pulling the string in the direction tangent to the branch. It is clear that the first method will fail at folds while the second one will succeed. Let us now give the mathematical description of the pseudo-arclength continuation method.

The arclength s along the curve $f(x, \lambda) = 0$ is defined by $ds^2 = dx^\sim dx + d\lambda^2$, where $dx^\sim$ denotes the transpose of dx. Suppose we have a solution (x_0, λ_0) of $f(x, \lambda) = 0$, as well as the normalized tangent vector $(\dot{x}_0, \dot{\lambda}_0)$. *Pseudo-arclength continuation* consists in solving the equations:

$$f(x_1, \lambda_1) = 0, \tag{3.6a}$$

$$(x_1 - x_0)^\sim \dot{x}_0 + (\lambda_1 - \lambda_0)\dot{\lambda}_0 - \Delta s_0 = 0. \tag{3.6b}$$

Hence, *both* x_1 and λ_1 are unknowns (Δs_0, instead of $\Delta\lambda_0$ as above, is the fixed quantity for a given continuation step). One looks for the point (x_1, λ_1) along the solution branch

which is located in an hyperplane that is at a distance Δs_0 from (x_0, λ_0) and that is perpendicular to the tangent vector $(\dot{x}_0, \dot{\lambda}_0)$ (see Fig. 3.2)[5].

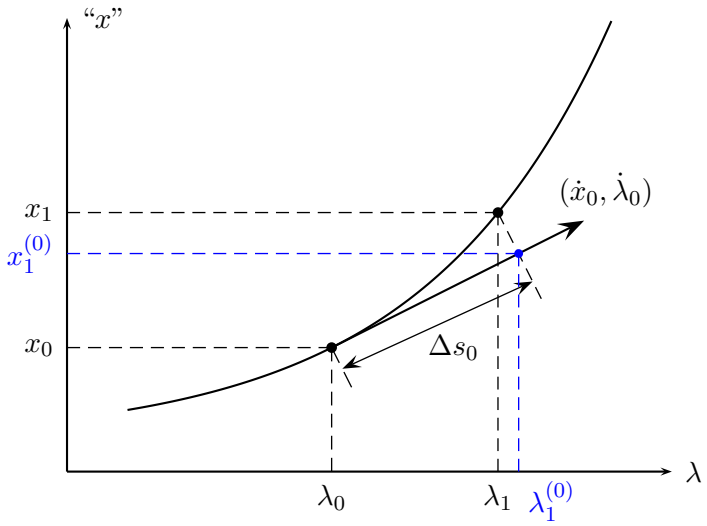

Figure 3.2. *Illustration of the pseudo-arclength continuation method. The arrow indicates the continuation direction. The blue dot represents the tangent predictor.*

The Newton-Raphson method applied to (3.6) writes:

$$\begin{pmatrix} f_x(x_1^{(i)}, \lambda_1^{(i)}) & f_\lambda(x_1^{(i)}, \lambda_1^{(i)}) \\ \dot{x}_0^\sim & \dot{\lambda}_0 \end{pmatrix} \begin{pmatrix} \Delta x_1^{(i)} \\ \Delta \lambda_1^{(i)} \end{pmatrix} = - \begin{pmatrix} f(x_1^{(i)}, \lambda_1^{(i)}) \\ (x_1^{(i)} - x_0)^\sim \dot{x}_0 + (\lambda_1^{(i)} - \lambda_0)\dot{\lambda}_0 - \Delta s_0 \end{pmatrix}$$
$$x_1^{(i+1)} = x_1^{(i)} + \Delta x_1^{(i)}$$
$$\lambda_1^{(i+1)} = \lambda_1^{(i)} + \Delta \lambda_1^{(i)} \tag{3.7}$$

and the tangent predictor for the first guess is given by:

$$x_1^{(0)} = x_0 + \Delta s_0 \, \dot{x}_0,$$
$$\lambda_1^{(0)} = \lambda_0 + \Delta s_0 \, \dot{\lambda}_0.$$

Upon convergence, the next tangent vector is computed from:

$$\begin{pmatrix} f_x(x_1, \lambda_1) & f_\lambda(x_1, \lambda_1) \\ \dot{x}_0^\sim & \dot{\lambda}_0 \end{pmatrix} \begin{pmatrix} \dot{x}_1 \\ \dot{\lambda}_1 \end{pmatrix} = \begin{pmatrix} 0 \\ 1 \end{pmatrix}. \tag{3.8}$$

The normalization equation $\dot{x}_0^\sim \dot{x}_1 + \dot{\lambda}_0 \dot{\lambda}_1 = 1$ ensures that the orientation of the branch is preserved if Δs_0 is sufficiently small. After solving (3.8), the new tangent vector must be rescaled to have unit length: $||\dot{x}_1||^2 + \dot{\lambda}_1^2 = 1$.

Pseudo-arclength continuation is the continuation method used in AUTO. Geometrically, it is the most natural continuation method, since the continuation direction is adapted at each step as to always be tangent to the solution branch[6].

[5] In "genuine" arclength continuation, Δs_0 would represent the distance between (x_0, λ_0) and (x_1, λ_1), and (3.6b) would be replaced by $(x_1 - x_0)^\sim (x_1 - x_0) + (\lambda_1 - \lambda_0)^2 - \Delta s_0^2 = 0$. The pseudo-arclength constrain (3.6b) has the advantage of being linear.

[6] Actually, pseudo-arclength continuation is not the only continuation method in which the continuation direction is tangent to the solution branch; in particular, the Moore-Penrose continuation method used in MATCONT has also this property [DGK03].

It is interesting to mention that because (3.3) can represent many other things than the annulation of a vector field, continuation methods can be used for many other purposes than computing branches of fixed points in ODE. It is applied below to the computation of periodic solution branches in ODE, but it can also be used in problems where the notion of stability is not even defined. Pseudo-arclength continuation is especially appropriate in any problem of type (3.3) where the solution branch exhibits an almost vertical portion as a function of the parameter. Such an application of pseudo-arclength continuation is described in Sec. 6.2.2.1.

3.5 Branch points and branch switching

A *branch point* is a point X_0 at which $\text{Rank}(f_X^0) = n - 1$ and through which two solution branches[7] with two distinct tangents pass. The detection of branch points is carried out in AUTO in the way described in the next section. The exact computation of the tangent vector of the bifurcating branch requires the evaluation of f_{XX}^0 (see, e.g., [Doe00]). However, an approximation of this tangent vector, which does not require the computation of second derivatives, can be obtained as follows. Let $\dot{X}_0$ be the tangent vector of the current branch[8]. The tangent vector of the bifurcating branch can be approximated by the null vector[9] of f_X^0 which satisfies

$$\phi_2 \perp \phi_1,$$

where $\phi_1 = \dot{X}_0$.

3.6 Monitoring stability and detecting bifurcations

The stability of a fixed point x_0 is determined by the eigenvalues of the Jacobian f_x^0. If all the eigenvalues have negative real parts, then the fixed point is stable, while if one eigenvalue has positive real part, then the fixed point is unstable (see, e.g., [Sey88]). Bifurcation points are characterized by the existence of at least one eigenvalue with zero real part.

The detection of bifurcations is done through the evaluation of scalar test functions $q(s)$, which become zero at the corresponding bifurcation. One obvious such test function is the real part of the eigenvalue closest to the imaginary axis at the current point, which is expected to change sign at a bifurcation. This test function is used in AUTO (together with the monitoring of the number of eigenvalues in the left half-plane) for the detection of Hopf bifurcations. However, the detection of folds is done via monitoring the test

[7] It is important to realize that the two branches contain solutions of the *same* one-parameter family of equations (3.3); in particular, a Hopf point along a fixed-point branch of an ODE is *not* a branch point since there is only one fixed-point branch passing through a generic Hopf bifurcation, the second branch being a periodic-solution branch. Examples of branch points are transcritical and pitchfork bifurcations. Branch points are non-generic in one-parameter families of solutions, however there may be physical reasons (e.g., symmetries in the underlying physical system) for which branch points are nevertheless present in a given model.

[8] This vector is estimated by "stepping over" X_0 in the continuation procedure, since (3.8) is expected to have a unique solution for X close to X_0. This usually does not require any additional computation since it is unlikely to hit exactly the branch point during the continuation.

[9] A null vector of a matrix M is a vector belonging to the nullspace of M, *i.e.*, a vector v such that $Mv = 0$.

function $q(s) = \dot{\lambda}(s)$, of which folds are simple zeroes. We believe that the detection of folds is implemented in this way because folds are geometrical properties of solution branches, which can occur also in problems where the notion of stability is not defined, so that it is more general to look for folds via $q(s) = \dot{\lambda}(s)$ rather than as saddle-node bifurcations of a branch of fixed points – the same test function can be used independently of the problem type. Similarly, the occurrence of branch points, independently of the bifurcation they represent, is monitored in AUTO via the computation of the determinant of the Jacobian F_X where

$$F(X;s) = F(x,\lambda;s) = \begin{pmatrix} f(x,\lambda) \\ (x-x_0)^{\sim}\dot{x}_0 + (\lambda-\lambda_0)\dot{\lambda}_0 - s \end{pmatrix},$$

so that

$$F_X^0 = \begin{pmatrix} f_x^0 & f_\lambda^0 \\ \dot{x}_0^{\sim} & \dot{\lambda}_0 \end{pmatrix}$$

(see [DKK91a] for details).

Note that the success of the detection of bifurcations relies on the smallness of the continuation stepsize Δs, since two bifurcations can possibly occur for close values of s.

Once a change of sign of a test function is detected, a secant iteration scheme is used to locate the bifurcation precisely:

$$s^{(i+1)} = s^{(i)} - \frac{s^{(i)} - s^{(i-1)}}{q(s^{(i)}) - q(s^{(i-1)})} q(s^{(i)}).$$

3.7 Two-parameter continuation

Two-parameter continuation consists in computing a branch of bifurcation points (saddle-nodes, Hopf bifurcations,...) in a two-parameter plane (λ, μ). The most straightforward way to do this is to append the test function $q(s)$ defining the bifurcation to the equations to solve, the second parameter μ being included in the pseudo-arclength equation:

$$\begin{aligned} &f(x(s),\lambda(s),\mu(s)) = 0, \\ &q(s) = 0, \\ &(x(s)-x_0)^{\sim}\dot{x}_0 + (\lambda(s)-\lambda_0)\dot{\lambda}_0 + (\mu(s)-\mu_0)\dot{\mu}_0 - \Delta s_0 = 0. \end{aligned} \tag{3.9}$$

The continuation must of course be started from an already computed bifurcation point. System (3.9) is called a *minimally augmented system*, because it only has one extra equation compared to (3.6). However, there might be numerical difficulties in solving such a minimally augmented system, therefore it is usually preferred to solve a *bordered system*, which contains more equations and unknowns than (3.9), but which is easier to handle numerically [BCD$^+$02].

3.8 Starting the continuation

Continuation is not a miracle tool: it can only compute solution branches for which a starting solution is known, or solution branches which are connected to a previously computed branch. There are basically three types of starting solutions: those for which an explicit expression is known, those which are obtained by direct numerical integration,

and those which are obtained by prior continuation with respect to another parameter. This second parameter can either be already present in the equations, or it can introduced specifically for the purpose of the preliminary continuation.

3.9 Periodic solutions

A periodic solution $x(t)$ of (3.1) satisfies

$$x(t+P) = x(t), \quad \forall t \in \mathbb{R}, \tag{3.10}$$

for some $P \in \mathbb{R}$ called the period of the solution.

3.9.1 Autonomous equations

If (3.1) is an autonomous ODE, *i.e.*, if the vector field f does not depend explicitly on time, then (3.10) is equivalent to

$$x(P) = x(0).$$

Hence, any periodic solution of an autonomous ODE, independently of its stability, can be expressed as the solution of a boundary-value problem. Note that, in contrast with the fixed-point case where the solutions searched for are points in an n-dimensional space (Sec. 3.1), here the unknowns are n-dimensional *functions* $x(\cdot)$, defined over the whole real interval $[0, P)$. Because the period P of the solution is usually an unknown of the problem, the boundary-value problem is reformulated as

$$\begin{cases} x'(t) = Pf(x(t), \lambda) \\ x(1) = x(0) \end{cases} \tag{3.11}$$

where the transformation $t \to t/P$ has been performed, so that the interval of periodicity is fixed, with its boundaries located at 0 and 1.

The solution of (3.11) is not uniquely defined because if $x(t)$ is a periodic solution, then so is $x(t+\sigma)$ for any $\sigma \in \mathbb{R}$. A *phase condition* is needed to determine the solution unequivocally. In the context of continuation, the phase condition is usually defined in terms of the previous solution computed along the periodic solution branch. Let $(x_0(\cdot), P_0, \lambda_0)$ be the computed solution, and let $(x_1(\cdot), P_1, \lambda_1)$ be the next solution to be computed. A numerically very suitable phase condition is the following. Let $\tilde{x}(t)$ be a solution with period P_1 at $\lambda = \lambda_1$, so that $\tilde{x}(t+\sigma)$ is also a solution for any σ. Take $x_1(t)$ as the solution $\tilde{x}(t+\hat{\sigma})$ which minimizes

$$D(\sigma) \equiv \int_0^1 ||\tilde{x}(t+\sigma) - x_0(t)||^2 dt$$

(see Fig. 3.3 for an illustration of the effect of this phase condition).

The optimal solution $\tilde{x}(t+\hat{\sigma})$ satisfies $D'(\hat{\sigma}) = 0$, *i.e.*,

$$\int_0^1 (\tilde{x}(t+\hat{\sigma}) - x_0(t))^{\sim} \, \tilde{x}'(t+\hat{\sigma}) \, dt = 0.$$

Writing $x_1(t) \equiv \tilde{x}(t+\hat{\sigma})$ gives

$$\int_0^1 (x_1(t) - x_0(t))^{\sim} \, x_1'(t) \, dt = 0.$$

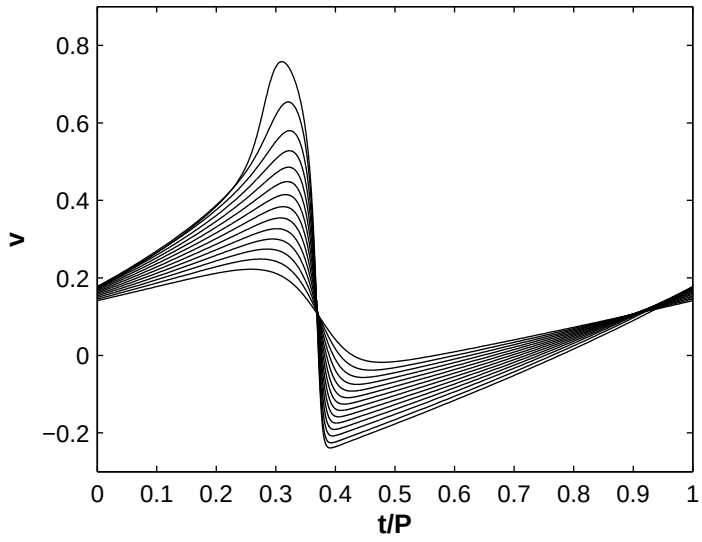

Figure 3.3. *The v component, as a function of the (normalized) time t/P, of a sample of periodic solutions belonging to the left, almost vertical, portion of branch in the bifurcation diagram of Fig. A.1. The phase-plane trajectories corresponding to these time evolutions are shown in the left panel of Fig. A.2. The effect of the phase condition* (3.12) *is to keep the two "peaks" in almost exactly the same place from one solution to the next. This is very convenient for the continuation method since it guarantees that the values of the variables for a given value of t will be a good first estimate of the values of the variables for the same value of t a little further along the solution branch. Indeed, "relaxation" methods for solving boundary-value problems, which are the type of boundary-value methods used in continuation softwares, work by iterating on the values of the variables at each point of a mesh covering the whole interval between the two boundaries.*

Integration by parts, using periodicity, gives

$$\int_0^1 x_1(t)^{\sim} x_0^{'}(t)\, dt = 0. \tag{3.12}$$

This is the (integral) phase condition used in AUTO.

In order to trace out a branch of periodic solutions, a continuation equation must be appended to (3.11) and (3.12). In the context of periodic solutions $x(\cdot)$ defined over the interval $[0, 1)$, the pseudo-arclength equation writes (compare with (3.6b)):

$$\int_0^1 (x_1(t) - x_0(t))^{\sim}\, \dot{x}_0(t)\, dt + (P_1 - P_0)\dot{P}_0 + (\lambda_1 - \lambda_0)\dot{\lambda}_0 - \Delta s_0 = 0. \tag{3.13}$$

Equations (3.11) (where x should be identified with x_1, P with P_1, and λ with λ_1), together with (3.12) and (3.13), define a (generalized) boundary-value problem for the unknowns $x_1(\cdot)$, P_1, and λ_1, which must be solved at each continuation step. The resolution of such a problem requires its discretization, which transforms the boundary-value problem into a nonlinear set of algebraic equations of type (3.3). This set of equations is then solved by a root finding method such as the Newton-Raphson method. The most widely used discretization method for boundary-value problems in ODE is the method of orthogonal collocation with piecewise polynomials (see, e.g., [Doe00]). This is the method used in AUTO.

The stability of a periodic solution $(x_0(\cdot), \lambda_0, P_0)$ is governed by the *Floquet multipliers*, which are the eigenvalues of the *monodromy matrix* (e.g., [Sey88]). The (i,j)th element ($i = 1, \ldots, n$, $j = 1, \ldots, n$) of the monodromy matrix quantifies the effect, on the ith component of $x_0(1)$, of a perturbation of the jth component of $x_0(0)$. A periodic solution always has a Floquet multiplier equal to one, which reflects the fact that perturbing the solution in the direction tangent to the trajectory has a neutral effect. If all other Floquet multipliers lie within the unit circle, then the periodic solution is stable, otherwise it is unstable. In AUTO, the detection of cycle bifurcations involves, as for fixed points, the evaluation of test functions which change sign at the corresponding bifurcation. For period-doubling and torus bifurcations, the test function involves the Floquet multiplier closest to the unit circle[10] (*i.e.*, of modulus closest to 1), while for saddle-node bifurcations, the function $q(s) = \dot{\lambda}(s)$ is again used.

3.9.2 Non-autonomous equations

In non-autonomous ODE, where the vector field depends explicitly on time, it is in general not true that solving the problem

$$\begin{cases} \dot{x}(t) = f(x(t), t, \lambda) \\ x(t+P) = x(t) \quad \forall t \in \mathbb{R} \end{cases} \tag{3.14}$$

is equivalent to solving the problem

$$\begin{cases} \dot{x}(t) = f(x(t), t, \lambda) \\ x(P) = x(0) \end{cases}. \tag{3.15}$$

This is correct if the vector field f is periodic in time, *i.e.*, if $f(x, t+T, \lambda) = f(x, t, \lambda)$, and if $P = MT$ where M is an integer[11]. Indeed, in that case, the evolution of x during the time interval $[iP, (i+1)P)$, $i = 1, 2, \ldots$ is guaranteed to be identical to its evolution during the time interval $[0, P)$ since the vector field repeats identically. In this work, we are interested in non-autonomous ODE of the form (see Chap. 4):

$$\dot{x}(t) = g(x(t), \lambda) + h(t, \lambda), \tag{3.16}$$

where

$$h(t+T, \lambda) = h(t, \lambda),$$

i.e., in periodically forced systems where the periodic forcing appears in an additive fashion only, and is independent of x. In such systems, one has trivially $f(x, t+T, \lambda) = f(x, t, \lambda)$, so that (3.15) can be used to look for periodic solutions of period $P = MT$. Note that the condition $P = MT$ is in fact not a restriction since *all* periodic solutions of (3.16) have a period which is an integer multiple of the forcing period. Indeed, assume $\tilde{x}(t)$ is a periodic solution of (3.16) with period P. Because $\tilde{x}(t)$ verifies the ODE for all times, we have

$$\dot{\tilde{x}}(t) = g(\tilde{x}(t), \lambda) + h(t, \lambda)$$

or, equivalently,

$$\dot{\tilde{x}}(t+P) = g(\tilde{x}(t+P), \lambda) + h(t+P, \lambda).$$

[10] After excluding the one multiplier which is always equal to 1.

[11] We assume that T is the smallest period of f.

Expressing the periodicity of $\tilde{x}(t)$ in the last equation leads to the equality $h(t+P,\lambda) = h(t,\lambda)$, which is correct only if $P = MT$ since h is periodic with period T.

Continuation softwares such as AUTO do not accept non-autonomous vector fields as input. The obvious way around this is to define an additional variable τ which evolves like time, $\dot{\tau} = 1$, and to rewrite the vector field as $f(x(t),\tau(t),\lambda)$. But then the extended ODE no longer admits a periodic solution, and can therefore not be studied within the special toolbox provided by AUTO for periodic solutions, and within which only some concepts of stability specific to periodic solutions are defined. The other option is to manage rewriting the periodic forcing in terms of the *periodic* solutions of an auxiliary autonomous ODE, which is then appended to the vector field for the continuation process. This is rather straightforward to do for sinusoidal forcing (see the demo "frc" in the AUTO manual [DCF+98]), but this is not feasible for all functional forms of forcing, unless a truncated Fourier expansion of the forcing function is used. Many additional differential equations might then be needed to obtain a satisfying representation of the forcing, and this increases unnecessarily the computational effort needed to perform the continuation.

In this work, we opted for the first solution, *i.e.*, we submitted to AUTO the boundary-value problem:

$$\begin{cases} x'(t) = Pf(x(t),\tau(t),\lambda) \\ \tau'(t) = P \\ x(1) = x(0) \\ \tau(0) = 0 \end{cases} \tag{3.17}$$

and made minor modifications to the source code in order to "switch on" the computation of Floquet multipliers for boundary-value problems of type (3.17)[12], and to enable in the same time the detection of period-doubling and torus bifurcations. We also enabled the two-parameter continuation of bifurcations.

Note that, in (3.17), P is not an unknown, as it is in (3.11), but is equal to $P = MT$, where the integer M is fixed prior to the computation of a given solution branch. Hence, it is not included in the pseudo-arclength equation for the continuation. Also, there is no additional phase condition to specify, since the equation $\tau(0) = 0$ plays the role of this phase condition.

To our knowledge, this method for computing the periodic solutions of a periodically forced system has not been used previously in ODE, but a similar method (in that it also makes use of the fact that the period of the periodic solutions in a periodically forced system of type (3.16) must be an integer multiple of the forcing period) has been applied to stroboscopic (Poincaré) maps of periodically forced oscillators (see, e.g., [KSA86]).

[12] It seems indeed reasonable that the notion of the monodromy matrix and Floquet multipliers extends to periodic solutions of periodically forced systems, *i.e.*, to solutions of problems of type (3.17). These solutions have $n+1$ components, with the last component being non-periodic and representing time. Since this $(n+1)$th component is unaffected by perturbations of the other components, all the elements of the $(n+1)$th row in the monodromy matrix are zero, except the last element which is equal to 1 (perturbing time has a neutral effect on time). The existence of a Floquet multiplier always equal to one therefore appears immediate in this type of system.

Chapter 4

Periodically forced slow-fast systems

This chapter provides a common introduction to the following two chapters, in which we present our original contribution to the study of the periodically forced FHN model in its excitable (Chap. 5) and its oscillatory (Chap. 6) regimes. Below, we first motivate the study of a periodically forced slow-fast system from the cardiac point of view, and introduce the "physiological" notion of an $M : N$ rhythm which will be used in the following. We then detail the equations used in the next two chapters, and give graphical examples of $M : N$ rhythms in these equations. We end up the present chapter with a brief "inventory" of the different types of theoretical studies that have been carried out until now on periodically forced slow-fast systems, in order to situate our work among the different approaches that have been taken.

4.1 Cardiac cells

In vivo, cardiac cells can be thought of as being submitted to periodic electrical stimulation via the action of the SA node, the natural pacemaker of the heart. This is of course a simplification, since cardiac cells are actually coupled bidirectionally with their neighbours, but it is a useful first approximation in the aim of understanding cardiac rhythms and arrhythmias. In this spirit, many *in vitro* studies have been carried out where isolated cardiac cells, or small groups of cardiac cells, were submitted to a periodic train of current pulses[1], in order to understand their response under controlled conditions. Part of these studies involved excitable cells (e.g., [DMJ89, GJAM89, HS89, CMJ90, HADJ90, LDD$^+$91, RL95, YSLG97, YJAG99]), while others involved spontaneously beating cells (e.g., [ADV$^+$91, GGS81, GSG90, GS90, GSG88]).

Periodic responses of cardiac cells to periodic electrical stimulation are classified as $M : N$ *rhythms*, where M is the number of regularly timed stimuli before the pattern repeats (so that MT is the period of the rhythm if T is the stimulation period), and N the number of action potentials that the pattern contains. The healthy situation is the $1 : 1$ rhythm, where every stimulus gives rise to the same AP. Frequently encountered pathological patterns which retain a periodic character include: $2 : 2$ rhythms or *alternans*, where there is a beat-to-beat alternation in the morphology of the AP; $2 : 1$ rhythms, where every second AP fails; and $M : M - 1$ or Wenckebach rhythms ($M \geq 3$), where a gradual beat-to-beat increase in the activation time[2] is observed before an AP

[1] By "pulses" we mean stimuli with a duration short compared with the APD.

[2] The *activation time*, or *latency*, is the time needed for an AP to reach maximum upstroke velocity

is skipped (see, e.g., [YJAG99]). In the whole heart, the $M:N$ terminology refers to the state of synchronization of one region of the heart to another; e.g., the number N of beats of the ventricules observed for M beats of the atria.

4.2 The system studied in this thesis

In order to model the periodic injection of an electrical current into a cardiac cell, we submit the FHN model (2.5) to periodic forcing by introducing an extra term in the equation for the potential:

$$\begin{cases} \dfrac{dv}{dt} = v(1-v)(v-0.2) - w + I(t) \\ \dfrac{dw}{dt} = \varepsilon(v - 0.4w - d) \end{cases} . \tag{4.1}$$

We use a train of Gaussian-shaped pulses:

$$I(t) = I_0 \sum_{j=-\infty}^{\infty} \exp\left(-(t-jT)^2/\sigma^2\right), \tag{4.2}$$

where I_0 is the stimulation amplitude and T the stimulation period. The value of σ is chosen as to insure that the stimulus is effectively "on" during a time much shorter than the APD[3]. For $\varepsilon = 0.005$ and $\varepsilon = 0.002$ (the two values of ε used in this work), we have chosen respectively $\sigma = 1$ and $\sigma = 2.5$, in order to have approximately the same ratio between the duration of the stimulus and that of the AP (decreasing ε does indeed lengthen the AP). The infinite sum is truncated for numerical purposes; we keep only the terms which have a noticeable effect on the vector field inside the integration interval at the numerical precision used (double precision). The studies described in Chaps. 5 and 6 are restricted to stimulation periods $T > T_{min} \simeq 10\sigma$, for which the overlap of successive stimuli can be neglected.

Figures 4.1 and 4.2 show examples of 1:1, 4:3, and 2:1 rhythms for the periodically forced FHN model (4.1)–(4.2) with $\varepsilon = 0.005$. In Fig. 4.1, $d = 0$ (excitable regime) and in Fig. 4.2, $d = 0.2$ (oscillatory regime). The main difference between the two regimes is of course that in the excitable case, no AP can occur in the absence of stimulus; the upstroke of an AP always coincides with the occurrence of a stimulus, while in the oscillatory case, there are spontaneous APs (e.g., in the middle right panel of Fig. 4.2, only the second AP is caused by a stimulus, the other ones are spontaneous responses, which are only possibly a bit deformed by the stimulus). One consequence is that $M:M-1$ rhythms are Wenckebach rhythms according to the definition given above only in the excitable regime: indeed, there cannot be a systematic increase in activation time from one beat to the next if APs can occur in the absence of stimulation. Another consequence is that in the oscillatory regime, there can be $M:N$ rhythms with $N > M$ (see bifurcation diagrams in Chap. 6), while this is impossible in the excitable regime.

once it is triggered by the stimulus [YSLG97].

[3]Strictly speaking, the Gaussian function never goes to zero, but it becomes negligible very fast: $I(t) < 10^{-N} I_0$ for $|t| > \sigma\sqrt{N \ln 10}$.

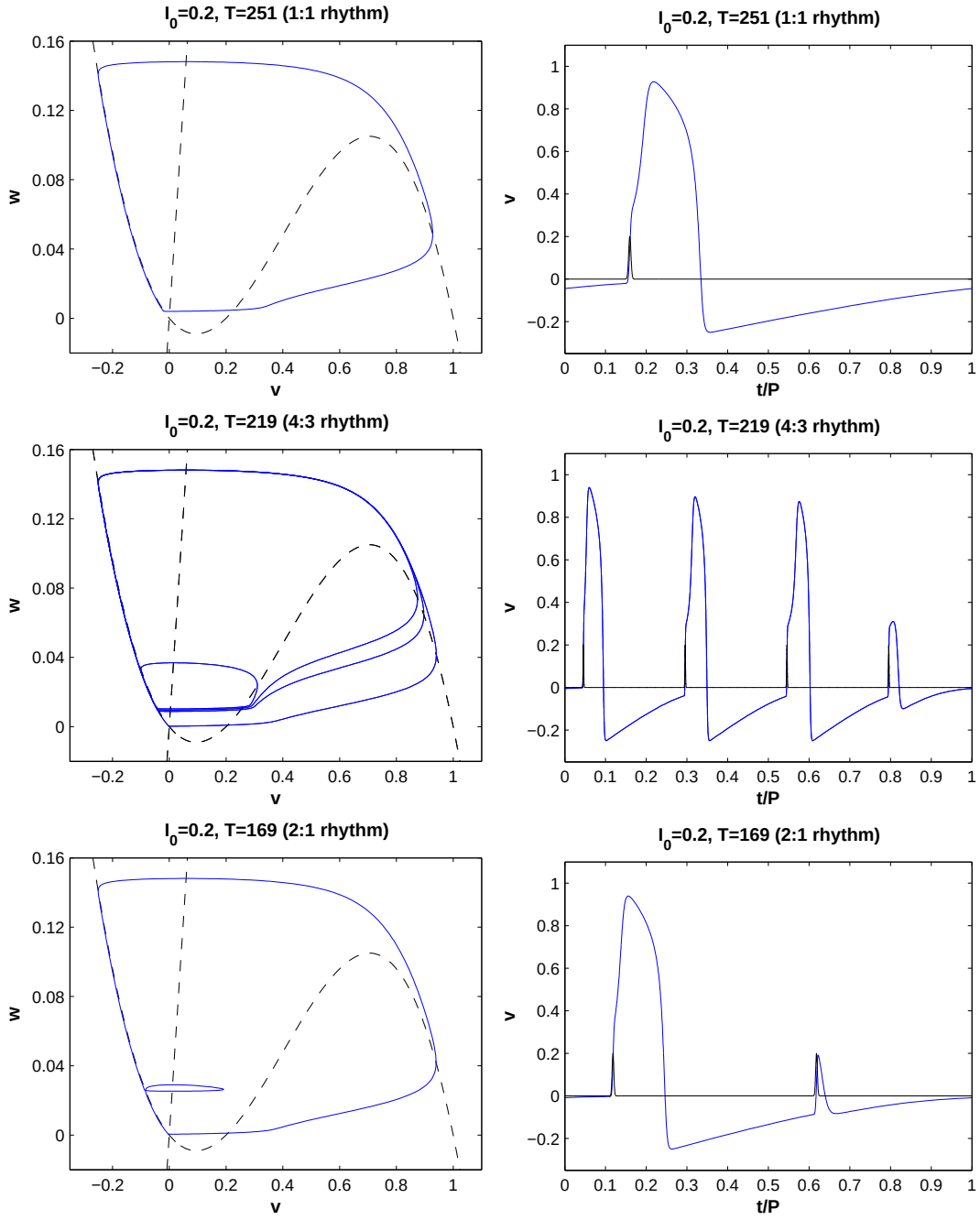

Figure 4.1. *Examples of $M:N$ rhythms in the excitable regime ($d = 0$) for $I_0 = 0.2$. Left: trajectory in the phase plane. The dashed curves are the nullclines. Right: time evolution of the potential over one period of the solution (time has been rescaled by $t \to t/P$ where P is the period of the solution). The black trace is the train of Gaussian-shaped pulses.*

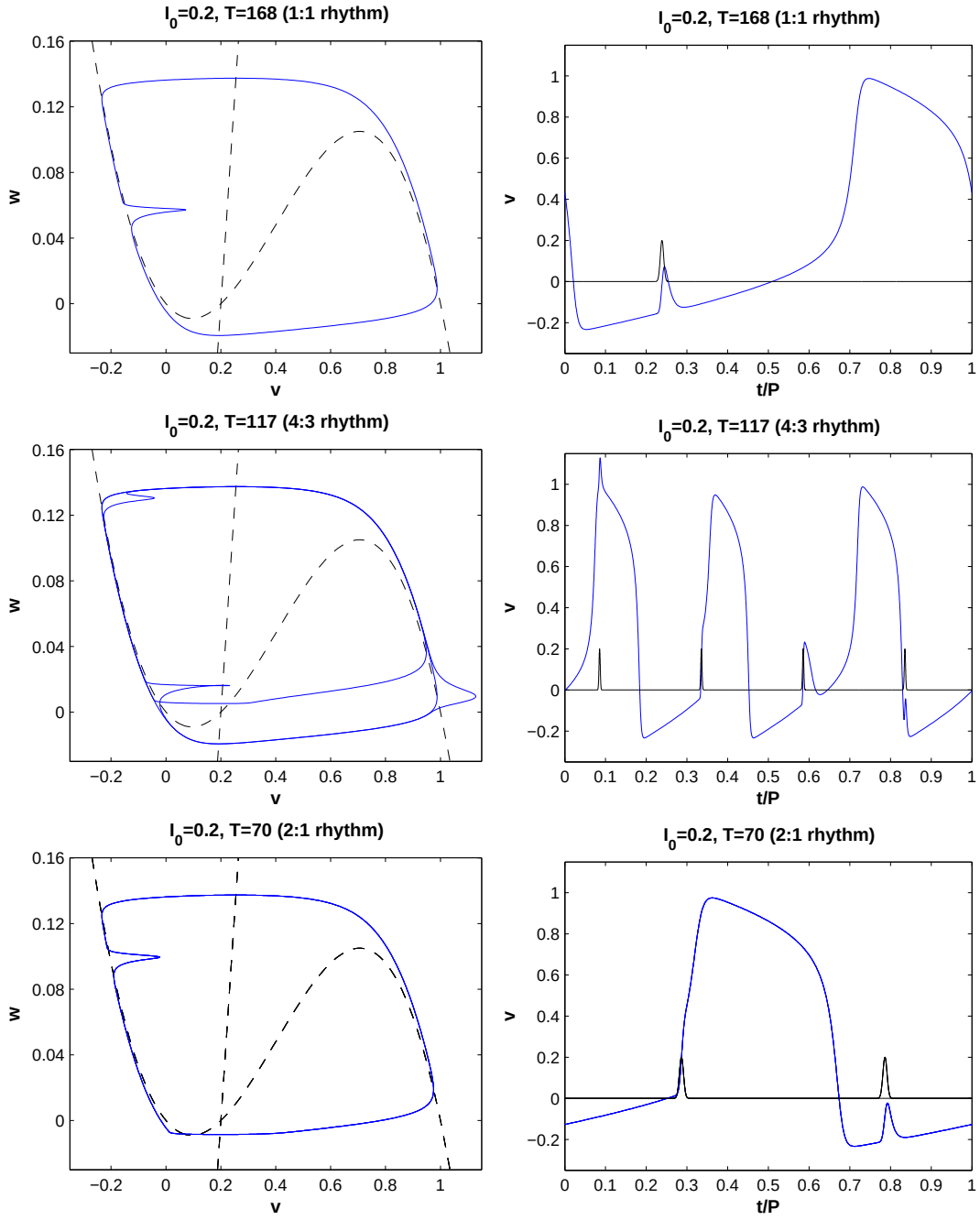

Figure 4.2. *Examples of $M:N$ rhythms in the oscillatory regime ($d = 0.2$) for $I_0 = 0.2$. Left: trajectory in the phase plane. The dashed curves are the nullclines. Right: time evolution of the potential over one period of the solution (time has been rescaled by $t \to t/P$ where P is the period of the solution). The black trace is the train of Gaussian-shaped pulses.*

4.3 $M:N$ rhythms

It is important to stress that the definition of an $M:N$ rhythm given above (which we will sometimes refer to as the "physiological" definition of an $M:N$ rhythm in the following, as it involves the notion of AP) is somewhat loose, because there is no universal definition of an AP. Indeed, in physiology, the AP is defined sometimes in terms of the maximum voltage reached, sometimes in terms of the area under the voltage curve, ..., and there is no general consensus about the value that the quantity used in the definition should overcome to have an AP. This is also true in ODE models of slow-fast systems such as the BVP-FHN model, where to obtain a unequivocal definition of the threshold manifold, one has to make an arbitrary assumption about its behaviour away from the repelling portion of the v-nullcline. There is however at least one category of periodically forced slow-fast systems for which the physiological notion of an $M:N$ rhythm is unequivocal and non-arbitrary, *i.e.*, that of forced relaxation oscillators at small stimulation amplitudes. Indeed, for these systems, the physiological notion of an $M:N$ rhythm coincides with the mathematical notion from the rotation number theory, as we explain in Chap. 6.

Despite the lack of a universal definition of an AP, there are nevertheless many situations, both in physiology and in models of periodically forced slow-fast systems, in which there is no doubt as to whether one is facing an $M:N$ rhythm or an $M:N+1$ rhythm (there is no doubt in this respect, e.g., in Figs. 4.1 and 4.2). And in the situations where the distinction is difficult to make, we believe (as far as ODE models such as the BVP-FHN model are concerned, at least) that there is no point in introducing an arbitrary definition to suppress the ambiguity, since usually, this ambiguity reflects the fact that the difference between an $M:N$ rhythm and an $M:N+1$ rhythm has become intrinsically weak (see, e.g., the discussion on that subject in Sec. 5.1).

4.4 The different theoretical works on the subject

There have been many theoretical and modelling studies on periodically forced slow-fast systems. These studies can be divided into two categories, depending on whether they are carried out on the full original equations (e.g., an ODE or a stroboscopic map of it[4]) or on an approximation of the original model (e.g., a piecewise linear ODE or a one-dimensional (1D) discrete map), for which the numerical computations are easier, and for which one can even occasionally obtain closed-form solutions. Such approximations also often provide easier insight into the system behaviour, because their dimension allows a graphical representation of the system, and/or because they relate quantities more directly related to the physiology/physics than the variables of the original model.

In the first category, one finds mainly studies on the VDP oscillator (e.g.,[FH78, MPL93]; see [Jac90] for a review), and on the BVP-FHN model both in its excitable regime [FGPV88, ADO90, SD92, RTF94, RL88, DS95, KCM$^+$96, YNPS99, GX01, RF06] and in its oscillatory regime [NSD$^+$94, YNPS99, RF06]. These studies use either sinusoidal or pulsatile forcing. Sinusoidal forcing can give rise to behaviours that are qualitatively different from those seen with pulsatile forcing; e.g., with sinusoidal forcing one can have bursting rhythms that one does not see with pulsatile forcing, in which several

[4]In this work, what we call a stroboscopic map or Poincaré map of a periodically forced ODE is a discrete map obtained by sampling the flow at time intervals equal to the forcing period, and the study of which is *equivalent* to the study of the full ODE.

action potentials ride on the crest of each cycle of the sinusoidal input (see, e.g., Fig. 16 of [ADO90]). All the electrophysiological studies referred to in Sec. 4.1 use pulsatile forcing. The effect of sinusoidal forcing on cardiac cells has indeed rarely been studied.

The reduction of an ODE model of a periodically forced slow-fast system into a simpler model (often, a 1D discrete map) has been carried out in two ways. In the first way, one assumes the singular limit, so that the motion of the unforced system is restricted to the two stable pieces of the critical manifold (see Appendix A), with instantaneous jumps between these two pieces [GM79, GP82, GB86, Din88, CO00, XOW96, OX99, GHW03]. In some of these works, the vector field is in addition approximated by piecewise-linear functions. In the second way, although the singular limit is not taken, one makes use of the fact that there exists, in slow-fast systems, a "privileged" trajectory to which the state-point usually returns rapidly following a perturbation (for a relaxation oscillator, this trajectory is the limit cycle; for an excitable system it is the path followed by a "standard" AP[5]). Two possibilities then exist. The first one consists in characterizing the response of the slow-fast system to a *single* stimulus pulse delivered at various points along the special trajectory by measuring the value taken by an appropriate scalar quantity, and then, assuming a sufficiently fast return of the state-point back to this trajectory, one derives a 1D "forward map" that is then iterated to predict the response of the system to periodic stimulation. The second possibility consists in constructing a 1D "return map" by measuring the value taken by the characteristic quantity at the moments at which successive stimuli arrive during *periodic* stimulation. For relaxation oscillators, the quantity measured is usually the phase along the cycle, and the 1D map is a circle map (the "phase-resetting map", see Sec. 6.2.1), while for an excitable system, quantities such as the AP duration, the latency to an AP, or the area under the voltage waveform have been used, and the 1D map is a map of the interval[6]. Examples of works[7] where a forward map has been studied are [PSB$^+$64, GGS81, GGBS84, CGG$^+$89, YNPS99] for forced relaxation oscillators, and [RTF94, DS95, YNPS99, CO00] for forced excitable systems. Return maps have been used in [GGBS84, ADV$^+$91, NSD$^+$93] to study forced relaxation oscillators, and in [SD92, KCM$^+$96, Cyt04] to study forced excitable systems.

The different approaches just described can be further classified according to the methods used for computing the solutions of the system. Numerical methods are usually needed, although closed-form solutions have also been found for some simplified models. Numerical methods can be divided into two main categories: time-integration of the model (ODE or map) as a initial-value problem, and continuation. Time integration can provide valuable information about the transient behaviour of the system, but it is not an efficient tool if one is interested in how asymptotic solutions change as a parameter of the system is varied. Moreover, it cannot be used to compute unstable solutions. Continuation, on the other hand, allows computing asymptotic solutions beyond the parameter value at which they become unstable – it does not rely on integrating the equations until all transients have decayed (see Chap. 3). However, it relies on the vector field or the map being sufficiently smooth, so that piecewise-linear equations, or equations involving non-smooth forcing, cannot be studied by continuation. We are

[5]This path appears as the thick curve passing close to the *right* branch of the v-nullcline in the left panel of Fig. 2.5, and subsequently following the left branch down to the fixed point.

[6]A map of the interval is a map from some real interval I into itself, the boundaries of this interval being distinct (in contrast with the circle).

[7]In part of the works listed, the scalar quantity used to construct the 1D map was not measured in an ODE but in an experimental system.

aware of only two prior continuation analyses of periodically forced slow-fast systems; one concerned with an excitable system [ADO90], and the other one with a relaxation oscillator [MPL93]. Both use an ODE model and sinusoidal forcing. The continuation analysis made in [ADO90], using the FHN model, is not an exhaustive study but rather consists in a few numerical illustrations of theoretical results proved in the first part of the paper. The study reported in [MPL93] is a thorough study, but the system under investigation, the sinusoidally forced Bonhoeffer-van der Pol model, exhibits symmetries which give rise to degenerations in the results.

In the present work, we use continuation to study the periodic solutions of eqs. (4.1)–(4.2), which is an ODE model of a slow-fast system forced by a smooth, pulsatile function. The excitable and oscillatory regimes of the slow-fast system are considered successively in Chaps. 5 and 6. In Chap. 6, we study in addition an approximation of the ODE, namely the phase-resetting map obtained by computing the phase-resetting response of the relaxation oscillator to a stimulus of the type appearing in the sum (4.2).

Chapter 5

The periodically forced excitable FHN model

In this chapter, we present a continuation and bifurcation analysis of the periodic solutions of (4.1)–(4.2) with $d = 0$, done with the AUTO continuation software [DCF+98]. Two values of ε are considered in turn: $\varepsilon = 0.005$ (with $\sigma = 1$) and $\varepsilon = 0.002$ (with $\sigma = 2.5$). We use the stimulation period T as bifurcation parameter and study the evolution of the bifurcation diagram as the stimulation amplitude I_0 is raised from zero. Two-parameter continuation in the (T, I_0) plane is also used to determine the precise values of I_0 at which some phenomena of interest begin or end. Our results are discussed in the light of prior experimental and modelling works on periodically forced excitable cells (most of these studies concern cardiac cells, but some also involve squid giant axons). Sec. 5.3.1 is dedicated to a "listing" of works where phenomena similar to those we observe have also been reported; Sec. 5.3.2 consists in a detailed comparison of our results to those of two prior studies. The first of these studies is concerned with experimental results on isolated cardiac cells stimulated by a periodic train of current pulses; the second one involves 1D maps derived from a pulse-forced FHN model. Most of the content of this chapter has been published [CD07].

In the bifurcation diagrams that follow, each periodic solution is represented by a point, which is the maximum value v_{max} of the v coordinate of the solution over one period. Branches of solutions with period at most $8T$ are shown (often not all the branches of period $\leq 8T$ computed are shown for the sake of clarity of the figure). Stable solutions are drawn in black and unstable solutions are drawn in grey. The presence of saddle-nodes (SNs) is indicated by crosses and that of period-doubling points (PDs) by purple circles. No Neimark-Sacker bifurcation (bifurcation to quasiperiodicity, sometimes also called "torus" bifurcation) was met along the branches we have followed for $T > T_{min} \simeq 10\sigma$. The starting periodic solution for computing a given periodic solution branch is obtained either via prior direct numerical integration, or via prior continuation, with I_0 as bifurcation parameter, from the fixed point existing at $I_0 = 0$ or from a periodic solution computed for another value of I_0.

5.1 Results for $\varepsilon = 0.005$, $\sigma = 1$

5.1.1 Evolution of the bifurcation diagram for increasing I_0

The first important observation is that the bifurcation diagram always possesses a period-1 branch, *i.e.*, a branch made of solutions that are characterized by a period $P = 1T$. We will refer to this branch as B_1. For very low and very high stimulation amplitudes, B_1 contains no bifurcation point and is everywhere stable (Fig. 5.1, lowest and highest curves). When the stimulation amplitude I_0, raised from zero, reaches some critical value, a pair of PD points appears on B_1. They split the branch into two regions of stable solutions separated by a region of unstable solutions (e.g., Fig. 5.1, intermediate curves). Continuation of these two PD points in the (T, I_0) parameter-plane shows that they belong to a unique closed curve (Fig. 5.2). It is interesting to point out that of all the bifurcation points we have detected, these two PD points are the first ones to appear and the last ones to disappear as the stimulation amplitude is raised. They thus bound the interval of stimulation amplitudes in which "non-trivial" behaviour can be observed in the system, and for this reason we have introduced the notations I_0^- and I_0^+ to label the limits of the corresponding interval of amplitudes. For $\varepsilon = 0.005$ and $\sigma = 1$, the values of these limit amplitudes are $I_0^- = 0.1421$ and $I_0^+ = 0.5966$.

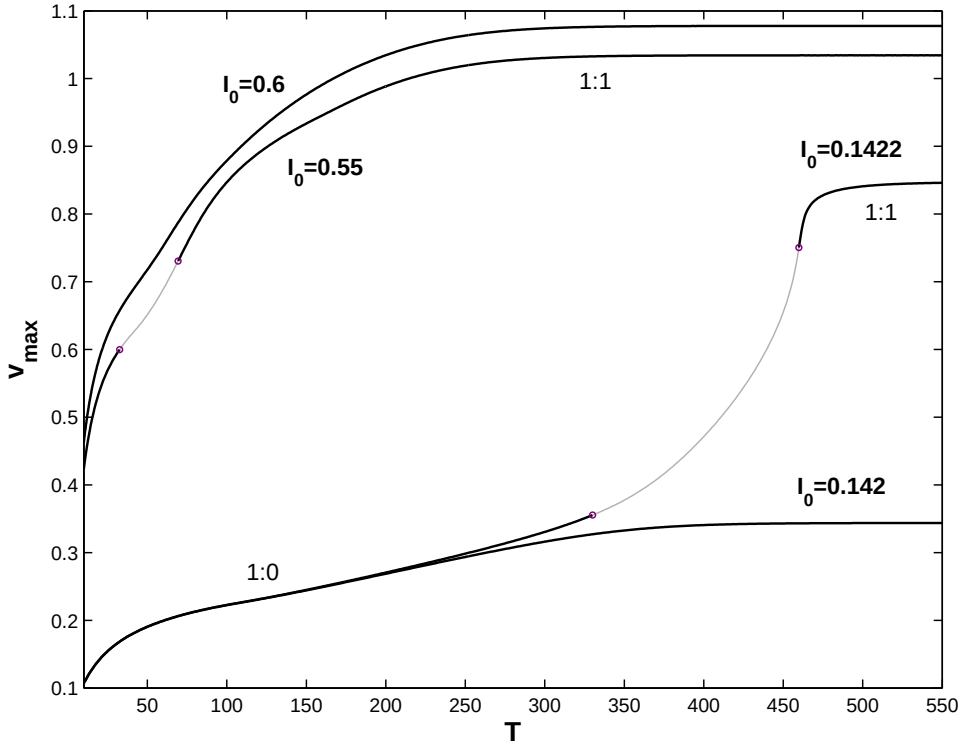

Figure 5.1. *Period-1 branch B_1 for $I_0 = 0.142$, $I_0 = 0.1422$, $I_0 = 0.55$ and $I_0 = 0.6$. Black curves represent stable solutions, grey curves represent unstable solutions. Circles are PD bifurcations.*

For I_0 just below I_0^- (Fig. 5.1, bottom curve), all the solutions on the stable period-1

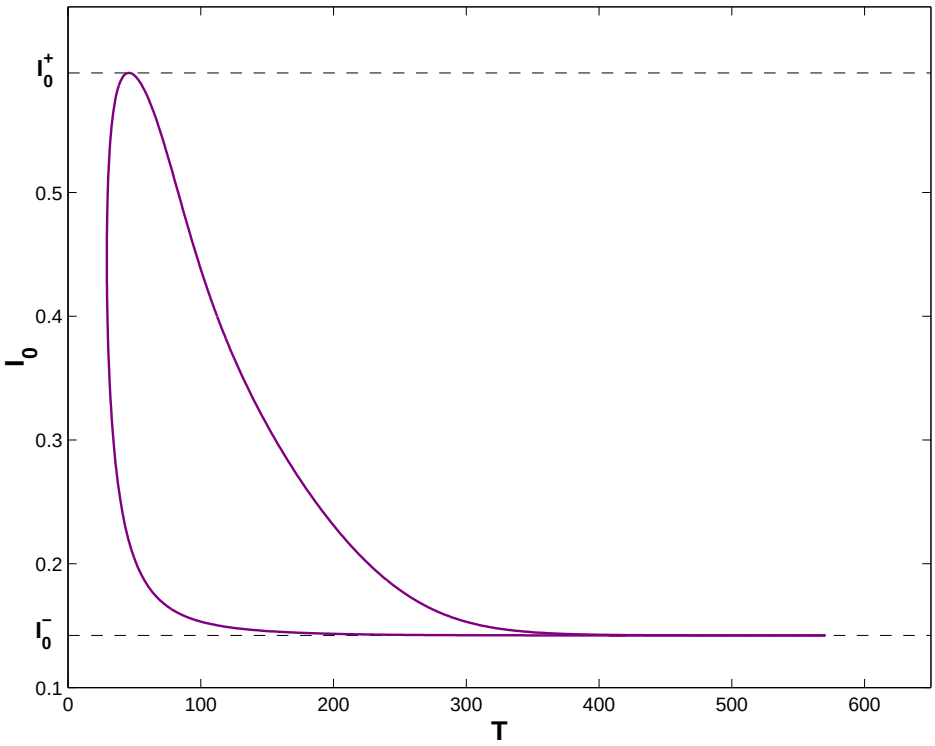

Figure 5.2. *Locus of the pair of PD points on B_1 in the (T, I_0) parameter-plane for $\varepsilon = 0.005$ and $\sigma = 1$. Notice how abruptly the pair of PD points appears at $I_0 = I_0^-$ compared to the way it disappears at $I_0 = I_0^+$* (cf. *discussion in text).*

branch are $1:0$ rhythms. Indeed, the inspection of the corresponding phase-plane trajectories shows that they are undoubtedly subthreshold responses (Fig. 5.3, top left panel). At the opposite, for I_0 just above I_0^+ (Fig. 5.1, top curve), the stable solutions with large T correspond to $1:1$ rhythms, while those with a small period are characterized by phase-plane trajectories lying completely above the right knee of the v-nullcline (Fig. 5.3, bottom right panel). It is therefore not possible to tell whether the latter correspond to subthreshold or suprathreshold responses without making an assumption about how the threshold manifold behaves away from the middle branch of the v-nullcline (*cf.* discussion in Sec. 2.2.2). A physiologist might qualify these responses as subthreshold since they lack the plateau phase characteristic of a cardiac AP.

Consider now values of the stimulation amplitude between the two limits just underscored. For I_0 just above I_0^-, B_1 is very different from what it was for I_0 just below I_0^-, as is shown in Fig. 5.1. It contains two bifurcation points, which are PD points. The stable region on the left part of B_1 contains $1:0$ rhythms, as for $I_0 < I_0^-$, while that on the right part is now composed of $1:1$ rhythms (Fig. 5.3, upper right panel). The two stable regions are separated by a large unstable region. This means that the two PD points move very far apart over a tiny range of stimulation amplitudes close to that ($I_0 = I_0^-$) at which they are born as a pair (Fig. 5.2). On the other hand, they come close to each other very "gently" as the amplitude is raised towards $I_0 = I_0^+$ (Fig. 5.2). This asymmetry is actually related to the fact that the divergence of the trajectories from the threshold curve of the excitable system fades in the region of the right knee (see Sec. 2.2.2), and that this divergence is much stronger, in particular, at ordinates close to that

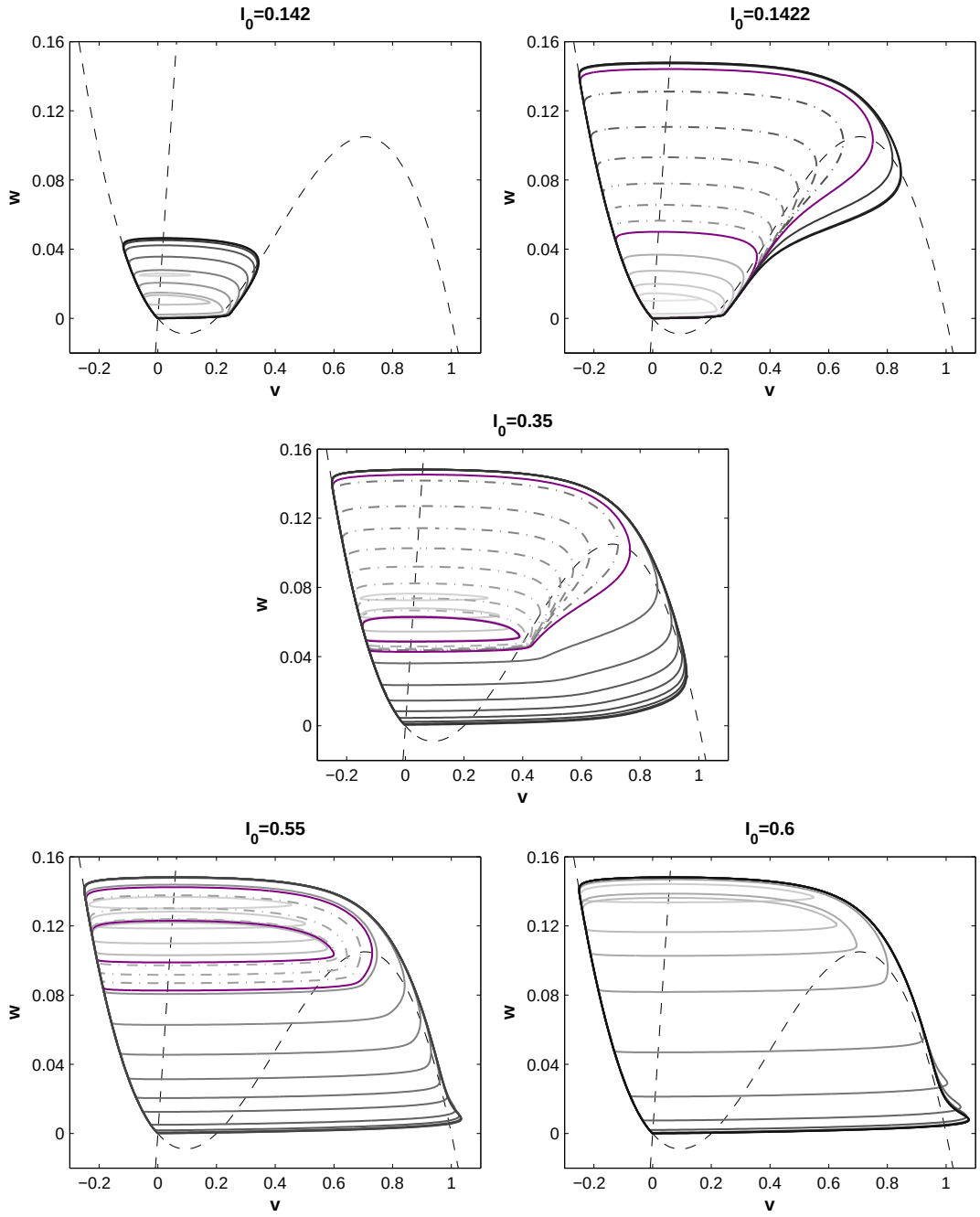

Figure 5.3. *Phase-plane trajectories for a sample of period-1 solutions for* $I_0 = 0.142$ *(upper left),* $I_0 = 0.1422$ *(upper right),* $I_0 = 0.35$ *(middle),* $I_0 = 0.55$ *(lower left), and* $I_0 = 0.6$ *(lower right). The period of the solution increases from grey to black. Unstable solutions are shown dashed-dotted. Period-doubling solutions are drawn in purple. Most of the solutions in the two top panels, as well as the unstable solutions in the middle panel, are reminiscent of canards, in that they follow the threshold manifold of the unforced equations over a substantial distance (see Appendix A).*

of the fixed point. To explain this, let us first admit that all the solutions on B_1 remain $1:0$ rhythms until $I_0 = I_0^-$, as seems to indicate the upper left panel of Fig. 5.3 (in which

I_0 is very close to I_0^- from below). In addition, note that, under the approximation that the effect of our stimulus is a horizontal translation of the state-point to the right[1], the stable fixed point is the point on the left branch from which it is easiest to bring the state-point on the right of the threshold manifold, given the shape of the v-nullcline[2]. Then, it must be true that for an amplitude smaller than I_0^-, the stimulus is unable to bring points located on the left branch to the right of the threshold manifold. Indeed, the state-point always ends up on the left branch[3], close from above to the fixed point, after some time, so that if a suprathreshold response could be elicited from the left branch for $I_0 < I_0^-$, $1:1$ rhythms could be induced by a periodic stimulation of sufficiently large period. The very different aspect of the right part of B_1 for $I_0 = 0.1422$ compared to $I_0 = 0.1420$ (Fig. 5.1, lower curves) can be explained by the fact that for I_0 just above I_0^-, the stimulus is able to bring the state-point from the left branch to the right of the threshold curve, but only for stimulation periods so large that the state-point is virtually back to the stable fixed point of the unforced equations when this happens (Fig. 5.3, upper right panel). Because the divergence of the trajectories from the threshold curve is very important in the vicinity of the fixed point, a slight change in stimulation amplitude with I_0 close to I_0^- can then lead to very different responses for large values of T. Second, it appears that the unstable region that exists on B_1 for $I_0^- < I_0 < I_0^+$ is made of solutions (dashed-dotted curves in Fig. 5.3) for which the stimulus puts the state-point in the vicinity of the threshold manifold[4]. For I_0 just above I_0^-, the region of unstable solutions extends over a large range of stimulation periods because stimuli given at very close points along the left branch, with ordinates just greater than that of the fixed point, can give rise to solutions with very different periods. Indeed, these stimuli bring the state-point in the region of the phase plane where the trajectories diverge the most (the lower part of the middle branch), so that the time needed before coming back to the left branch can be very different. As I_0 is increased, the range of points along the left branch from which the stimulus can bring the state-point in the vicinity of the threshold curve moves up (this range is resp. defined by w close to 0, 0.4 and 0.8 for I_0 equal to 0.1422, 0.35 and 0.55, *cf.* Fig. 5.3). This causes the unstable region to shrink since trajectories starting on one or the other side of the threshold manifold at high ordinates take paths of less different durations to reach the left branch than at lower ordinates. When I_0 reaches I_0^+, the unstable region disappears completely. One can interpret this as meaning that, for $I_0 \geq I_0^+$, the stimulus brings any point located on the left branch to the opposite side of the threshold manifold, *i.e.*, that all responses elicited from the left branch are suprathreshold. This is, in fact, a way of defining *a posteriori* the location of the threshold manifold in the neighbourhood of the right knee.

[1]Strictly speaking, our Gaussian-shaped stimulus has no beginning and no end, but its effect on the vector field is however essentially restricted to a finite period of time. Throughout our reasoning, we assume that the stimulus "starts" and "ends" at the points in the phase-plane trajectories of Fig. 5.3 at which the trajectories look "broken"; *i.e.*, that the stimulus takes the state-point "from" the first of these two points "to" the second, which has approximately the same w-coordinate as the first one, and that the dynamics is essentially governed by the unforced equations outside of the portion of trajectory bounded by these two points.

[2]At least, this is true of the points on the left branch which have an ordinate smaller than the right knee: indeed, since the trajectory defining the threshold turns left in the vicinity of the right knee, and heads subsequently towards the left branch, its "right" is no longer defined past that moment.

[3]Throughout our reasoning, we assume that the state-point returns to the fixed point along the left branch, which is actually only a (good) approximation for non-zero values of ε (see also Appendix A).

[4]Note that part of the stable solutions for $I_0 = 0.142$ and $I_0 = 0.1422$ have also this characteristic (Fig. 5.3).

It would imply, in particular, that all the periodic solutions on B_1 for $I_0 = 0.6$ (upper curve in Fig. 5.1 and bottom right panel of Fig. 5.3) are $1:1$ rhythms. Conversely, one can assume that $1:0$ rhythms still exist for $I_0 > I_0^+$, but then the location of the boundary between stable $1:0$ and $1:1$ rhythms on B_1 becomes completely arbitrary for $I_0 > I_0^+$.

In the bifurcation diagrams that follow (Figs. 5.4–5.14), we will see that a phenomenon similar to that which occurs on B_1 happens on the other branches: the different stable rhythms on a given branch/loop are separated by large unstable regions at relatively small stimulation amplitudes above I_0^-, but these unstable regions shrink as the amplitude is raised, until they finally disappear. The attitude we have adopted for labeling the stable portions of branches in the bifurcation diagrams is the following: we have assumed that if a stable segment corresponds to an $M:N$ rhythm for I_0 just above I_0^- (which can be determined without ambiguity for the reasons mentioned previously), then it remains an $M:N$ rhythm for larger amplitude. Whether or not this assumption is "correct" will depend on the precise definition chosen for the threshold curve, but given that the difference between a stable $M:N$ rhythm and a stable $M:N-1$ rhythm becomes anyway weaker as the amplitude is raised, we believe that the answer to this question has no importance.

Let us now analyse characteristics of the bifurcation diagram other than B_1 for I_0 just above I_0^-. The bifurcation diagram for $I_0 = 0.1422$ is shown in Fig. 5.4. The two PD points on B_1 are connected by a period-2 branch. We will refer to this period-2 branch as B_2. The left origin of B_2 is a subcritical bifurcation, while a supercritical bifurcation is observed at the right connection with B_1. Because the $1:1$ rhythm loses stability through a supercritical PD bifurcation as the stimulation period is decreased, a stable $2:2$ rhythm is met when the bifurcation point is passed. This $2:2$ rhythm remains stable only over a rather narrow stimulation period interval. However, B_2 contains another stable region which extends over a large range of T values, and which is found to correspond to a $2:1$ rhythm. One can see from Fig. 5.4 that there exists a range of T values over which the $2:1$ rhythm is bistable with the $1:0$ rhythm.

The zoom on the right part of the bifurcation diagram in Fig. 5.4 shows that like the $1:1$ solution, the $2:2$ rhythm becomes unstable through a supercritical PD bifurcation, and gives rise to a $4:4$ rhythm. In fact, a whole cascade of PD bifurcations might occur there (we have only tracked the first few bifurcations). Another PD cascade is starting at the point where the $2:1$ rhythm becomes unstable for increasing values of T (left part of the inset in Fig. 5.4). Between these two (partial) PD cascades, a stable $3:2$ rhythm is present. It belongs to an "isolated loop", *i.e.*, a closed solution branch distinct from the other branches. In the regions between this $3:2$ loop and the PD cascades, where only unstable solutions are visible in Fig. 5.4, chaotic-like[5] solutions were found by direct numerical integration.

For $I_0 = 0.143$, a pair of saddle-nodes has appeared on B_1 on the right of the rightmost PD point (Fig. 5.5, inset). Two-parameter continuation shows that the birth of this pair of SNs occurs at $I_0 = 0.1426$. As a result, the $1:1$ rhythm loses stability for the first time at a SN bifurcation when the stimulation period T is decreased. Following the branch, stability is then recovered for a short distance after the second SN, before reaching the PD bifurcation point. It is thus possible to observe $1:1 \leftrightarrow 1:1$ bistability in a tiny range of stimulation periods ($385.085 < T < 385.155$ for $I_0 = 0.143$). In addition,

[5]We have only used direct numerical integration, so we cannot be certain it is chaos.

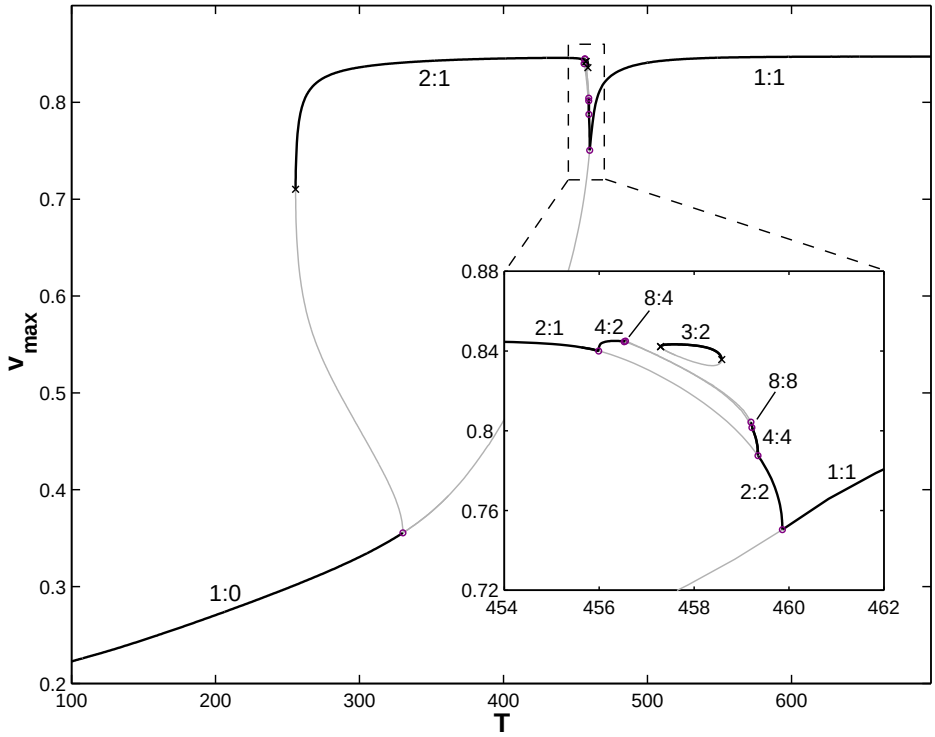

Figure 5.4. *Bifurcation diagram for* $I_0 = 0.1422$, $\varepsilon = 0.005$, *and* $\sigma = 1$.

the range of stimulation periods over which the $2^k : 2^k$ PD cascade ($k \in \mathbb{N}$) extends is entirely contained within that over which the main (upper) $1:1$ rhythm extends[6]. As a consequence (in addition to the presence of $1:1 \leftrightarrow 2^k : 2^k$ bistability), if the stimulation period is decreased gradually with initial conditions in the basin of attraction of the main $1:1$ rhythm, no $2^k : 2^k$ rhythm is reached past the point where the main $1:1$ rhythm becomes unstable (upper SN on B_1). Instead, a (very high-order, not shown in Fig. 5.5) $N : N-1$ or Wenckebach (W) rhythm is established. Like the $3:2$ rhythm of Fig. 5.4, each of these stable W rhythms belongs to a loop which is isolated from the other loops and isolated from the branches connected to B_1. The important proximity of the different branches[7] prevents however from realizing this from Fig. 5.5. Only the loops containing the first few W rhythms ($3:2$, $4:3$, $5:4$) are shown in Fig. 5.5, but very high-order ($N \gg 10$) stable W rhythms have been identified by direct numerical integration. It is also interesting to point out that a $2^k : 2^{k-1}$ PD cascade no longer stems from the $2:1$ rhythm; the PD bifurcation through which the $2:1$ rhythm loses stability for increasing stimulation periods has turned subcritical. On the left part of B_2, both a pair of SNs and a pair of PDs have appeared (only one of the two PD points is visible in Fig. 5.5, but both PD points are visible in Fig. 5.6).

For $I_0 = 0.15$ (Fig. 5.6), the $1:0 \leftrightarrow 2:1$ bistability described earlier is no longer

[6] Assuming the ranges ΔT_k over which the successive stable $2^k : 2^k$ rhythms extend shrink sufficiently quickly as the integer k increases (the computation of the first few ΔT_k makes us think that this is actually the case).

[7] We believe that this peculiar proximity is due to the smallness of ε, but we have not checked with a larger value of ε that this is indeed the case, as we have done in a similar situation for the periodically forced FHN oscillator (Chap. 6).

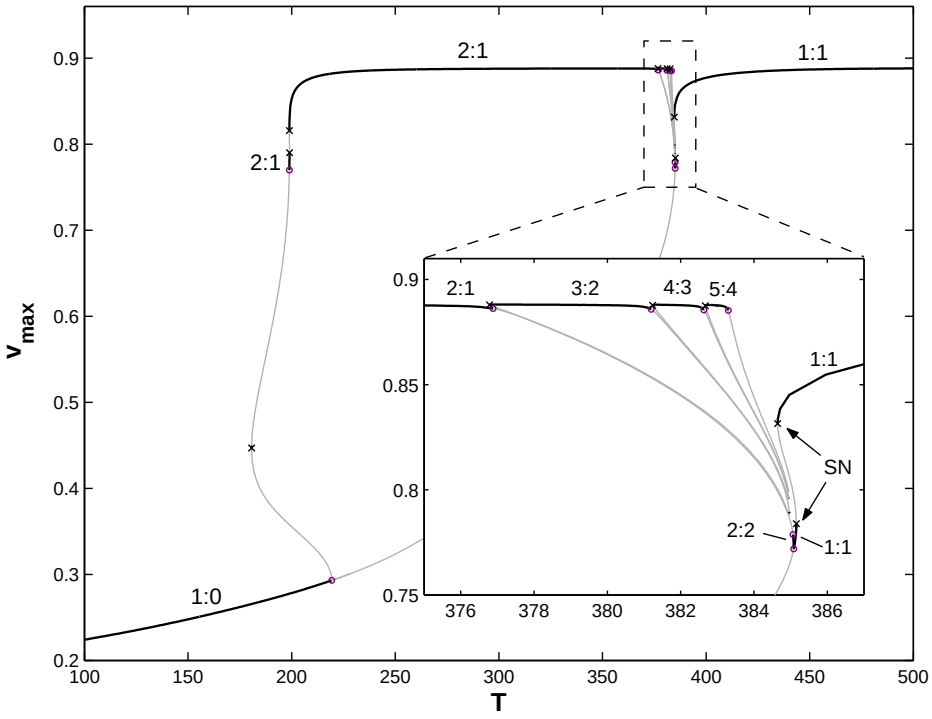

Figure 5.5. *Bifurcation diagram for* $I_0 = 0.143$, $\varepsilon = 0.005$, *and* $\sigma = 1$.

present. Indeed, at $I_0 = 0.1438$, the SN bounding the stable $2:1$ rhythm on the left has moved right relatively to the PD point through which the $1:0$ loses stability. A stable $2:0$ rhythm is present on the left part of B_2. It does not stem directly from the stable $1:0$ rhythm (the PD bifurcation through which the $1:0$ rhythm loses stability is still subcritical), but is bistable with the $1:0$ rhythm. In the interval of stimulation periods between the stable $2:0$ and $2:1$ rhythms, a stable $3:1$ rhythm is present.

For $I_0 = 0.2$ (Fig. 5.7), more $N:1$ rhythms can be found. Like Wenckebach rhythms, $N:1$ rhythms belong to loops which are isolated from the main branches and isolated from each other. Successive $N:1$ rhythms do not always show up with increasing values of N as the stimulation period is decreased (the "rotation number" $1/N$ is thus non-monotonic in this region), and, for a given value of N, it is possible to find several $N:1$ loops, corresponding to different types of $N:1$ rhythms. In addition, for $I_0 = 0.2$ (Fig. 5.7), the left PD point on B_1 has turned supercritical and a cascade of period-doubled $2^k:0$ rhythms is displayed when the stimulation period is increased from the $1:0$ rhythm. Although we have not checked this observation rigorously, it is interesting to mention that this PD cascade seems to be the first step of a Metropolis U-sequence (e.g., [Str00]). Indeed, each loop containing a stable $N:1$ rhythm also exhibits a stable $N:0$ rhythm in a tiny stimulation period interval near its left tip (these $N:0$ rhythms are invisible in Fig. 5.7 but their presence can be "guessed" in Fig. 5.11), and each of these $N:0$ rhythms constitutes itself the first step of a $2^k N:0$ period-doubling cascade. The order in which these PD cascades succeed to each other for increasing stimulation period is consistent with the U-sequence for the loops we have computed for Fig. 5.7.

While for $I_0 = 0.2$, tiny ranges of bistability exist between successive W rhythms and between the $2:1$ and $3:2$ rhythms (Fig. 5.7, inset), for $I_0 = 0.3$, "gaps" exist

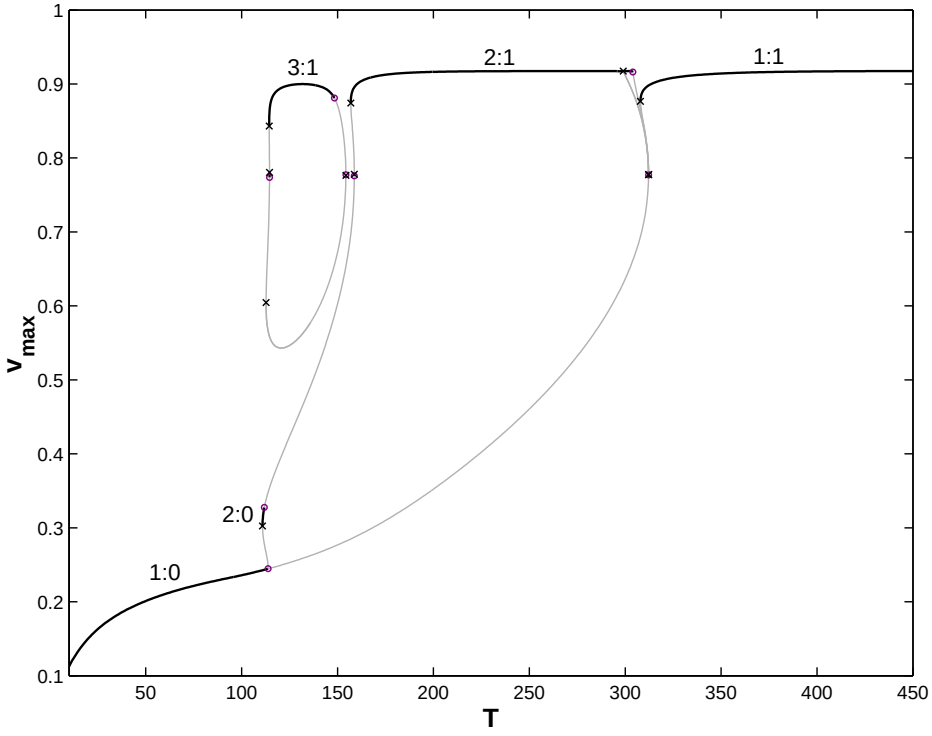

Figure 5.6. *Bifurcation diagram for* $I_0 = 0.15$, $\varepsilon = 0.005$, *and* $\sigma = 1$.

between these stable rhythms (Fig. 5.8). In these regions, stable solutions of higher period are present, although they are not shown in Fig. 5.8. For example, a $5:3$ rhythm, a $7:4$ rhythm,... can be observed between the $2:1$ and the $3:2$ solutions. Similarly, a $7:5$ rhythm,... can be seen between the $3:2$ and the $4:3$ solutions, etc. Such an organisation is reminiscent of the well-known Farey tree, which characterizes, notably, the organisation of phase-locking in the sine-circle map (e.g., [AFH94]). Another evolution of the bifurcation diagram can be appreciated in Fig. 5.8: a pair of SNs has appeared on the right part of B_2, with the consequence that the $2:1$ rhythm loses stability through a SN (instead of a PD) as the stimulation period is increased[8].

The pair of SNs on the right of B_1 disappears for $I_0 = 0.3030$. The $2^k:2^k$ period-doubling cascade can then be "experienced" again when the stimulation period is decreased past the main $1:1$ rhythm (actually, the PD cascade is no longer bistable with the main $1:1$ rhythm a little before the pair of SNs disappears, as can be seen from Fig. 5.8). Before W rhythms are met, other PD cascades (interspersed by chaotic-like solutions) are encountered as the stimulation period is further decreased. This is because, in a similar fashion to what happens with $N:1$ rhythms, each loop containing a $N:N-1$ rhythm in Fig. 5.8 exhibits also a $N:N$ rhythm at its right end, and these $N:N$ rhythms give rise to $2^kN:2^kN$ period-doubling sequences for decreasing stimulation period.

As can be appreciated from Fig. 5.5 – 5.9, W rhythms remain stable in smaller and smaller ranges of stimulation periods as the stimulation amplitude is raised. They even-

[8]Another consequence is that a secondary stable $2:1$ rhythm is now present in a tiny range of stimulation periods near the lower SN, and causes $2:1 \leftrightarrow 2:1$ bistability to exist, but this bistability is of course restricted to a range of T values as minuscule as that over which the secondary $2:1$ rhythm is stable.

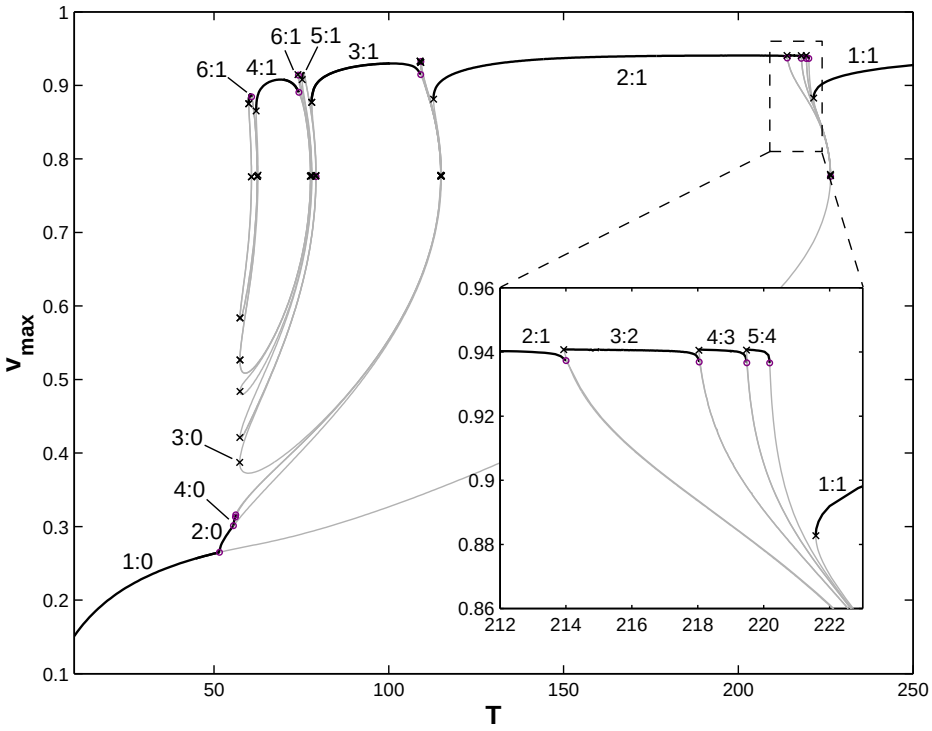

Figure 5.7. *Bifurcation diagram for* $I_0 = 0.2$, $\varepsilon = 0.005$, *and* $\sigma = 1$.

tually disappear, together with the loop they belong to, the highest-period W rhythms vanishing first. Before the $3:2$ loop finally disappears ($I_0 = 0.3398$), the rightmost SN on B_2 moves right relatively to the $3:2$ loop, so that $2:1 \leftrightarrow 3:2$ bistability re-appears[9] in the bifurcation diagram (Fig. 5.9). It remains present only over a small range of stimulation amplitudes. When the same SN on B_2 moves right of the right PD point on B_1, it is the turn of $2:1 \leftrightarrow 1:1$ bistability to settle in the system (Fig. 5.10). The $2:1$ rhythm is simultaneously bistable with the period-doubled rhythms stemming from the $1:1$ rhythm. For $I_0 = 0.4$ (Fig. 5.11), only the first of these period-doubled rhythms, the $2:2$ rhythm, is still present. Indeed, the only bifurcation points that remain on the right part of B_2 is a pair of SNs – the right pair of PD points has disappeared for $I_0 = 0.3569$.

For $I_0 = 0.45$ (Fig. 5.12), only one of the two SNs on the right part of B_2 is still present. The other one has disappeared through a collision with the right PD point on B_1 at $I_0 = 0.4308$, which has made that PD bifurcation subcritical. This codimension-2 bifurcation[10] is called a *generalized period-doubling* (GPD). A second GPD bifurcation occurs at $I_0 = 0.4733$, through which the PD bifurcation on B_1 becomes supercritical again. For stimulation amplitudes between the two GPD bifurcations (e.g., $I_0 = 0.45$, Fig. 5.12), one observes a direct transition from the stable $1:1$ rhythm to the stable $2:1$ rhythm as the stimulation period is decreased.

[9]It was present at smaller stimulation amplitudes (Fig. 5.7) but its cause was different, *i.e.*, the bifurcation points whose relative position was responsible for the bistability were other bifurcation points.

[10]The *codimension* of a bifurcation is the number of parameters one needs to tune to meet the bifurcation in a generic system.

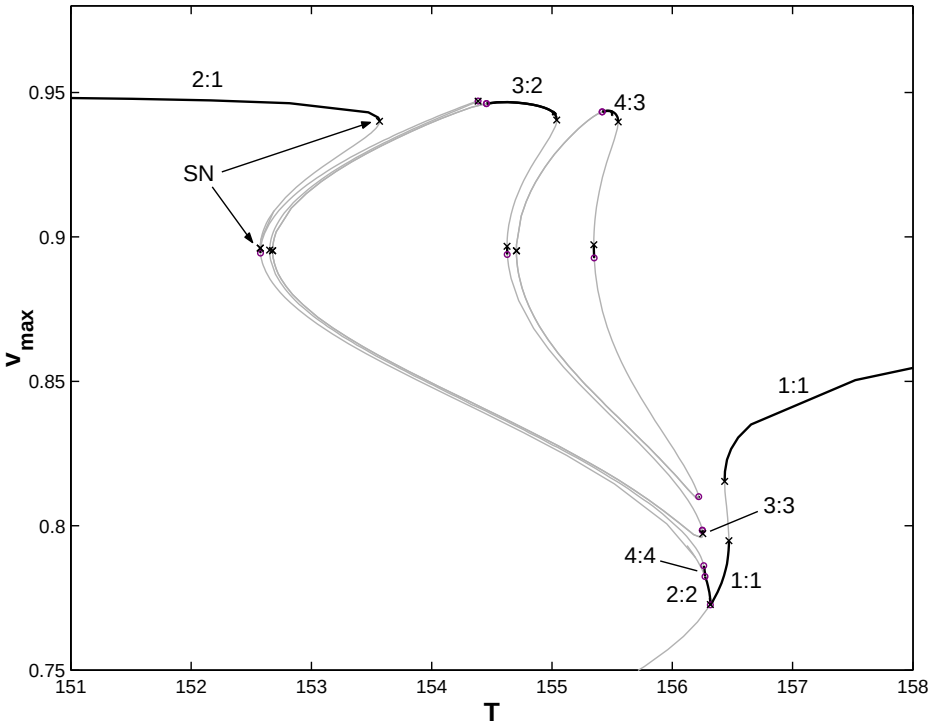

Figure 5.8. *Zoom on the right part of the bifurcation diagram for* $I_0 = 0.3$, $\varepsilon = 0.005$, *and* $\sigma = 1$.

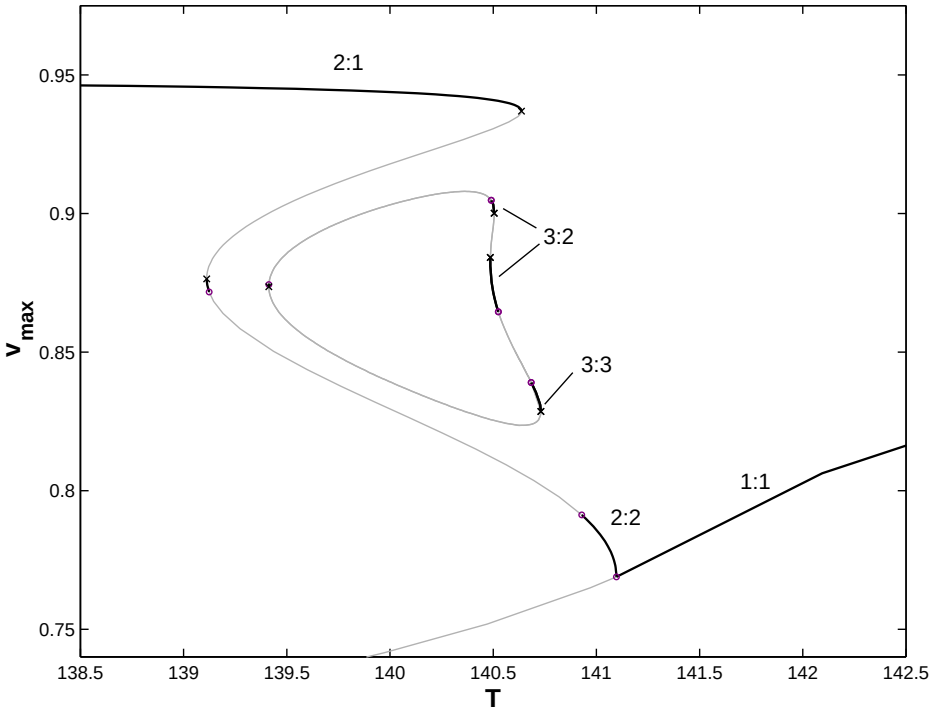

Figure 5.9. *Zoom on the right part of the bifurcation diagram for* $I_0 = 0.33$, $\varepsilon = 0.005$, *and* $\sigma = 1$.

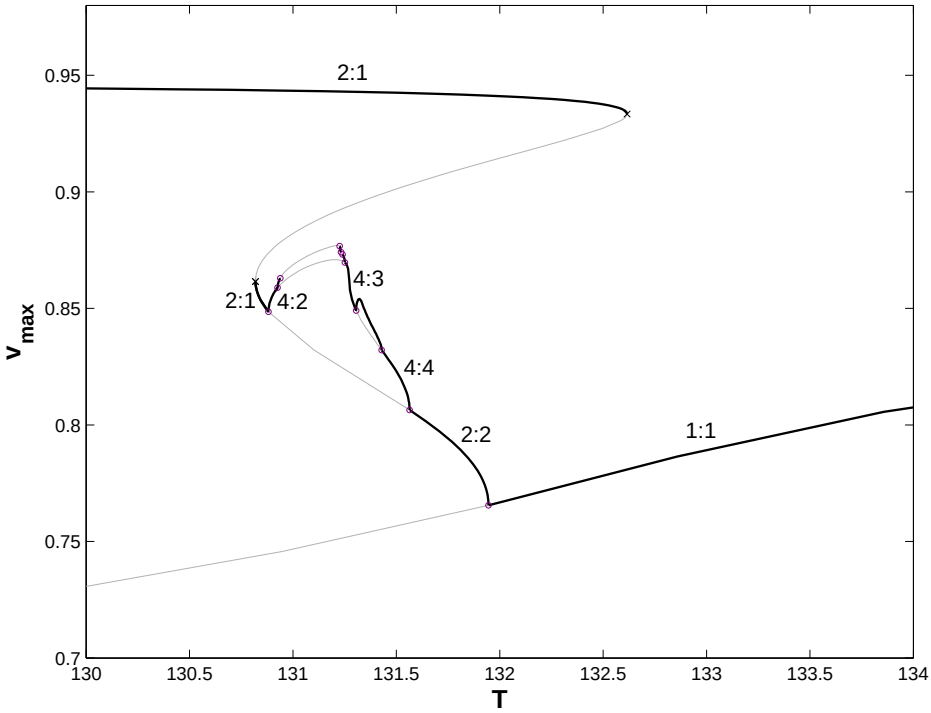

Figure 5.10. *Zoom on the right part of the bifurcation diagram for* $I_0 = 0.35$, $\varepsilon = 0.005$, *and* $\sigma = 1$.

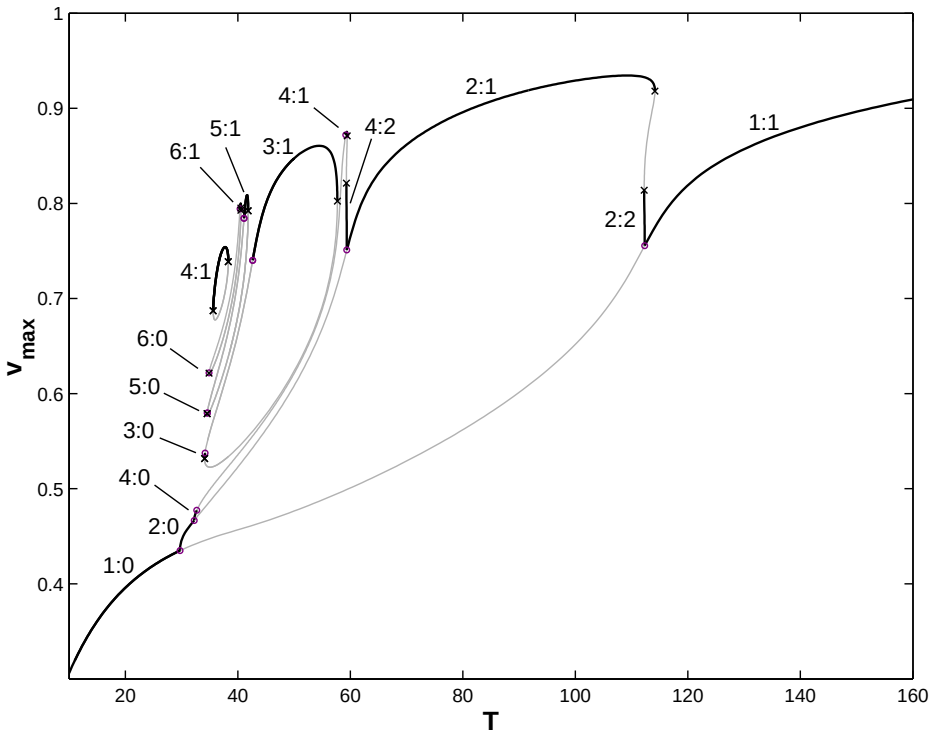

Figure 5.11. *Bifurcation diagram for* $I_0 = 0.4$, $\varepsilon = 0.005$, *and* $\sigma = 1$.

The $2:1 \leftrightarrow 1:1$ bistability vanishes ($I_0 = 0.4829$) just before the remaining pair of SNs on the right part of B_2 disappears ($I_0 = 0.4847$). For $I_0 > 0.4847$, there is no longer a region of unstable solutions between the stable $2:2$ and $2:1$ rhythms (e.g., $I_0 = 0.5$, Fig. 5.13) and the two stable rhythms transform continuously into each other as the stimulation period is increased or decreased. For $I_0 = 0.5248$, the last pair of PD points on B_2 disappears, causing the branch to become everywhere stable (e.g., $I_0 = 0.55$, Fig. 5.14). The stable $2:0$ and $2:1$ rhythms then also transform continuously into each other as the stimulation period is varied. B_2 finally disappears for $I_0 = I_0^+$ (Fig. 5.1).

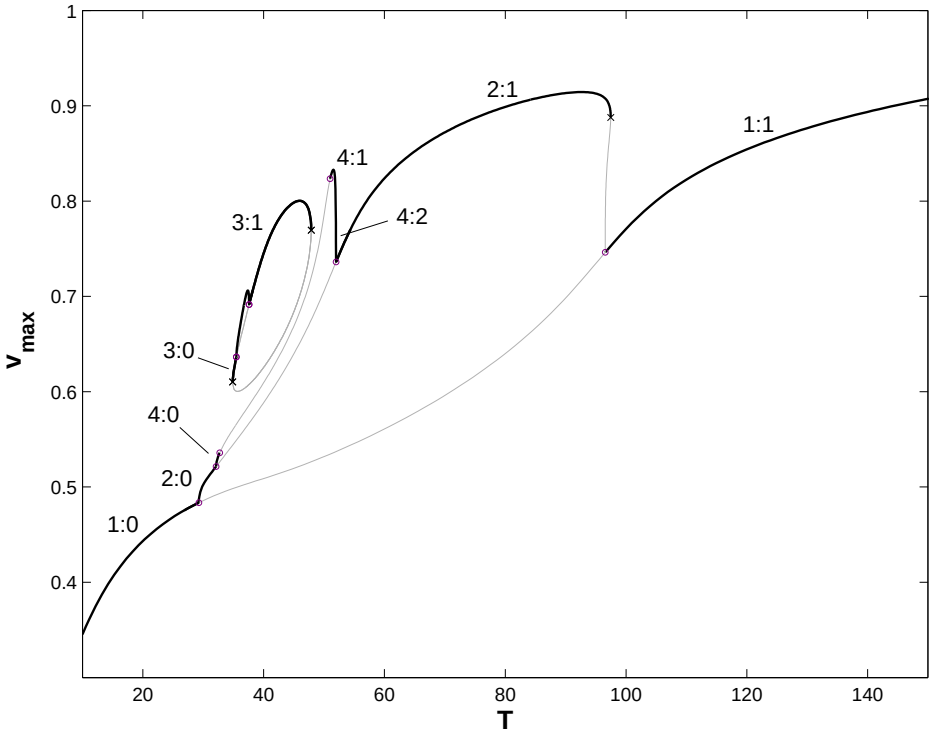

Figure 5.12. *Bifurcation diagram for* $I_0 = 0.45$, $\varepsilon = 0.005$, *and* $\sigma = 1$.

5.1.2 Ranges of I_0 over which phenomena of interest persist

The interval $\Delta I_0^{+-} = I_0^+ - I_0^-$ provides a useful reference to which the intervals of stimulation amplitudes over which the different phenomena persist can be compared. For example, $1:0 \leftrightarrow 2:1$ bistability, although present over a non-negligible range of stimulation periods in Figs. 5.4 and 5.5, persists only in a very small portion of ΔI_0^{+-} (0.4%). The $3:2$ loop is present in our system in a large range of stimulation amplitudes ($\simeq$ 43% of ΔI_0^{+-}), a range larger than that in which $1:1 \leftrightarrow 2:1$ bistability occurs ($\simeq$ 32% of ΔI_0^{+-}). This is not in good agreement with the experimental results on isolated cardiac cells since W rhythms have been observed only in a small range of stimulation amplitudes just above the threshold intensity I_t for obtaining a $1:1$ rhythm [DMJ89, HADJ90], while $2:1 \leftrightarrow 1:1$ bistability is usually easier to observe (M.R. Guevara, personal communication). In periodically stimulated squid giant axons, on the other hand, W rhythms are still observed for $I_0 = 2.1 I_t$ [THM$^+$90]. Unfortunately, the behaviour of squid axons for $I_0 > 2.1 I_t$ is not addressed in [THM$^+$90]. In our model,

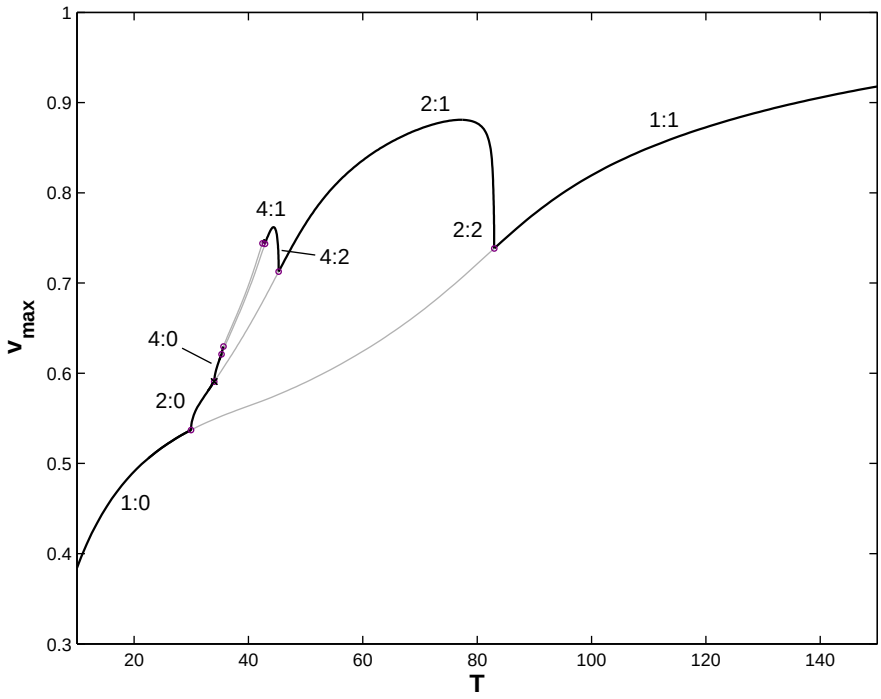

Figure 5.13. *Bifurcation diagram for* $I_0 = 0.5$, $\varepsilon = 0.005$, *and* $\sigma = 1$.

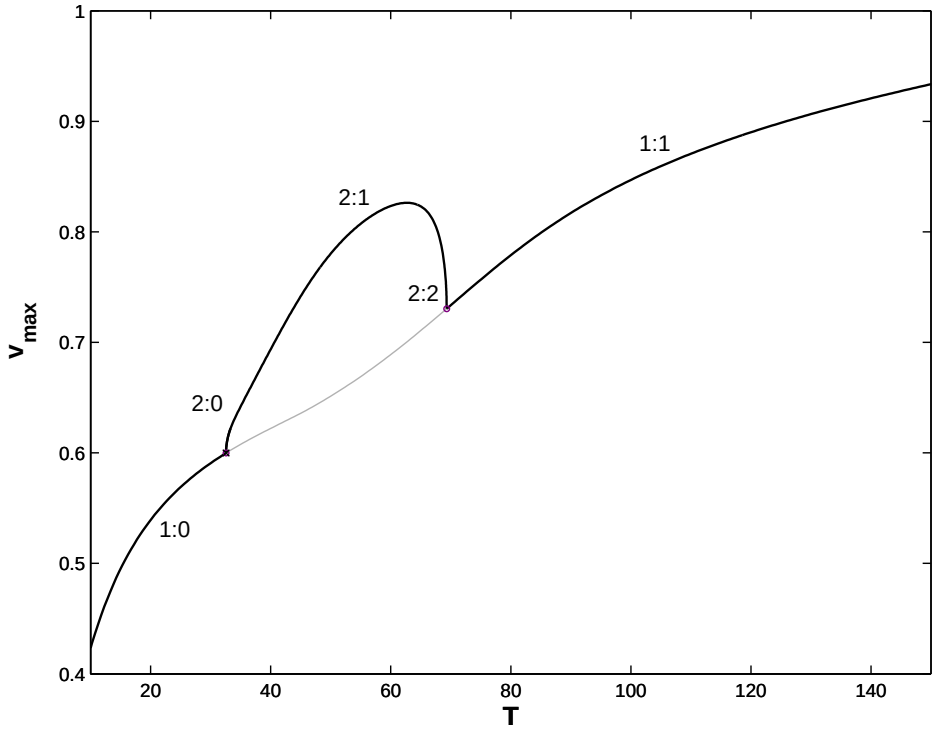

Figure 5.14. *Bifurcation diagram for* $I_0 = 0.55$, $\varepsilon = 0.005$, *and* $\sigma = 1$.

none of the stable W rhythms identified remains present for $I_0 > 2.4I_0^-$.

In the following subsection, we investigate the effect of reducing ε on the aspect of the bifurcation diagram, paying particular attention to the effect on the ranges of existence and stability of W rhythms. Indeed, the occurrence of W rhythms in the excitable FHN model is intimately linked to the fact that, for $\varepsilon \neq 0$, the time needed to come back to the left branch of the v-nullcline increases as the stimulus puts the state-point closer and closer to the threshold manifold of the unforced equations (Fig. 4.1, middle panel). It is not possible to generate W rhythms for $\varepsilon = 0$ because the behaviour of the system is truly "all-or-none" for this value of ε, *i.e.*, no delay is induced by the threshold curve except if the stimulus puts the state-point exactly on it. It therefore makes sense to check whether reducing the value of ε changes the range of I_0 or T values over which W rhythms occur, possibly allowing a better reproduction of the experimental results on cardiac cells. In the next subsection, we thus consider $\varepsilon = 0.002$ (using values of ε smaller than 0.002 causes numerical problems) and because reducing ε lengthens the action potential, we increase in compensation the duration of the stimulus by setting $\sigma = 2.5$.

5.2 Results for $\varepsilon = 0.002$, $\sigma = 2.5$

5.2.1 Evolution of the bifurcation diagram for increasing I_0

For $\varepsilon = 0.002$ and $\sigma = 2.5$, we have $I_0^- = 0.05780$ and $I_0^+ = 0.3043$. The evolution of the bifurcation diagram as the stimulation amplitude is raised from $I_0 = I_0^-$ is very similar to what happens for $\varepsilon = 0.005$, except for the following points.

Due to the smaller value of ε, the value of the stimulation amplitude at which the pair of SNs appears on B_1 is numerically indistinguishable from I_0^- at which the pair of PD points appears. As a consequence, it is not possible for $\varepsilon = 0.002$ to compute a bifurcation diagram similar to that of Fig. 5.4, where it is shown that for I_0 just above I_0^-, the $1:1$ rhythm loses stability through a PD point as the stimulation period is decreased and gives rise to a cascade of period-doubled $2^k:2^k$ rhythms. This situation was nevertheless already restricted to an extremely small range of stimulation amplitudes for $\varepsilon = 0.005$ (0.1% of ΔI_0^{+-}).

Secondly, $2:1 \leftrightarrow 1:1$ bistability arises (for $I_0 = 0.1257$) in a different way than for $\varepsilon = 0.005$, when the pair of SNs on B_1 is still present. It appears in the bifurcation diagram through the fact that the leftmost SN on B_1 has moved left below the rightmost SN on B_2 (Fig. 5.16). There is first $3:2 \leftrightarrow 1:1$ bistability (Fig. 5.15) and then $2:1 \leftrightarrow 1:1$ bistability (Fig. 5.16). This situation has for consequence that one gets a direct transition from the stable $1:1$ rhythm to the stable $2:1$ rhythm at an amplitude lower than that at which this transition involves a stable $2:2$ rhythm, in contrast to what happens for $\varepsilon = 0.005$ and $\sigma = 1$. We will come back on this point in section 5.3.2.1 since it yields a distinction between the two cases as the agreement with experimental results on cardiac cells is concerned. For larger stimulation amplitude (Fig. 5.17), even tristability phenomena occur: one involves the $2:1$, $1:1$, and $2:2$ rhythms, and another one involves the $2:1$ and two $1:1$ rhythms. However, the $2:2$ rhythm in the first case, and the lowest $1:1$ rhythm in the second case, are stable in so tiny intervals of stimulation periods that the intervals in which tristability occurs are negligible.

As for $\varepsilon = 0.005$, two GPD bifurcations take place between the right PD on B_1 and the closest SN on B_2, respectively for $I_0 = 0.2342$ and for $I_0 = 0.2754$. The $1:1 \rightarrow 2:1$

transition is direct a second time in the interval of stimulation amplitudes between the two GPD bifurcations. $2:1 \leftrightarrow 1:1$ bistability ends up for $I_0 = 0.2767$.

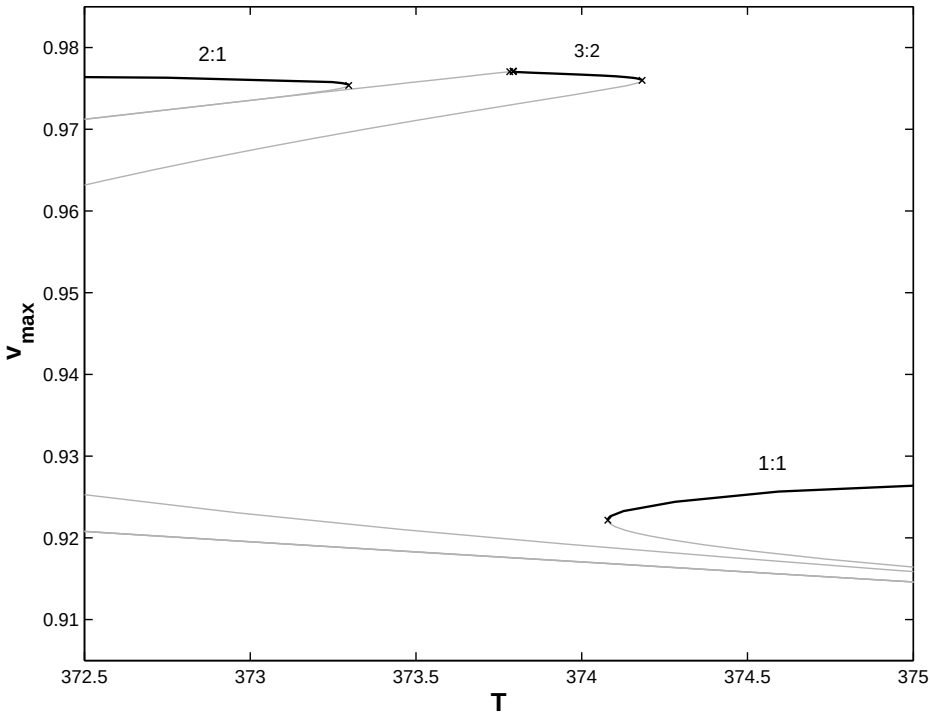

Figure 5.15. *Zoom on the right part of the bifurcation diagram for* $I_0 = 0.122$, $\varepsilon = 0.002$, *and* $\sigma = 2.5$.

5.2.2 Ranges of I_0 over which phenomena of interest persist

The fraction of ΔI_0^{+-} in which the $3:2$ loop is present is actually larger for $\varepsilon = 0.002$ (64%) than for $\varepsilon = 0.005$ (43%). However, the interval of stimulation periods ΔT_{32} over which the $3:2$ rhythm is stable for a given value of I_0 is very small in a much larger part of the range $\Delta I_{0,32}$ of stimulation amplitudes where the $3:2$ rhythm exists for $\varepsilon = 0.002$ than for $\varepsilon = 0.005$ ($\Delta T_{32} \leq 0.05$ in about 55% of $\Delta I_{0,32}$ for $\varepsilon = 0.002$, while for $\varepsilon = 0.005$, $\Delta T_{32} \leq 0.05$ in only about 5% of $\Delta I_{0,32}$)[11]. It can also be noted that the range of stimulation amplitudes over which $1:1 \leftrightarrow 2:1$ bistability is present has nearly doubled (61% of ΔI_0^{+-} against 32% for $\varepsilon = 0.005$).

5.3 Prior related studies

5.3.1 Reports of similar phenomena

In the present section, we give a brief review of experimental and/or theoretical works on periodically forced excitable systems in which the phenomena we have described

[11] It should be noted that the evolution of the size of ΔT_{32} as a function of I_0 is not easy to determine because, as can be seen from, e.g., Figs. 5.4 and 5.7–5.9, it is not always the same bifurcation points which bound the portion of the $3:2$ loop over which the $3:2$ rhythm is stable, and there can also be more than one such stable segment along the loop.

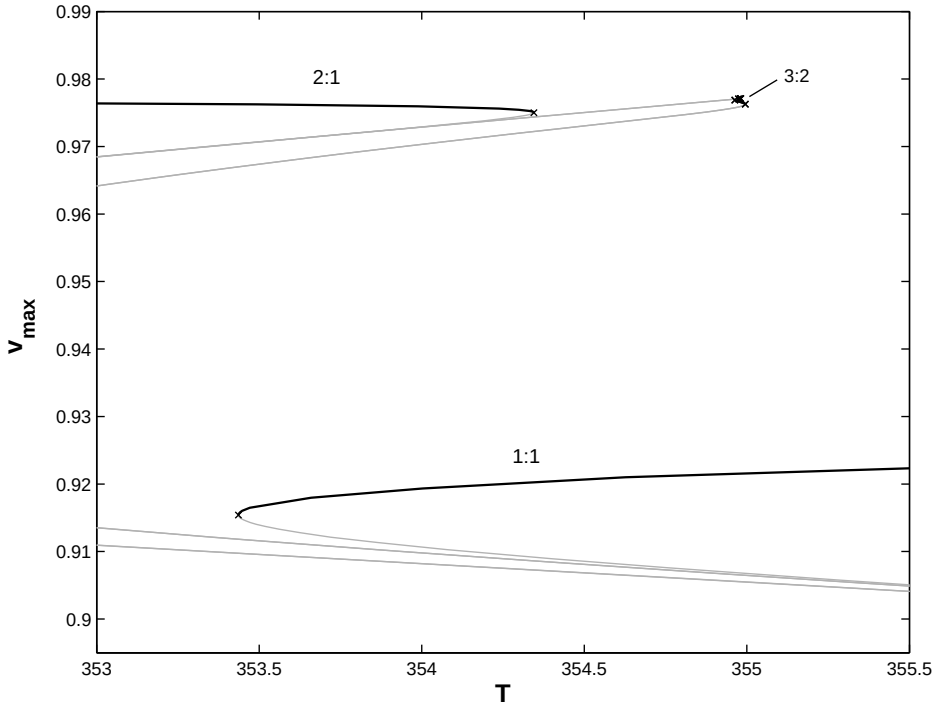

Figure 5.16. *Zoom on the right part of the bifurcation diagram for* $I_0 = 0.13$, $\varepsilon = 0.002$, *and* $\sigma = 2.5$.

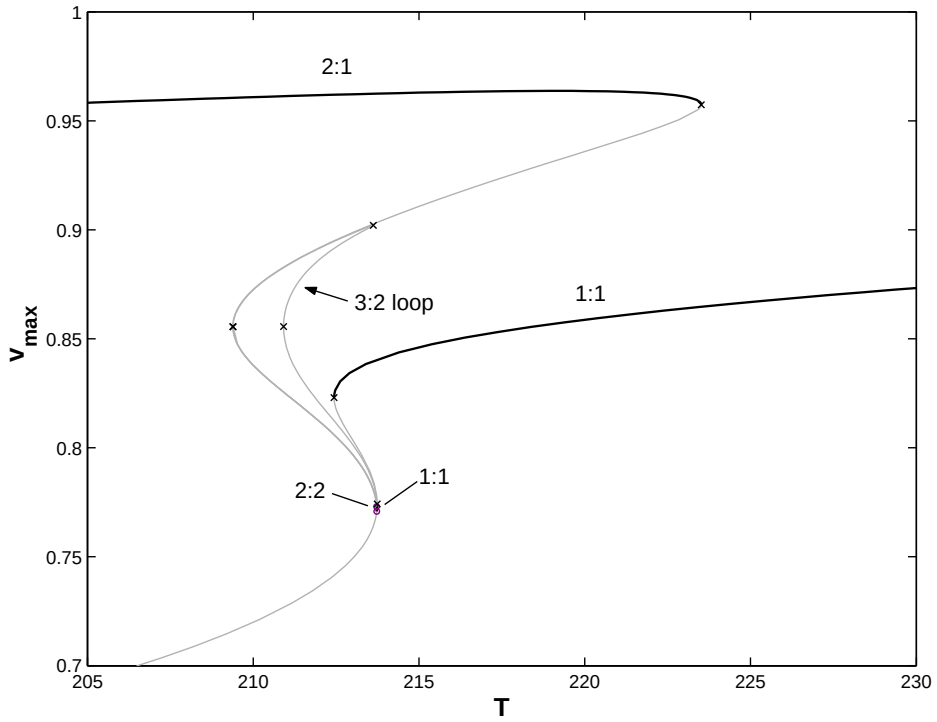

Figure 5.17. *Zoom on the right part of the bifurcation diagram for* $I_0 = 0.2$, $\varepsilon = 0.002$, *and* $\sigma = 2.5$.

above have also been reported. Some of these works use 1D discrete map models of periodically forced excitable systems, which we refer to as "1D maps" below. We discuss the phenomena in the order in which they were encountered in Secs. 5.1 and 5.2 (*i.e.*, for increasing stimulation amplitude). Unless otherwise stated, the sequences of phenomena discussed below were observed as the stimulation period was varied.

The existence of a period-1 branch in the bifurcation diagram for all values of I_0 is a proven result for the periodically forced FHN model [KRS04]. The result holds no matter the functional form of the periodic forcing, and no matter whether the FHN model is in the excitable or in the oscillatory regime.

$2:1 \leftrightarrow 1:0$ bistability (Fig. 5.4 and 5.5) has been observed previously in the FHN model where a weak sinusoidal forcing was applied to the slow variable [GX01]. It is also accounted for by 1D maps modelling the occurrence of partial devil's staircases in periodically forced excitable systems [YR03].

The $2^k:2^k$ ($k \in \mathbb{N}$) period-doubling sequence (Fig. 5.4, Fig. 5.8), followed by a chaotic regime, has been observed in toad ventricules [SRG$^+$89] and in dog Purkinje fibres [GOW97].

The occurrence of complex dynamics, including chaos, even at small stimulation amplitudes, had been previously noticed in the excitable FHN model [YNPS99].

We are not aware of prior reports of $1:1 \leftrightarrow 1:1$ bistability (e.g., Fig. 5.5 and 5.8) in forced excitable systems, but this form of bistability has been observed in forced oscillators (see, e.g., [RVR84, RPE02] and our discussion in section 6.3.3). However, another "self-bistability" phenomenon, the coexistence of two different stable $2:2$ rhythms, belonging to the same branch, is reported in [VR94] for a 1D map model of a forced excitable system (compare, e.g., our Fig. 5.8 to Fig. 6(b) in [VR94]). In both that study and ours, $1:1 \leftrightarrow 2:2$ bistability accompanies the self-bistability phenomenon (compare, e.g., the inset of our Fig. 5.5 to Fig. 5(b) in [VR94]) but the mechanism underlying the bistability is different (two SNs on the period-1 branch in our model, two SNs on the period-2 branch in the 1D map of [VR94]). $1:1 \leftrightarrow 2:2$ bistability has also been found in an ODE model of ischemic ventricular tissue as the external potassium ion concentration was varied at fixed stimulation amplitude and period [ALG02].

The occurrence of the subthreshold $2^k:0$ ($k \in \mathbb{N}$) period-doubling sequence (Fig. 5.7, 5.11–5.13) has been reported in [KCM$^+$96], article in which the response of squid giant axons to periodic stimulation is studied experimentally and modeled with a forced excitable FHN system. The period-doubling sequence reported in [RL88] for a sinusoidally forced excitable FHN system looks to us subthreshold as well.

Bistability between successive W rhythms and between $2:1$ and $3:2$ rhythms (inset of Fig. 5.7) has been observed in 1D maps [YR03]. Absence of bistability between these rhythms (Fig. 5.8), with complex dynamics occurring in the "gaps", has been observed in the FHN model [SD92], as well as in a family of 1D maps derived from the FHN model [Cyt04].

Farey-tree-like organisations have been observed in different types of quiescent cardiac cells [HS89, CMJ90, HADJ90], in ODE models of cardiac tissue [VCMJ90], in squid giant axons [THM$^+$90], in the excitable FHN model [FGPV88, YNPS99], and in 1D maps [DS95, IAJ98, YR03].

$2:1 \leftrightarrow 1:1$ bistability (Fig. 5.10–5.12) has been observed in isolated rabbit ventricular cells [YJAG99], aggregates of embryonic chick ventricular cells [GSG90] and small pieces of bullfrog cardiac muscle [HBG99]. It is accounted for by the Luo-Rudy ODE model [YJAG99] and by 1D maps [LG90, XOW96, OX99, YJAG99].

$2:1 \leftrightarrow 2:2$ bistability (Fig. 5.10–5.12) has been observed in isolated rabbit ventricular cells [GAJvG89] and small pieces of bullfrog cardiac muscle [HBG99]. It is accounted for by the Beeler-Reuter ODE model [LG90] and by 1D maps [LG90, OX99].

The transition $\{1:1 \to 2:2 \to 2:1 \to 4:2 \to \dots\}$ (Fig. 5.11–5.13), has been observed in isolated ventricular cells [HS89, GSG90], in the Beeler-Reuter model [VCMJ90, LG90] and in 1D maps [VCMJ90, LG90]. It has also been observed in squid giant axons [GFJ80], under the same form as in our Fig. 5.13 (that is, without bifurcation between the $2:2$ and $2:1$ rhythms and between the $4:2$ and $4:1$ rhythms).

The transition $2:2 \to 2:1 \to 2:0$ without bifurcation (Fig. 5.14) has been observed at high stimulation amplitudes in spontaneously beating aggregates of embryonic chick ventricular cells [GS90] and in the singular Poincaré oscillator (circular limit cycle with infinitely fast return to the limit cycle following a perturbation) subjected to impulsive forcing [GG82]. The transition $1:1 \to 1:0$ without bifurcation (Fig. 5.1) is also observed in the singular Poincaré oscillator. It also occurs for stimulation amplitudes larger than those at which the transition $2:2 \to 2:1 \to 2:0$ without bifurcation is seen.

Finally, let us mention that the occurrence of PD cascades, chaotic dynamics, and bistability was also reported in [FGPV88, DS95, YNPS99], for periodically forced excitable FHN equations, and in [DS95, OX99, YNPS99, CO00], for 1D maps derived from such equations, but the detail of the sequences of rhythms encountered was not given.

5.3.2 Two-parameter studies

In this section, we discuss in detail two studies in which the influence of both the period and the amplitude of the stimulation on the response of an excitable system to periodic forcing were investigated. The first one concerns *in vitro* experiments in which isolated excitable cardiac cells were periodically stimulated by an electrical current. The second one is purely theoretical and involves 1D maps derived from a periodically forced FHN model.

5.3.2.1 Experimental results on periodically driven cardiac excitable cells

In [YJAG99], a summary is given of the ways the $1:1$ rhythm can lose stability in periodically driven single cells isolated from rabbit ventricular muscle. The stimulation consisted of a periodic train of current pulses, the duration of which was small (5-20 ms) compared with the action potential duration ($\sim$ 300 ms). The following scenarios were reported. For low stimulation amplitudes, the transition $1:1 \to N:N-1 \to 2:1$ was seen as the stimulation period was decreased. For intermediate stimulation amplitudes, the transition $1:1 \to 2:1$ was direct (*i.e.*, no other rhythms are seen in between) and was accompanied by bistability between the two rhythms. The average stimulation amplitude at which this transition was seen was about 1.2 times the threshold amplitude to obtain a $1:1$ rhythm at the stimulation period $T = 1000$ ms. For high stimulation amplitudes, alternans were observed before the system settled in the $2:1$ pattern, *i.e.* the transition $1:1 \to 2:2 \to 2:1$ was seen as the stimulation period was decreased. Moreover, in this latter case both $2:1 \leftrightarrow 1:1$ bistability and $2:1 \leftrightarrow 2:2$ bistability were encountered.

Let us now describe how our results fit/disagree with the experimental findings reported in [YJAG99]. First, we should mention that the ranges of stimulation amplitudes referred to in [YJAG99] are essentially defined in a relative fashion, *i.e.* "high stimulation

amplitudes" simply lie above "low stimulation amplitudes" and "intermediate stimulation amplitudes" lie in between. The lowest bound for "low stimulation amplitudes" is the minimum amplitude to obtain a $1:1$ rhythm, which corresponds in this work to I_0^-. For reasons given earlier, we have additionally an upper bound for "high stimulation amplitudes", which is I_0^+.

For $\varepsilon = 0.005$ and $\sigma = 1$, we find five main scenarios between I_0^- and I_0^+:

1. the transition $1:1 \to 2:2 \to \ldots \to N:N-1 \to 2:1$, without $2:1 \leftrightarrow 1:1$ bistability ($\simeq 7\%$ of ΔI_0^{+-});
2. the transition $1:1 \to N:N-1 \to 2:1$, without $2:1 \leftrightarrow 1:1$ bistability ($\simeq 34\%$ of ΔI_0^{+-});
3. the transition $1:1 \to 2:2 \to \ldots \to 2:1$, with both $2:1 \leftrightarrow 1:1$ and $2:1 \leftrightarrow 2:2$ bistability ($\simeq 23\%$ of ΔI_0^{+-});
4. the direct $1:1 \to 2:1$ transition, with $2:1 \leftrightarrow 1:1$ bistability ($\simeq 9\%$ of ΔI_0^{+-});
5. the transition $1:1 \to 2:2 \to 2:1$, without bistability ($\simeq 25\%$ of ΔI_0^{+-}).

The first scenario is not reported in [YJAG99], however we find it to be restricted to a rather small fraction of ΔI_0^{+-}. The second scenario is observed experimentally at small stimulation amplitudes. The third scenario is also described in [YJAG99], however it is reported that the transition $1:1 \to 2:1$ is at first direct (scenario 4) and involves a $2:2$ rhythm (scenario 3) only for larger stimulation amplitudes, while we find the opposite. We observe the third scenario from $I_0 = 0.3374$, amplitude at which the rightmost SN on B_2 moves to the right of the right PD point on B_1 (start of $2:1 \leftrightarrow 1:1$ bistability, compare Figs. 5.9 and 5.10), until $I_0 = 0.4308$, amplitude at which the right PD bifurcation on B_1 becomes subcritical through a GPD bifurcation, causing the disappearance of the stable $2:2$ rhythm (compare Figs. 5.11 and 5.12). The fourth scenario is then seen until $I_0 = 0.4733$, amplitude at which a second GPD bifurcation occurs. Above the second GPD bifurcation, the right PD bifurcation on B_1 becomes supercritical again and the third scenario is observed a second time until $I_0 = 0.4829$, amplitude at which the $2:1 \leftrightarrow 1:1$ bistability ceases. Finally, the fifth scenario is not reported in [YJAG99]. It is however possible that this scenario requires stimulation amplitudes larger than those used in [YJAG99] to be observed in excitable cardiac cells, since it arises in our model for stimulation amplitudes higher than the last (in the order of increasing stimulation amplitudes) scenario reported in [YJAG99]. In addition, as mentioned above, this scenario has been observed in spontaneously beating aggregates of embryonic chick ventricular cells [GS90] and in squid giant axons [GFJ80], in both cases at large stimulation amplitudes.

For $\varepsilon = 0.002$ and $\sigma = 2.5$, four scenarios emerge in our model:

1. the transition $1:1 \to N:N-1 \to 2:1$, without $2:1 \leftrightarrow 1:1$ bistability ($\simeq 26\%$ of ΔI_0^{+-});
2. the direct $1:1 \to 2:1$ transition, with $2:1 \leftrightarrow 1:1$ bistability ($\simeq 50\%$ of ΔI_0^{+-});
3. the transition $1:1 \to 2:2 \to \ldots \to 2:1$, with both $2:1 \leftrightarrow 1:1$ and $2:1 \leftrightarrow 2:2$ bistability ($\simeq 11\%$ of ΔI_0^{+-});
4. the transition $1:1 \to 2:2 \to 2:1$, without bistability ($\simeq 11\%$ of ΔI_0^{+-}).

The first three scenarios have been observed experimentally [YJAG99]. We obtain the first scenario only in about 26% of ΔI_0^{+-}, even if the $3:2$ loop is present in about 64% of ΔI_0^{+-}, notably because in a situation like that of Fig. 5.16, the $1:1 \to 2:1$ transition is direct (assuming B_1 is followed until the SN at which the main $1:1$ rhythm becomes unstable). In contrast with what happens for $\varepsilon = 0.005$, the second scenario occurs a first time in a range of stimulation amplitudes lower than that in which the third scenario occurs, which is consistent with the experimental observations. The stimulation amplitude at which the direct $1:1 \to 2:1$ transition is seen for the first time is about $2.2I_0^-$, which is a fair order of magnitude with respect to the results reported in [YJAG99]. Indeed, this transition arises in the experiments for a stimulation amplitude which is in average 1.2 times the threshold amplitude to obtain a $1:1$ rhythm at $T = 1000$ ms, and the "absolute" minimum amplitude to obtain a $1:1$ rhythm (which corresponds to our I_0^-), can only be smaller than this amplitude. For $\varepsilon = 0.005$, the transition $1:1 \to 2:1$ becomes direct at $I_0 \simeq 3.0I_0^-$. Finally, the fourth scenario, which occurs also for $\varepsilon = 0.005$, is not reported in [YJAG99]. Again, as explained earlier, it is possible that this situation simply requires stimulation amplitudes higher than those used in [YJAG99]. Note also that for $\varepsilon = 0.002$, this scenario is restricted to a much smaller range of stimulation amplitudes than the other three scenarios.

In summary, we obtain a better agreement with the results reported in [YJAG99] for $\varepsilon = 0.002$ than for $\varepsilon = 0.005$. A possible reason is that the greater upstroke velocity that characterizes the action potential for $\varepsilon = 0.002$ is more consistent with the actual behaviour of cardiac cells.

5.3.2.2 Theoretical results based on 1D map reductions of a periodically forced excitable system

In [Cyt04], it is shown that a 1D discrete map can account for the occurrence of Wenckebach rhythms in a periodically forced excitable system provided it exhibits the appropriate non-monotonicity, which is usually not the case of the traditional APD map (see [Cyt04] and refs. therein). The 1D map studied in [Cyt04] is derived from a forced FHN model in which the stimulation consists in periodically increasing the value of the sole potential. The map relates successive values of the prestimulus potential (while the APD map relates the APD to the preceding "diastolic interval" DI=T–APD, where T is the stimulation period). This first map is then simplified into a piecewise linear map which retains only the essential characteristics of the original map in the Wenckebach regime. Explicit calculation of entire classes of solutions is then possible, in particular the following results are obtained.

No matter the value of the stimulation amplitude, stable W rhythms appear as the stimulation period is increased through a SN and disappear through a PD bifurcation (Fig. 15 in [Cyt04]). Moreover, bistability between successive W rhythms is never encountered and instead, complicated rhythms, interspersed with chaotic cycles, are observed in the small interval of stimulation periods that separates successive stable W rhythms. In our model, for small stimulation amplitudes, stable W rhythms also arise as the stimulation period is increased through a SN and vanish through a PD point (Fig. 5.7). However, bistability is present between successive W rhythms and between the $2:1$ rhythm and the $3:2$ rhythm. This bistability phenomenon disappears when the stimulation amplitude is raised (Fig. 5.8), indeed making room for higher period rhythms in between successive W rhythms, but then the way through which stable W

rhythms appear and disappear is reversed: they are bounded by a PD point on the left and by a SN on the right. It is important to stress, however, that these discrepancies do not imply that the simplified 1D map of [Cyt04] does not reproduce correctly the phenomena occurring in the three-dimensional ODE model it is derived from. Indeed, the model studied in [Cyt04] is different from ours in that an instantaneous stimulus is used in [Cyt04], while we consider above a stimulation with non-zero duration and finite upstroke velocity (for the double reason that it seems more realistic and allows a continuation approach).

Finally, one can check that the summary given in Fig. 16 of [Cyt04] for the different stable rhythms and bistability phenomena that arise in function of the stimulation amplitude in the original smooth map is consistent with our own results : the five boxes of Fig. 16 in [Cyt04] correspond to the bifurcation diagrams of Figs. 5.8 and 5.10 – 5.13 in the present work (these diagrams are for $\varepsilon = 0.005$, $\sigma = 1$, but the situations illustrated in Fig. 5.10 – 5.13 are also found for $\varepsilon = 0.002$, $\sigma = 1$). Two situations that we report however, are not present in Fig. 16 of [Cyt04]: the situation in which the $1:1$ rhythm can directly be replaced by W rhythms as the stimulation period is decreased, the $2^k : 2^k$ period-doubled rhythms being bistable with the main $1:1$ rhythm (Fig. 5.5 – 5.7), and the situation in which bistability exists between successive W rhythms and between the $2:1$ rhythm and the $3:2$ rhythm (Fig. 5.5 – 5.7 as well). Since these situations are encountered in our model at stimulation amplitudes smaller than those at which the scenarios accounted for in [Cyt04] are observed, it might be that a smaller stimulation amplitude would allow to reveal these sequences in the 1D maps studied in [Cyt04]. In addition, let us remind that the direct $1:1 \to N:N-1$ transition is one of the experimental scenarios reported in [YJAG99] and that bistability between successive W rhythms and between $2:1$ and $3:2$ rhythms has been previously described in 1D map models of excitable systems [YR03].

5.4 Summary

We have shown that the evolution of the bifurcation diagram of the periodically forced excitable FHN model as the amplitude is raised is characterized by two limit amplitudes, I_0^- and I_0^+. These amplitudes define an interval outside which the behaviour of the system is trivial with a period-1 branch, B_1, everywhere stable. Inside this interval on the other hand, B_1 contains three main regions: two regions of stable solutions, which correspond respectively to $1:0$ and $1:1$ rhythms, and a region of unstable solutions between the two stable regions. In addition, a period-doubled branch, B_2, is connected on both ends to B_1. The $2:0$, $2:1$, and $2:2$ rhythms belong to this branch. Depending on the value of I_0, a variable (possibly infinite) number of additional period-doubled branches stem from B_2. The $N:1$ and $N:N-1$ rhythms ($N > 2$), when they exist, are themselves essentially located on loops isolated from the main "tree" and isolated from each other.

The different stable rhythms which belong to a common branch are separated by large unstable segments at small stimulation amplitudes, while these unstable segments shrink as the amplitude is raised, to finally disappear above some critical amplitude (note that $I_0 = I_0^+$ is this critical amplitude for the period-1 branch B_1). We have explained[12] that this phenomenon is related to the fact that the divergence of trajectories from the

[12]The reasoning was done with B_1, but a qualitatively similar argument can be applied to the other branches/loops.

threshold curve of the unforced equations fades in the vicinity of the right knee.

The predictions of our model have been compared to the results of prior experimental and theoretical studies. In particular, we are able to reproduce the different scenarios in which the $1:1$ rhythm can lose stability in paced isolated rabbit ventricular cells as the stimulation period is decreased [YJAG99]. The order in which these scenarios are observed experimentally as the stimulation amplitude is raised is better reproduced with $\varepsilon = 0.002$ and $\sigma = 2.5$ than with $\varepsilon = 0.005$ and $\sigma = 1$. The range of stimulation amplitudes in which Wenckebach rhythms exist is too large in comparison with what has been observed in cardiac cells [DMJ89, HADJ90]. It is however consistent with experimental results on squid giant axons [THM$^+$90].

Chapter 6

The periodically forced FHN relaxation oscillator

The present chapter consists in a study of the periodically forced FHN model (4.1)–(4.2) in its relaxation oscillation regime ($d = 0.2$, $\varepsilon = 0.005$, and $\sigma = 1$). After a reminder of some important theoretical results about periodically forced oscillators, the first part of the chapter is devoted to a continuation and bifurcation analysis of the ODE similar to that presented in Chap. 5. The second part of the chapter is itself devoted to the study of a circle map derived from the phase-resetting curve of the oscillator, the phase-resetting map (see Secs. 4.4 and 6.2.1). We examine to which extent this circle map constitutes a good approximation of the original ODE. We obtain the period-1 solution branches for the map without calculation, by a graphical operation on the phase-resetting curve (computations are needed only to locate the bifurcation points along the branches of period-1 orbits). We then compare these period-1 solutions to those of the ODE. This allows us to point out an important property of the bifurcation diagram of circle maps where the bifurcation parameter appears in an additive fashion only; namely, that the period-1 orbits belong to isolated loops when the topological degree of the map is one, whereas they belong to a unique branch when the topological degree is zero. In order to compare also the period-N orbits ($N > 1$) of the phase-resetting map to those of the ODE, we make use of the translational symmetry property of the bifurcation diagram of the phase-resetting map. This allows to avoid the explicit computation of the period-N orbits of the map. Finally, we discuss our results at the light of prior works where the phase-resetting response and/or the response to periodic stimulation of an oscillator has also been studied. The essential of the content of this chapter has been published [CGD09].

6.1 Ordinary differential equations

6.1.1 Theoretical background on periodically forced oscillators

Consider a planar oscillator described by a globally attracting limit cycle of period T_0 enclosing an unstable fixed point. If this oscillator is submitted to periodic forcing with period T and amplitude I_0, then the extended phase space of the system (the phase space with an additional dimension for the time), for each value of (T, I_0), is $\mathbb{R}^2 \times \mathbb{S}^1$. Indeed, the forcing being a periodic function of time unaffected by the oscillator, time

can be considered modulo the stimulation period T, and the state of the forcing can be represented by a phase varying between 0 and 1 (Fig. 6.1).

Figure 6.1. *The extended phase space of a periodically forced planar oscillator [AS82].*

6.1.1.1 Zero forcing amplitude

At zero stimulation amplitude, for any value of T, the extended phase space contains a globally attracting[1] invariant two-torus, given by the Cartesian product of the globally attracting limit cycle of the unforced equations by the circle $\mathbb{S}^1$ describing the forcing. It contains also an unstable limit cycle of period 1, enclosed within the torus, which is the Cartesian product of the unstable fixed point of the unforced system by $\mathbb{S}^1$ (Fig. 6.2). The globally attracting character of the invariant torus implies that, except for initial conditions on the unstable limit cycle, all the asymptotic dynamics occurs on the torus.

Figure 6.2. *The extended phase space of the forced FHN relaxation oscillator at zero amplitude, containing a globally attracting invariant two-torus and a repelling period-1 limit cycle [AS82].*

[1] A globally attracting invariant manifold contains all the attractors of the system, but may not be an attractor itself (see, e.g., [Wig90], Chap. 1).

The existence of a globally attracting invariant torus for the differential equations is equivalent to the existence of a globally attracting invariant circle for the "stroboscopic maps", or Poincaré maps, of the system (the 2D discrete maps[2] obtained by stroboscopically sampling the flow at time intervals equal to the forcing period T). Therefore, the stroboscopic maps of the system asymptotically reduce to circle maps $f : \mathbb{S}^1 \to \mathbb{S}^1$. These circle maps can be written under the form

$$\theta_n \to \theta_{n+1} = f(\theta_n) = \theta_n + T/T_0 \pmod 1.$$

Indeed, the limit cycle of the unforced equations (on which the oscillator still evolves since $I_0 = 0$) can always be re-parametrized by an angular variable $\theta = t/T_0 \pmod 1$, where t is the time elapsed since the state-point has crossed an arbitrary point on the limit cycle chosen as origin. This variable θ evolves at a constant rate on the unit circle, so that its increase between two crossings of a Poincaré section is always T/T_0. This type of map is called a *rigid rotation*, in reference to the constant rate of evolution along the unit circle.

6.1.1.2 Small forcing amplitude

At sufficiently small stimulation amplitude, both the invariant torus and the unstable limit cycle enclosed by the torus perturb smoothly, because they are *normally hyperbolic* invariant manifolds[3] when the stimulation amplitude is zero [Fen71, Wig94]. The normal hyperbolicity of the invariant torus at zero amplitude follows from the hyperbolicity[4] of the limit cycle of the unforced equations. Indeed, because this limit cycle is hyperbolic, the "growth" rate[5] of a perturbation transverse to the limit cycle is trivially larger than the growth rate of a perturbation tangent to the limit cycle, which is zero. Since the invariant torus at zero stimulation amplitude is given by the product of this limit cycle by S1, one of the two directions tangent to the torus is the direction tangent to the limit cycle, and the other tangent direction is the direction of "time". Because the forcing amplitude is zero, the growth rate of a perturbation in that second tangent direction is also zero. The (normal) hyperbolicity of the unstable limit cycle enclosed by the torus follows itself from the hyperbolicity[6] of the unstable fixed point of the unforced equations, by a similar reasoning. With the exception of the unstable limit cycle enclosed by the torus, no hyperbolic periodic solution can exist outside of the globally attracting torus at small forcing amplitude, because it would then have to exist at zero amplitude, while we made the assumption that no such orbit exists for $I_0 = 0$.

Hence, for sufficiently small I_0, the asymptotic dynamics is essentially restricted to an invariant torus, as it is the case at zero forcing amplitude. The stroboscopic maps of the system therefore also reduce asymptotically to circle maps $f : \mathbb{S}^1 \to \mathbb{S}^1$. These circle maps must be rigid rotations when $I_0 = 0$, so that, for sufficiently small I_0, they can be

[2] The Poincaré map is not unique because the timing of the first sampling is arbitrary.

[3] An invariant manifold is normally hyperbolic if, under the dynamics linearized about the invariant manifold, the growth rate (in absolute value) of perturbation vectors transverse to the manifold dominates the growth rate of perturbation vectors tangent to the manifold (e.g., [Wig94]). Figs. 4 and 5 of [Fen71] provide a nice illustration of why this condition is required for an invariant manifold to perturb smoothly.

[4] A limit cycle is hyperbolic if it has only one Floquet multiplier equal to one.

[5] In this case, this is rather a rate of decay, since the limit cycle is attracting.

[6] A fixed point is hyperbolic if it has no eigenvalue equal to zero.

written as:

$$\theta_n \to \theta_{n+1} = f(\theta_n) = \theta_n + I_0 G(\theta_n) + T/T_0 \pmod 1. \tag{6.1}$$

If I_0 and T are considered as parameters, the above equation defines a two-parameter family of circle maps, which has been extensively studied in the literature. Some of their important properties are now briefly recalled.

Consider the following general circle map, depending on the two parameters α and β:

$$\theta_n \to \theta_{n+1} = f(\theta_n; \alpha, \beta) = F(\theta_n; \alpha, \beta) \pmod 1, \tag{6.2}$$

where $F : \mathbb{R} \to \mathbb{R}$ is given by:

$$x \to F(x; \alpha, \beta) = x + \alpha g(x) + \beta, \tag{6.3}$$

and $g : \mathbb{R} \to \mathbb{R}$ satisfies:

1. $g \in C^1$ and $\left|\frac{dg}{dx}\right| \leq 1$,
2. $\forall x \in \mathbb{R}$, $g(x+1) = g(x)$.
3. $\int_0^1 g(x)dx = 0$.

The first two conditions on g are equivalent to requiring that f is a homeomorphism of the circle (that is, a continuous, invertible, circle map with continuous inverse) for $0 \leq \alpha < 1$. The third condition expresses that the mean of g over one revolution is zero or, equivalently, that β is the mean of the shift induced by the map over one revolution: $\beta = \int_0^1 (F(x) - x)\, dx$. So, it is easy to understand that every homeomorphism of the circle can be expressed under the form (6.2)–(6.3). In particular, only a redefinition of the parameters is necessary to express our equation (6.1) under this form. Indeed, this relation actually defines a homeomorphism of the circle since all stroboscopic maps of differential flows are homeomorphisms. Moreover, α, β and $g(x)$ can be defined as follows. If we introduce the notation $\bar{G} = \int_0^1 G(x)dx$, then we can assume $\alpha = I_0$, $\beta = T/T_0 + I_0\bar{G}$ and $\alpha g(x) = I_0(G(x) - \bar{G})$.

The essential of the asymptotic dynamics of circle homeomorphisms of the type (6.2)–(6.3) is described by the associated *rotation number*, which is defined as follows. For $\beta \in \mathbb{R}$ and $0 \leq \alpha < 1$, the rotation number of $f(x; \alpha, \beta)$ is:

$$\rho(\alpha, \beta) = \lim_{n\to\infty} \frac{F^n(x; \alpha, \beta) - x}{n} \tag{6.4}$$

where $F^n(x; \alpha, \beta)$ denotes the nth iterate of $F(x; \alpha, \beta)$, that is,

$$F^n(x; \alpha, \beta) = F\left(F^{n-1}(x; \alpha, \beta); \alpha, \beta\right).$$

The rotation number is thus the asymptotic average number of times the orbit winds around the unit circle per iteration of the map. When $\alpha = 0$ (rigid rotation), the rotation number is equal to β.

The rotation number has the following important properties (see, e.g., [Hal84], and refs. therein): For $\beta \in \mathbb{R}$ and $0 \leq \alpha < 1$,

1. $\rho(\alpha, \beta)$ exists and is independent of the x in the definition,

2. if $\rho(\alpha,\beta) = N/M \in \mathbb{Q}$, then there exists $\theta \in \mathbb{S}^1$ such that

$$F^M(\theta;\alpha,\beta) = F(\theta;\alpha,\beta) + N.$$

Let us now interpret these properties, and give some additional ones, in terms of the invariant torus of the differential equations. Geometrically, the rotation number corresponds to the average number of times the solution winds around a "meridian" of the torus per forcing period. When the rotation number is rational, the solution is periodic (property 2 above); when it is irrational, the solution is quasiperiodic, with the trajectory densely covering the torus. The uniqueness of the rotation number for a given value of $(T/T_0, I_0)$ (property 1 above) implies that the coexistence of periodic solutions of different period, as well as the coexistence of periodic and quasiperiodic motion, is forbidden on the torus (this would indeed imply the intersection of the trajectories). A stable periodic solution never exists alone on the torus, but is always paired with an unstable solution of the same period, with the stable solution being a nodal limit cycle, and the unstable one being a saddle limit cycle. Each rational point N/M on the T/T_0 axis constitutes the tip of a region in the $(T/T_0, I_0)$ parameter plane called an N/M *Arnol'd tongue* (or N/M *resonance horn*, or $M:N$ *phase-locking zone*), in which a periodic solution with period MT and rotation number N/M, called an $M:N$ *phase-locked rhythm*, exists. Generically, Arnol'd tongues open up into the upper half of the parameter plane as "wedges" (that is, with the two sides of the tongue not tangent to one-another)[7], bounded by saddle-node bifurcation curves.

6.1.1.3 Large forcing amplitude

At large stimulation amplitudes, the invariant torus is no longer guaranteed to persist as a differentiable invariant manifold, and indeed typically looses smoothness and breaks up. The aforementioned results then no longer hold and instead of studying the dynamics on a torus or circle maps, one has to revert to considering the full differential equations, or the associated stroboscopic maps of the plane. Although some general results do exist about the latter (e.g., [Pec90]), the dynamics of such systems is much less constrained than that of circle homeomorphisms, so that numerical tools (in particular, continuation) are often needed to study the details of the wealth of phenomena that can occur.

6.1.2 Results

We have computed period-M solution branches, with $M \leq 3$, of (4.1)–(4.2) with $d = 0.2$, $\varepsilon = 0.005$, and $\sigma = 1$. The normalized stimulation period T/T_0 (T_0 begin the period of the unforced relaxation oscillator) is used as bifurcation parameter and the stimulation amplitude I_0 is fixed in each bifurcation diagram. The stimulation period T is kept above $T_{min} \simeq 10\sigma$ and below some T_{max} which depends on the bifurcation diagram, but chosen large enough so that the $1:2$ rhythm is computed in each case ($2.25 < T_{max}/T_0 < 3$). As in Chap. 5, black curves represent stable periodic solutions, grey curves represent unstable periodic solutions, black crosses are saddle-node (SN) bifurcations, and purple

[7] Note that this is not the case of the classical sine circle map, for which all the Arnol'd tongues, except those of period-1, have their two sides tangent at the tip. This is because only the first mode in the Fourier expansion of the sine function has a non-zero coefficient (see, e.g., [MP96]).

circles are period-doubling (PD) bifurcations. The L_2-norm of the solutions, that is

$$\sqrt{\frac{1}{P}\int_0^P (v^2(t)+w^2(t))dt},$$

where P is the period of the solution, is plotted along the ordinate. The $M:N$ labels along the solution branches are assigned in the same way as in Chap. 5, except that the labeling can be started at $I_0 = 0$ (instead of $I_0 = I_0^-$) since all the $M:N$ rhythms already exist at zero amplitude in a periodically forced oscillator (*cf.* Sec. 6.1.1.2).

At small amplitudes, the "physiological" notion of an $M:N$ rhythm, where N is the number of action potentials (Sec. 4.1), coincides, for periodic solutions on the torus, with the mathematical notion of the rotation number theory, where N is the number of times the periodic solution winds around a meridian of the torus in the interval of period MT (Sec. 6.1.1). Indeed, because the stimulation amplitude is small, the effect in the phase plane of any stimulus given when the state-point lies close to the limit cycle of the unforced equations is only a slight deviation of the state-point from the limit cycle trajectory (this is the case, e.g., for the periodic solutions shown in the right panel of Fig. 6.4). In particular, the stimulus cannot bring the state-point to the portion of the threshold manifold (see Secs. 2.2.2 and 2.2.3) where an AP can be grown without going through a "complete" revolution around the limit cycle. Hence, the number N of APs is given by the unequivocal number of times the state-point winds around the limit cycle of the unforced equations. This number of windings is also the number N in the mathematical definition of an $M:N$ rhythm. Indeed, the phase plane representation shown, e.g., the right panel of Fig. 6.4, consists in a "projection" of the extended phase space $\mathbb{R}^2 \times \mathbb{S}^1$ onto $\mathbb{R}^2$ (projection "along" $\mathbb{S}^1$). In particular, because the invariant torus existing at zero amplitude perturbs smoothly at small stimulation amplitude, a trajectory in the phase plane everywhere close to the limit cycle of the unforced equations corresponds to the projection of a trajectory on the (perturbed) invariant torus onto the plane[8]. Therefore, the number of windings of such a trajectory in the phase plane around the limit cycle of the unforced equations is also the number N in the mathematical definition of an $M:N$ rhythm.

Let us now describe the evolution of the bifurcation diagram as I_0 is increased. For very small stimulation amplitudes, e.g., $I_0 = 0.1$ (Fig. 6.3), all stable periodic solutions belong to isolated closed loops in the bifurcation diagram. The only bifurcation points on these loops are saddle-nodes, which is consistent with the theoretical results described in Sec. 6.1.1.2. Most loops in Fig. 6.3 contain only two saddle-nodes, where the stable-unstable pairs of solutions meet, and which define their boundaries with respect to T/T_0 (and thus give the edges of the Arnol'd tongue in cross-section at that I_0). The period-1 loops, however, contain 3 pairs of saddle-nodes, which gives rise to regions of bistability. The zoom in Fig. 6.3, for instance, shows that there are two ranges of T/T_0 over which there is coexistence of two stable 1:1 rhythms ($0.9971 < T/T_0 < 0.9983$ and $1.003 < T/T_0 < 1.052$), which we term $1:1$ "self-bistability". Figure 6.4 shows one of these pairs of bistable $1:1$ rhythms. Continuation of the period-1 saddle-nodes in the two-parameter $(T/T_0, I_0)$ plane shows that the bistability exists all the way down to zero amplitude (Fig. 6.5). This does not contradict the persistence of the globally attracting torus mentioned in Sec. 6.1.1 since these solutions have the same period. In fact, the occurrence of such self-bistability at arbitrarily small stimulation amplitudes has been

[8]This is not the case of the phase-plane trajectories shown in Fig. 6.6, as explained later in the text.

shown to be a generic feature of periodically forced planar oscillators (see [MP96] and the discussion in Sec. 6.3.3). The regions in the two-parameter plane which are bounded by the "secondary" SN curves in Fig. 6.5 (dashed and dotted curves) have been termed *Arnol'd flames* [MP96, PK02].

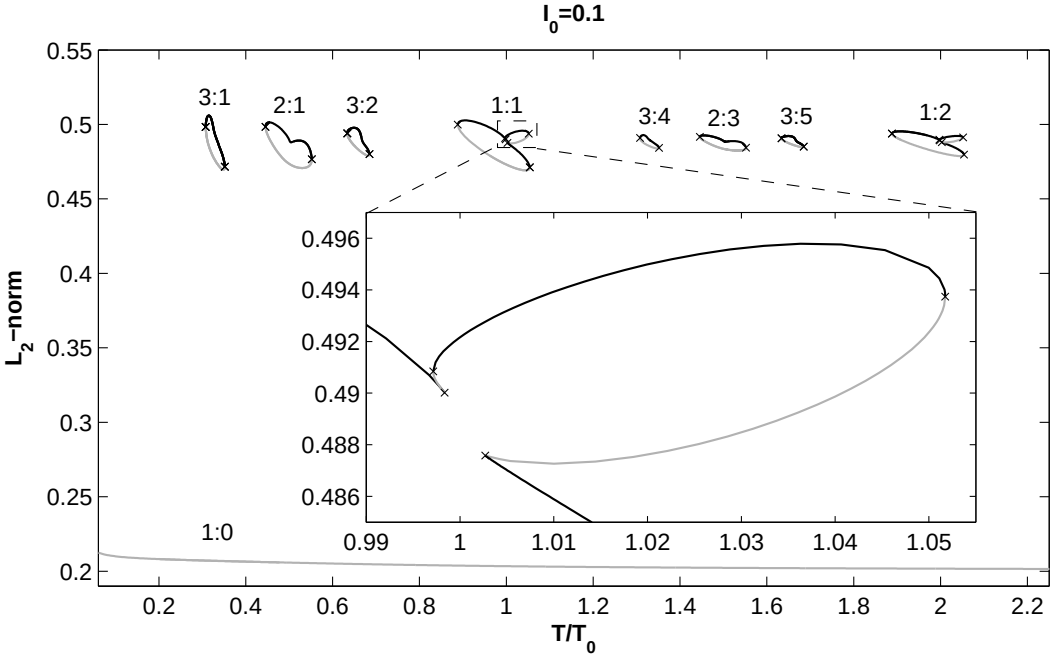

Figure 6.3. *Bifurcation diagram for* $I_0 = 0.1$. *Black curves indicate stable solutions; grey curves indicate unstable solutions. The only bifurcations present are saddle-nodes (x). The zoom on part of the* 1:1 *loop shows two of the three pairs of SNs on that loop, which give rise to* $1{:}1 \leftrightarrow 1{:}1$ *bistability (*1:1 *"self-bistability") in two ranges of* T/T_0.

In addition to the isolated loops, the bifurcation diagram at small I_0 contains an everywhere-unstable period-1 branch (bottom branch in Fig. 6.3). This branch reflects the persistence at finite I_0 of the unstable limit cycle existing in the extended phase space at zero amplitude. Indeed, projection of solutions from this branch on the (v, w) phase-plane show that the state-point remains in the vicinity of the unstable fixed point of the unforced system, passing closer and closer to it as the stimulation period increases (Fig. 6.6). These solutions are reminiscent of canards (see Appendix A), in that a portion of the trajectory follows the threshold manifold. The standard rotation number is not defined for these solutions since, for each given value of T/T_0, the solution does not lie on the invariant torus but constitutes the unstable limit cycle enclosed by the torus. However, they are clearly 1:0 rhythms according to the physiological definition of an $M{:}N$ rhythm (see Sec. 4.1).

Another characteristic of Fig. 6.3 is the approximate translational invariance of the bifurcation diagram. If the loops to the right of the 1:1 rhythm are shifted left by an amount $T/T_0 = 1$, then each $M : N$ loop for $T/T_0 > 1.2$ is paired with an $M : N-M$ loop for $T/T_0 < 1.2$, and the locations of the saddle-nodes on each pair of loops virtually coincide (Fig. 6.7). We shall return to consider this symmetry further later on (Sec. 6.2.2.5).

At a higher value of I_0, pairs of period-doubling points appear on the isolated loops. They are present, e.g., for $I_0 = 0.133$ (Fig. 6.8). In the ranges of T/T_0 where a period-

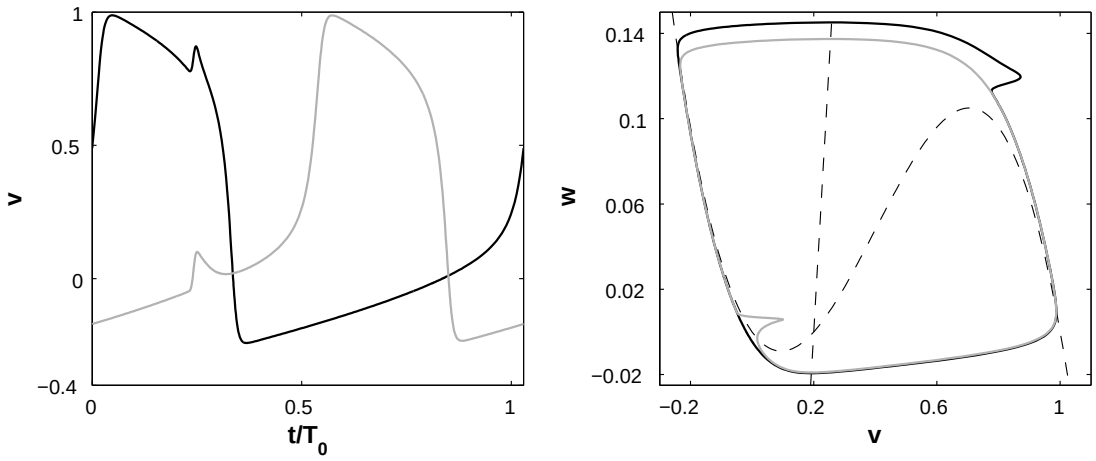

Figure 6.4. *The pair of bistable* 1:1 *rhythms existing at* $I_0 = 0.1$, $T/T_0 = 1.03$. *Left:* $v(t)$ *plotted over one period. Right: projection of the solutions on the* (v, w) *phase plane (solid curves). The trajectories are traveled counter-clockwise. Dashed curves give the nullclines of the unforced system.*

doubled solution is born, the invariant torus can no longer exist. Indeed, for a given value of T/T_0, the period-doubled solution cannot lie on the invariant torus because it would intersect the periodic solution from which it originates. Neither can it lie outside of this torus because this would imply a crossing of the invariant torus by the period-doubled solution.

One of the PD points from each pair is very close to the rightmost SN of each loop (e.g., at point C in Fig. 6.8), so that the two different bifurcations look like they are occurring at the same point in the figure. On some loops, the right PD point was not even identified by AUTO. This is because the continuation step used in these computations was not small enough to detect the two consecutive bifurcations (SN-PD). We have performed a two-parameter continuation of the left PD point for some loops and in each case, the PD bifurcation curve leads to the right PD point, as shown in Fig. 6.5 for the 1:1 loop. Figure 6.5 also shows that the proximity of the rightmost SN and PD points actually persists over a large range of parameters values, since the bottom part of the PD branch (thick purple curve) is indistinguishable from the nearest SN branch (solid black curve). The two bifurcation curves become more separated from each other as larger values of ε are used, and so we believe that their close proximity in Fig. 6.5 is related to the slow-fast nature of the system ($\varepsilon \ll 1$ in (4.1)). The fact that the two bifurcation curves extent greatly to the right (they actually extend further than the right limit of Fig. 6.5), in a quasi-horizontal manner, is also due to the smallness of ε.

The two PD points of each pair (e.g., A and C in Fig. 6.8) are connected by a branch of period-2 solutions. However, for the sake of clarity, we show in Fig. 6.8 the period-2 branch only for the 1:1 loop, and use a different colour scheme to indicate its stability (blue for stable solutions, orange for unstable solutions) in order to distinguish this branch from the period-1 branch. This period-2 branch is unstable for most of the range of T/T_0 values over which it exists, as the dominant orange colour indicates. A stable 2:2 rhythm is however present in the tiny region between point A (PD of period-1 solution) and point B (PD of period-2 solution). The two PD points A and B might thus be the first two members of a supercritical period-doubling cascade that produces period-

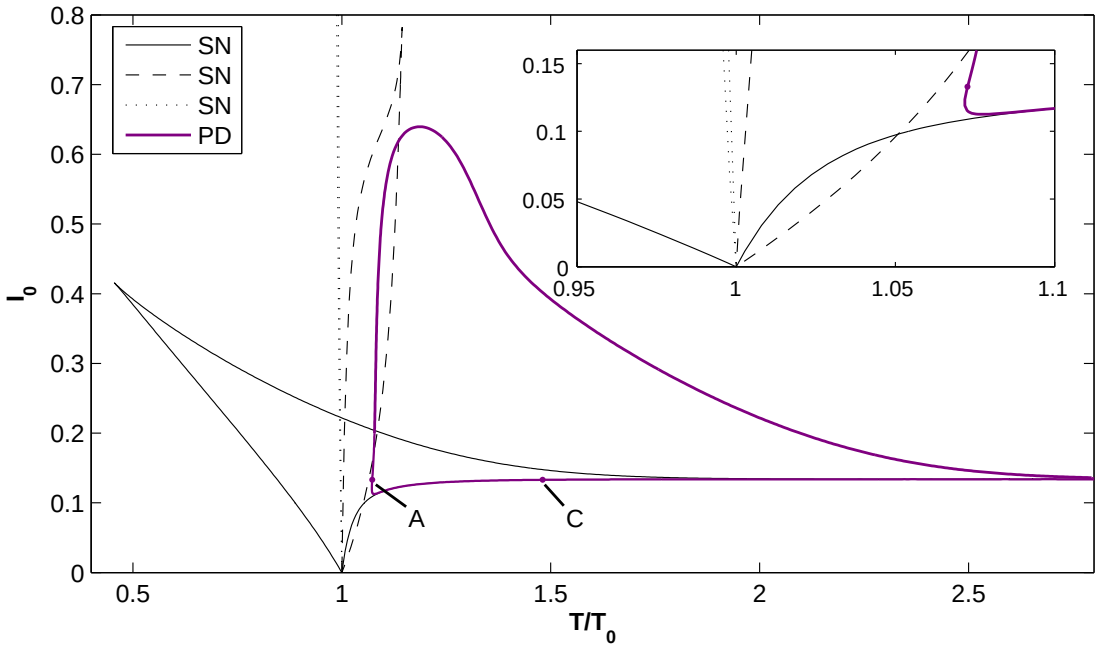

Figure 6.5. *Loci of the 3 pairs of SNs (thin solid, dashed, and dotted black curves) and of the pair of PDs (thick purple curve) on the* 1:1 *loop. The zoom shown in the inset allows the two SNs belonging to the narrowest locus (dotted curve) to be distinguished from each other. Points A and C are those from Fig. 6.8.*

doubled phase-locking zones within the Arnol'd tongues, and which can even progress to chaotic dynamics (e.g., [TK79, SDCM88]).

If the amplitude is raised just a little further, a spectacular change occurs in the bifurcation diagram: the period-1 loops merge with the everywhere-unstable period-1 branch, and the period-2 loops become period-2 branches attached to the period-1 branch through PD points. Indeed, for instance, for $I_0 = 0.135$ in Fig. 6.9, both the 1:1 loop, the 1:2 loop and the 2:3 loop have merged with the 1:0 branch, and the 2:1 loop is about to merge with a period-2 branch that has appeared below it. We were not able to determine numerically which of the period-1 loops merges first with the unstable period-1 branch: we find that all merge for $I_0 = I_{th} = 0.1338 \pm 0.0001$. The period-2 branch just below the the 2:1 loop in Fig. 6.9 also appears at $I_0 = I_{th}$, via the birth of a pair of PD points on the period-1 branch. We are convinced that this very delicate behaviour is related again to the slow-fast nature of the system, since the successive mergings can be distinguished if a larger value of ε is used (e.g., using $\varepsilon = 0.02$ and $\sigma = 0.25$). The 3:4 and 3:5 solutions, like the 3:1 and 3:2 solutions, still form closed loops in the bifurcation diagram for $I_0 > I_{th}$. But because the unstable parts of these loops pass very close to the period-1 and period-2 branches, this is not easy to realize at first sight (we have used orange in Fig. 6.9 to highlight the unstable segments of the period-3 loops). The crossings of the 3:4 and 3:5 loops with the 2:3 loop are only apparent (two different solutions can have the same L_2-norm). The rightmost SN on the 3:5 loop is very close to a SN on the period-1 branch, and remains so over a finite range of stimulation amplitude. This characteristic is yet again due to the small value of ε. Finally, the dotted grey curves in the background of Fig. 6.9 superimpose the bifurcation diagram for $I_0 = 0.133$ (disregarding stability), in order to underscore the huge change

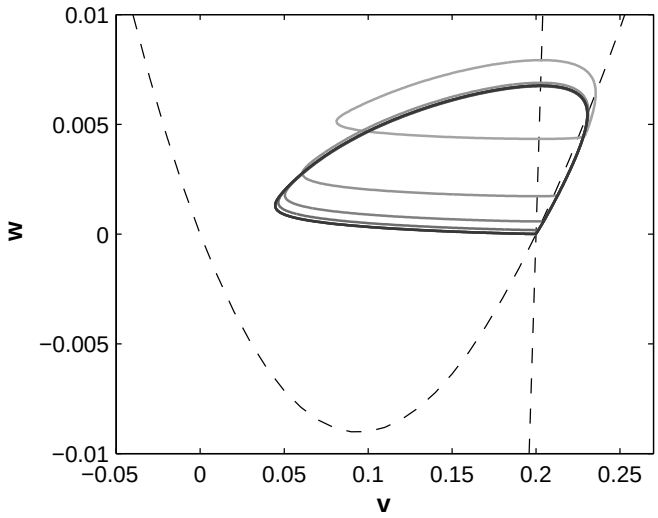

Figure 6.6. *Projections onto the* (v, w) *phase-plane of solutions belonging to the unstable* $1:0$ *branch for* $I_0 = 0.1$*, computed with AUTO. The unstable fixed point of the unforced system lies at the intersection of the nullclines (dashed curves).* T/T_0 *varies from* 0.234 *(lightest grey curve) to* 2.46 *(black curve).*

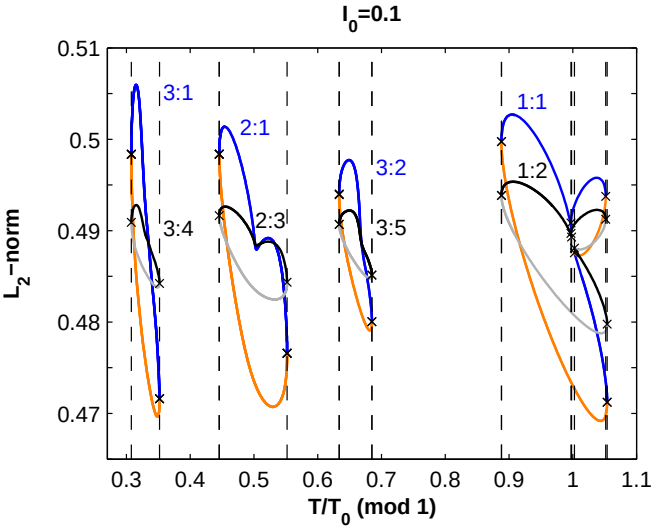

Figure 6.7. *Illustration of the approximate translational symmetry of the bifurcation diagram for* $I_0 = 0.1$*. The loops to the right of the* $1:1$ *rhythm are shifted left by an amount* $T/T_0 = 1$*. For the unshifted loops, blue indicates stable solutions, orange indicates unstable solutions. The locations of the SNs for the shifted loops are highlighted by vertical dashed lines, to allow comparison with the corresponding bifurcations for the unshifted loops.*

that has occurred in the qualitative picture following the minute change of amplitude from $I_0 = 0.133$ to $I_0 = 0.135$.

For $I_0 = 0.2$ (Fig. 6.10, upper panel), the $2:1$ loop has merged with the period-2 branch below it. The $3:2$ loop, in a fashion similar to the $3:5$ loop, now has its rightmost SN virtually touching the period-1 branch.

For $I_0 = 0.5$ (Fig. 6.10, middle panel), we no longer find stable $3:2$ and $3:5$ rhythms.

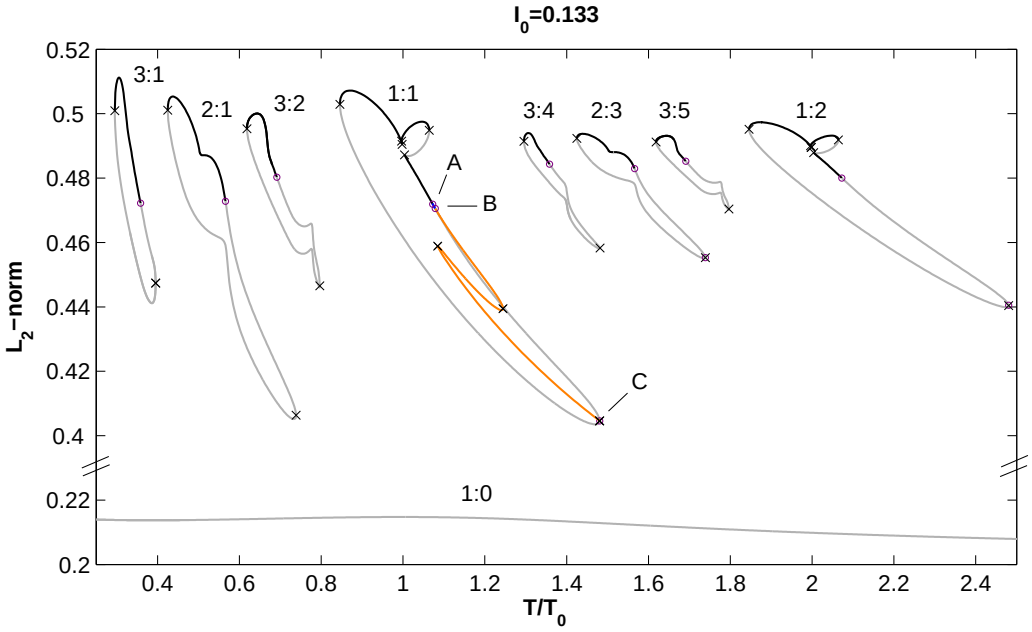

Figure 6.8. *Bifurcation diagram for* $I_0 = 0.133$. *Pairs of PD points (o) have appeared on the loops, with the rightmost PD point of each pair being very close to a SN (x), as at point C. The rightmost PD point has sometimes been missed by the computation (*cf. *text). The period-2 branch that connects each pair of PD points is shown only for the* 1:1 *loop. It is stable in the tiny region between point A and point B (blue) and unstable virtually everywhere between point B and point C (orange). The PD point A belongs to the period-1 branch while the PD point B belongs to the period-2 branch. Note the y-axis break.*

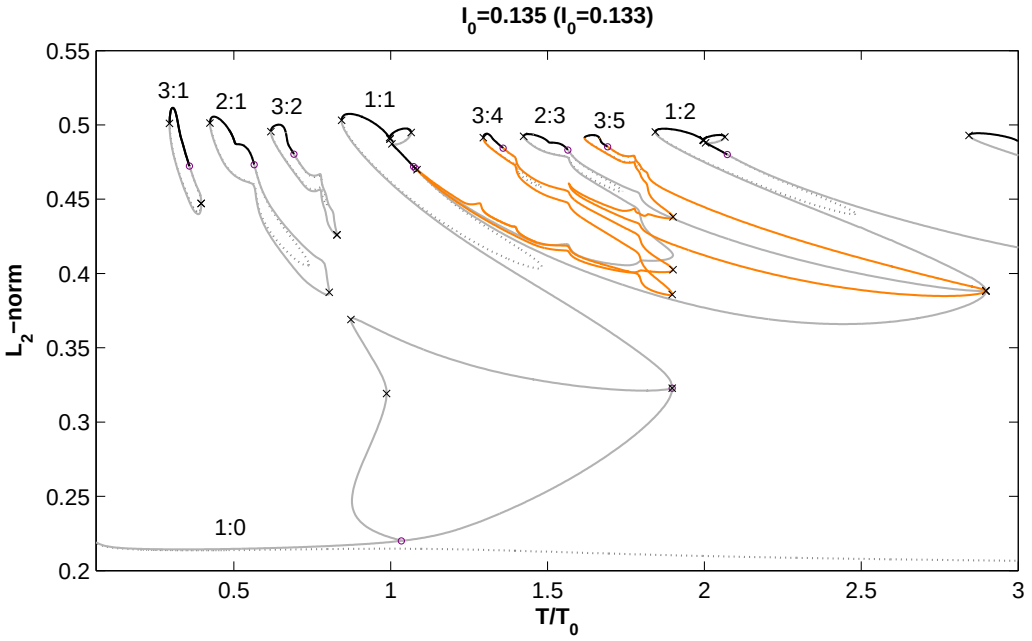

Figure 6.9. *Bifurcation diagram for* $I_0 = 0.135$. *The unstable segments of the* 3:4 *and* 3:5 *loops are drawn in orange, in order to facilitate their identification. The dotted curves in the background repeat the bifurcation diagram for* $I_0 = 0.133$ *(disregarding stability), in order to underline the huge qualitative change that has occurred.*

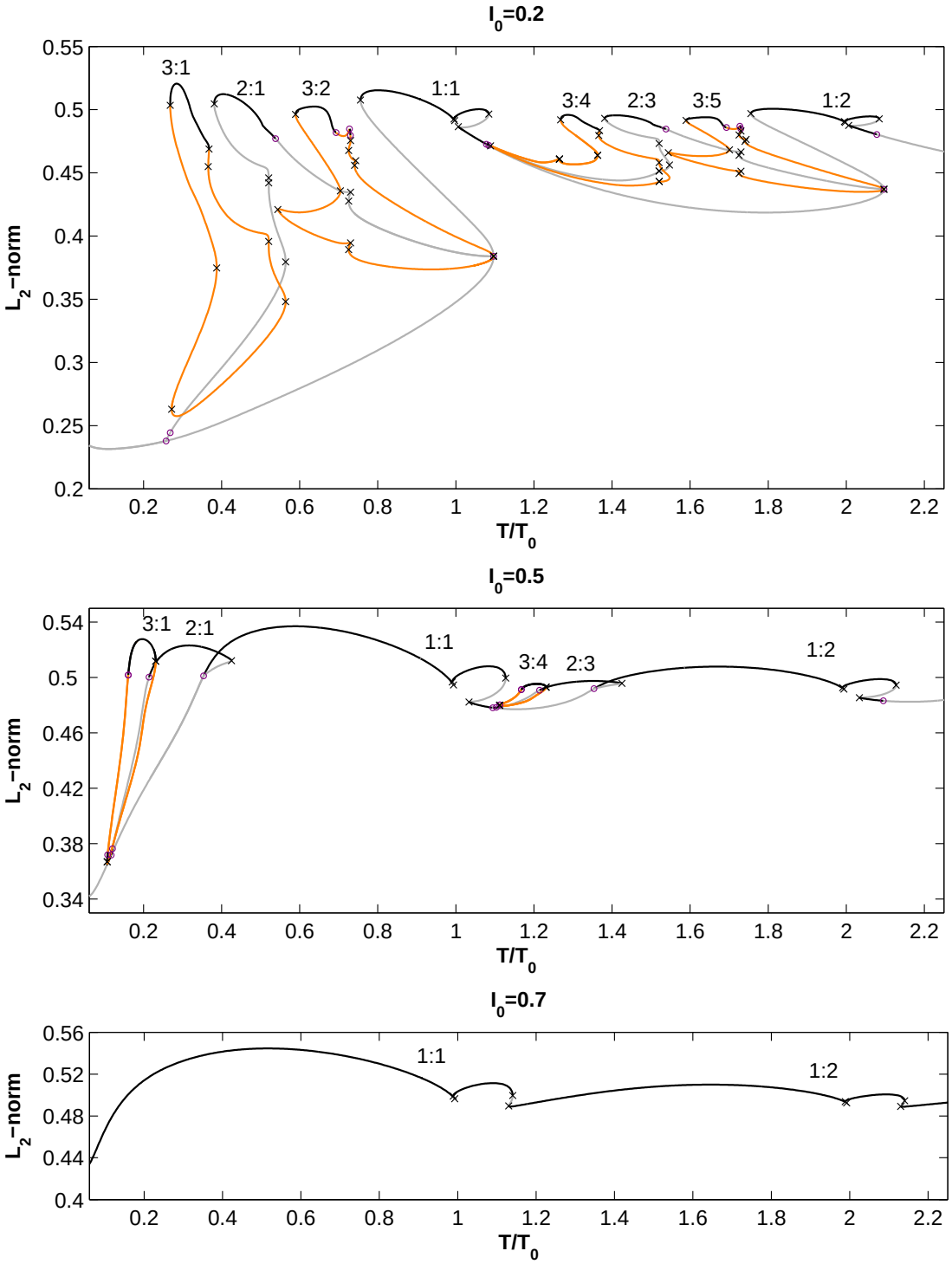

Figure 6.10. *Bifurcation diagrams for* $I_0 = 0.2$, 0.5 *and* 0.7. *The unstable portions of the period-3 loops are drawn in orange.*

Instead, $2:1 \leftrightarrow 1:1$ bistability and $2:3 \leftrightarrow 1:2$ bistability are seen. $3:1 \leftrightarrow 2:1$ bistability and $3:4 \leftrightarrow 2:3$ bistability are also present.

For $I_0 = 0.7$ (Fig. 6.10, lower panel), only the period-1 branch remains. All the period-doubled branches have disappeared through collision and annihilation of the PD points on each branch. All the loops have also disappeared, and it is likely that the period-1 branch is truly the only periodic solution left, since the external forcing is expected to dominate the dynamics of the system at very large stimulation amplitudes, as in several other models of periodically forced oscillators [DFSM89, GS94, GP83, KSA86, KST91, Pec90, SDCM88, VR89, PK02]. One of the two pairs of saddle-nodes still present on the $1:1$ branch for $I_0 = 0.7$ (the rightmost pair) disappears at slightly larger stimulation amplitudes ($I_0 = 0.782$), as can be seen from the closing of the dashed curve in Fig. 6.5. The remaining pair (dotted curve in Fig. 6.5) only disappears at a huge stimulation amplitude ($I_0 = 155$).

6.2 Phase-resetting map and comparison with the ODE

6.2.1 Prerequisite

6.2.1.1 Definitions

Consider an ODE possessing a stable limit cycle of period T_0 and suppose that the state-point lies initially on the limit cycle. If a *single* stimulus is given to the oscillator, the trajectory will asymptotically return to the limit cycle, unless the stimulus kicks the state-point out of the basin of attraction of the limit cycle (for the model we consider in this work, this would require the state-point to be kicked precisely onto the unstable fixed point enclosed by the limit cycle). However, if one compares the evolution of the oscillator to what it would have been in the absence of perturbation, there will generically be a temporal shift ΔT: the perturbed oscillator will reach a given point of the limit cycle with an advance or a delay compared to the time the unperturbed oscillator would have reached it. Two curves are used to quantify this effect [Win00]:

- The *phase-resetting curve* (PRC) gives the phase shift

$$\Delta\phi = \Delta T / T_0, \tag{6.5}$$

that is the temporal shift normalized by the intrinsic period, as a function of the phase

$$\phi = t_c / T_0 \pmod 1.$$

In this expression, the "coupling time" t_c is the time of delivery of the stimulus, measured from the moment at which the state-point has crossed an arbitrary point on the limit-cycle called "phase zero". For a cell which fires periodically, a common choice of phase zero is a point on the upstroke of the action potential [Sco79, GGS81, GGBS84, GSG86, GJ90, ADV$^+$91, TZF$^+$07]. The temporal shift and the phase shift are by convention positive when the asymptotic effect of the stimulus is to advance the state-point along the limit cycle ("phase-advance"), and negative for the reverse ("phase-delay") (e.g., [GS87, GJ90]). $\Delta\phi$ is usually defined modulo one, but we prefer not to restrict $\Delta\phi$ to $[0, 1)$ in this work for reasons we explain in Sec. 6.2.1.3.

- The *phase transition curve* (PTC) gives the "new phase"

$$\phi' = \phi + \Delta\phi \pmod 1 \tag{6.6}$$

as a function of the "old phase" ϕ. As a map from $\mathbb{S}^1$ to $\mathbb{S}^1$, the PTC is characterized by its *topological degree*, which is the net number of times ϕ' winds around the unit circle while ϕ winds once around the unit circle, or the mean slope of the PTC. The topological degree is also referred to as the "phase-resetting type" [Win00]. The notion of topological degree is related to that of *shifted cycle*, which is the locus of the points reached at the end of the stimulus[9] by all points belonging initially to the limit cycle (e.g., [GW84]). For a globally attracting limit cycle surrounding a single unstable fixed point in the plane, the topological degree changes from one to zero when the shifted cycle intersects the fixed point (*i.e.*, the shifted cycle encloses the fixed point when the topological degree is one, and no longer encloses it when the topological degree is zero).

Because the effect of the stimulus depends not only on the old phase, but also on the amplitude of the stimulus, there exists one PRC/PTC for each value of the amplitude. The phase shift and the new phase can only be measured exactly an infinite time after the stimulus has been given, since it takes an infinite time for the state-point to return to the limit cycle. However, when the limit cycle is sufficiently attracting, it is a good approximation to consider that the state-point is back to the limit cycle within a few intrinsic periods following the application of the stimulus or, in systems where there is a distinctive event occurring during the cycle (such as an action potential), within a few occurrences of that event.

6.2.1.2 Phase-resetting measurement

For the FHN oscillator we study in this work, it turns out to be a good approximation to consider that the state-point has reached its asymptotic new phase by the second AP following the stimulus (*i.e.*, we obtain virtually the same PRC and PTC if we wait for a third AP). Therefore, for each value of I_0 of interest, we computed the PRC in the following way (Fig. 6.11).

Starting with initial conditions corresponding to the chosen phase zero ($v_0 \simeq 0.519$, $w_0 \simeq -0.0149$), we applied a stimulus to the oscillator at a phase $\phi = t_c/T_0 \in [0, 1)$. For our gaussian-shaped stimulus pulse, t_c was taken as the time at which the stimulus goes through its maximum. The increment in ϕ from one run to the next was at most 0.001 (a smaller increment was used in the regions of phase where the PTC is particularly steep).

Following each stimulation, we waited for the occurrence of two APs and then measured the time t_{p2} at which the potential v (solid traces in Fig. 6.11) goes through the "event marker" $\{v = v_0,\ dv/dt > 0\}$ on the second AP. Crossing this event marker is indeed equivalent to crossing phase zero when the state-point is on the limit cycle. On the other hand, an unperturbed oscillator (dotted trace in Fig. 6.11) would have crossed the event marker on the same AP at $t = 2T_0$. Therefore, the temporal shift between the two oscillators by the second AP is $\Delta T_2 = 2T_0 - t_{p2}$ and the corresponding phase shift (called the "second transient phase shift" [Kaw81, GS87, GJ90]) is $\Delta\phi_2 = \Delta T_2/T_0$. As we stated above, no significative difference was observed when measuring instead ΔT_3 (temporal shift by the third AP), so that we could safely assume $\Delta T \simeq \Delta T_2$ and

[9] This notion is therefore rigorously defined only for a finite-duration stimulus.

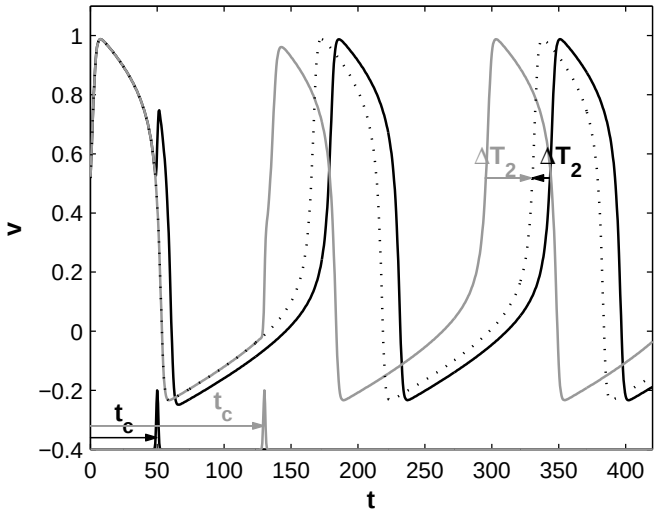

Figure 6.11. *Phase shift measurement for two different trials with $I_0 = 0.2$ (solid traces). The dotted trace shows the evolution of the v-variable for the unperturbed oscillator. For $t_c = 50$ (black trace), $\Delta T_2 < 0$ ("phase delay"); for $t_c = 130$ (grey trace), $\Delta T_2 > 0$ ("phase advance").*

$\Delta\phi \simeq \Delta\phi_2$. On the other hand, there were significant differences between ΔT_2 and ΔT_1 for some combinations of I_0 and ϕ.

The (arbitrary) criterion we used to acknowledge the occurrence of an AP is that the potential v becomes greater than $v_{AP} = 0.706$, which is the value of the potential at the right knee of the v-nullcline of the unforced equations (see, e.g., Fig. 6.4). We required additionally that the potential has first to decrease below 0 before a new AP can be elicited, so that deflections occurring during an AP (such as that caused by the stimulus in the black trace in Fig. 6.11) are not identified as additional APs.

The phase shifts we measure are always smaller than 1, since the "best" a stimulus of short effective duration can do is to cause the immediate occurrence of one extra action potential. On the other hand, $\Delta\phi$ can take all negative values; in particular it can be very negative if the stimulus moves the state-point close to the unstable fixed point of the system. Therefore we have $\Delta\phi \in (-\infty, 1)$.

Because a stimulus of sufficiently large amplitude is capable not only of advancing or delaying an existing AP, but also of eliciting an additional AP (see Fig. 6.13 and the animations "phiI0133tu.avi" and "phiI0135tu.avi" in supplementary material [epa]), there can be discontinuities of size 1 in the PRC (e.g., in Fig. 6.12 below) if $\Delta\phi$ is not defined modulo one. Indeed, for large enough amplitude, there exists a critical phase of stimulation such that for a phase smaller than this value, the perturbation immediately caused by the stimulus in the v waveform does not satisfy the definition of an AP we have adopted to construct the PRC, while it does satisfy this definition when the phase of stimulation is above the critical value (this critical phase exists no matter the definition of an AP chosen; only its value depends on the definition used). At this threshold value of the phase, a discontinuity is present in the PRC. Its size is effectively 1 provided the state-point is back to the limit cycle when the phase shift measurement is done, which is virtually the case by the second AP here. Such size-1 gaps in the PRC do not make the PTC discontinuous since ϕ' is defined modulo one. Gaps of size different from 1 appear in the first transient phase shift $\Delta\phi_1$, here (not shown) and elsewhere

[GGBS84, GS87, GSG86, GJ90, Kaw81, TZF$^+$07], and lead to discontinuities in the PTC if $\Delta\phi_1$ is used to estimate $\Delta\phi$. The reason why we wish to keep track of the size-1 gaps in the PRC, by not using the modulo in the definition of $\Delta\phi$, is given in the next section.

6.2.1.3 Phase-resetting map

In addition to its intrinsic interest as a characterization of the behaviour of an oscillator, the PTC or PRC can be used to derive a 1D discrete map (the "phase-resetting map") which, under certain conditions, can predict the behaviour of the oscillator under periodic forcing (see, e.g., [Sco79, YNPS99, CGG$^+$89, GGBS84, GG82, GGS81, PSB$^+$64]). Suppose that the ith stimulus is given when the state-point of the system lies on the limit cycle, at phase ϕ_i. Suppose also that it takes at most a time τ for the state-point to come back, to within a good approximation (to be defined, but this does not matter to the present argument), to the limit cycle after having been perturbed away from it. Then, if the stimulation period T is larger than τ, the state-point will be effectively back to the limit cycle when the next stimulus is applied, at phase ϕ_{i+1}. Calling ϕ_τ the phase at which the state-point comes back to the limit cycle, we have

$$\phi_{i+1} = \phi_\tau + \frac{T-\tau}{T_0} \pmod 1$$

since the state-point evolves on the limit cycle from ϕ_τ to ϕ_{i+1}. ϕ_τ is itself related to ϕ_i by

$$\phi_\tau = \phi'(\phi_i) + \frac{\tau}{T_0} \pmod 1$$

since $\phi'(\phi_i)$ is the asymptotic phase of the oscillator stimulated at ϕ_i when a hypothetically unperturbed oscillator would cross ϕ_i. So in the end, we have

$$\phi_{i+1} = f(\phi_i) = \phi'(\phi_i) + \frac{T}{T_0} \pmod 1 \tag{6.7}$$

where f is a circle map giving the phase just before the $i+1$st stimulus as a function of the phase just before the ith stimulus. It is obtained by simply shifting the PTC vertically by an amount T/T_0, and its topological degree is therefore the same as that of the PTC. The fixed points of the M^{th} iterate of the map represent period-M solutions for the periodically forced oscillator. They will coincide with solutions of the full ODE when the hypothesis $\tau < T$ is satisfied. One thus expects the map to work better at large stimulation periods. Equivalent ways of deriving (6.7) can be found, e.g., in [CGG$^+$89, CGM$^+$93, YNPS99].

In contrast with the family of circle maps discussed in Sec. 6.1.1.2, the phase-resetting map is not always a homeomorphism (that is, a degree-1 invertible map[10]), so that the original definition of the rotation number (6.4) cannot be used. The definition of the rotation number has however been generalized to non-invertible circle maps of any topological degree[11] [BG85]. Consider a circle map $f : \mathbb{S}^1 \to \mathbb{S}^1$ defined by the restriction to the circle of a real map $F : \mathbb{R} \to \mathbb{R}$, that is

$$\phi_i = f(\phi_{i-1}) = F(\phi_{i-1}) \pmod 1, \quad i \geq 1.$$

[10] Only circle maps of topological degree one can be homeomorphisms, but the reverse is not true – there can be non-invertible circle maps of topological degree one.

[11] Note that this is different from generalizing the rotation number to 2D maps, as is done, e.g., in [Pec90].

The rotation number for an initial condition ϕ_0 is defined by

$$\rho(f, \phi_0) = \limsup_{n\to\infty} \frac{1}{n} \sum_{j=0}^{n} \delta_j(\phi_j) \tag{6.8}$$

where

$$\delta_i(\phi_i) = F(\phi_i) - \phi_i, \quad i \geq 0.$$

In contrast with the rotation number of circle homeomorphisms (6.4), this generalized rotation number may depend on the initial condition (*i.e.*, coexistence of periodic solutions with different rotation numbers is possible in non-invertible circle maps).

For a periodic orbit of period M, $\{\phi_0^*, \phi_1^*, ..., \phi_M^*\}$ where $\phi_i^* = f(\phi_{i-1}^*)$, $i \geq 1$, and $\phi_M^* = \phi_0^*$, the rotation number is the rational number $\rho = N/M$ with

$$N = \sum_{j=0}^{M-1} \delta_j(\phi_j^*). \tag{6.9}$$

In this work, we use $F(x) = x + \Delta\phi(x \bmod 1) + T/T_0$. The map F is discontinuous at the critical phases at which, in the PRCs, an extra action potential is generated. This is an important feature because it guarantees that the changes of rotation number along the periodic solution branches of the circle map (see Sec. 6.2.2.3) will be linked to our definition of an AP, instead of being completely arbitrary[12]. For instance, it guarantees that the stimulation period T/T_0 at which, for large stimulation amplitudes, the $1:1$ rhythm changes into the $1:2$ rhythm along the period-1 branch will correspond to the generation of an extra action potential according to our definition (Fig. 6.14)[13].

6.2.2 Results

6.2.2.1 Phase resetting and phase transition curves

Fig. 6.12 shows the evolution of the PRC and PTC for increasing stimulation amplitude, computed by the direct numerical integration method described in Sec. 6.2.1.2.

For $I_0 = 0.1$ and $I_0 = 0.133$, the PRC is continuous and the PTC has topological degree 1. For $I_0 = 0.135$, the steepness of the curves has become so large around $\phi \sim 0.78$ that we could not determine their topology even by reducing the step in ϕ down to the minimum that double numerical precision allows ($\simeq 15$ significant decimal digits). That is why we do not show the PRC and PTC for this amplitude in Fig. 6.12. To get round this difficulty, we used a method originally developed for the computation of (un)stable manifolds of vector fields [KOD$^+$05]: we performed continuation of trajectories, defined as the solutions of a boundary-value problem where the initial conditions are fixed to phase zero and the integration time is set to $3T_0$, using the phase ϕ of the stimulus as the continuation parameter. Because AUTO uses pseudo-arclength continuation (which implies including all the state variables in addition to the free parameter in the definition of the step), the continuation stepsize reflects the change of

[12] Our definition is arbitrary as well, but at least it reflects as best as is possible with an arbitrary definition the conditions we think an AP should satisfy in the FHN model.

[13] If we had used instead $F(x) = x + (\Delta\phi(x \bmod 1) \bmod 1) + T/T_0$, that stimulation period would have simply been $T/T_0 = 1$, which is meaningless. Using the last-mentioned $F(x)$, or, equivalently, including the modulo in the definition of $\Delta\phi$ (6.5), is thus equivalent to erasing existing information (the size-1 gaps in the PRC) and then artificially reconstructing it.

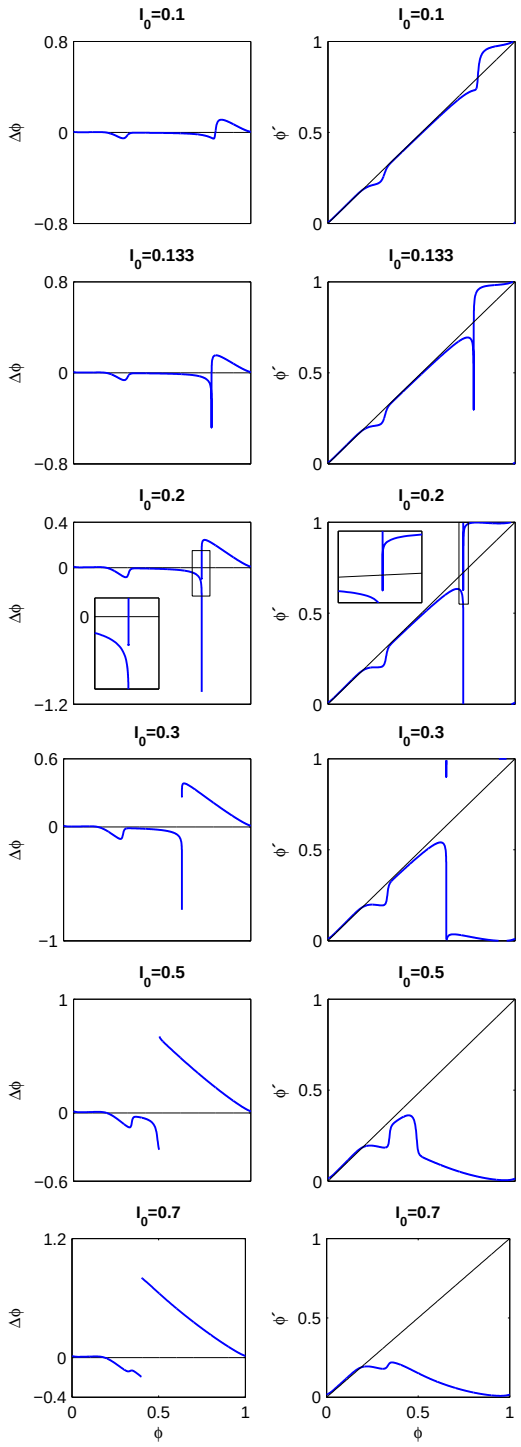

Figure 6.12. *Evolution of the PRC (left) and PTC (right) for increasing stimulation amplitude I_0. For $I_0 = 0.1$ and $I_0 = 0.133$, the PRC is continuous and the PTC is of degree 1. For $I_0 = 0.2$ and above, the PRC exhibits a discontinuity of size 1 and the PTC is of degree 0 (zooms help to see this for $I_0 = 0.2$). The curves were computed using the direct numerical integration method described in Sec. 6.2.1.2.*

the entire computed trajectory, and not only the change of the free parameter (as is the case of the stepsize in the direct numerical integration method used above). Therefore, we could follow much more finely, within the limits of double numerical precision, the evolution of the trajectories in the steeply changing region of the PTC. We could then deduce from the observed evolution that the topological degree is 0 at $I_0 = 0.135$. By repeating the procedure with different values of I_0, we could show that the change of topological degree occurs for $I_0 = I_{th} = 0.1338 \pm 0.0001$, which is also the amplitude at which the merging of the period-1 loops with the everywhere-unstable period-1 branch takes place in the bifurcation diagram of the original ODE. We explain the reasons for this coincidence in Sec. 6.2.2.4. In the supplementary material [epa], two animations "phiI0133uv.avi" and "phiI0135uv.avi", made from the trajectories computed by pseudo-arclength continuation, provide a nice way to see that the PTC is degree-1 at $I_0 = 0.133$ and degree-0 at $I_0 = 0.135$: these animations show the evolution in the phase plane of the point corresponding to ϕ' (approximated by the point reached at $t = t_c + 2T_0$) as the point corresponding to ϕ winds around the limit cycle once. They also reveal that the change of topological degree in the PTC of a relaxation oscillator involves canard-like trajectories: for ϕ in the steep region of the PTC, the trajectories follow the threshold manifold along a substantial part of their course (see also Fig. 6.13, lower panels). This is not surprising to the extent that, for stimulation amplitudes close to that at which the topological degree changes, one expects the stimulus to be able to bring the state-point "from" the limit cycle "to" the vicinity of the unstable fixed point[14], and that this unstable fixed point precisely belongs to the threshold manifold of the unforced equations along which canard-like trajectories can be generated (see Appendix A). Two other animations in [epa], "phiI0133tu.avi" and "phiI0135tu.avi", show the corresponding evolutions of the potential in time. These animations indicate that while a stimulus of amplitude $I_0 = 0.133$ is only able to advance or delay an existing AP in the v waveform of the FHN oscillator, a stimulus of amplitude $I_0 = 0.135$ is also able to "create" an additional AP in the v waveform (see also Fig. 6.13, upper and middle panels). This can be understood easily under the approximation that the effect of our stimulus is essentially a horizontal translation of the state-point to the right. Indeed, under this approximation, it is precisely when the shifted cycle stops enclosing the fixed point (which occurs at $I_0 = I_{th}$) that this shifted cycle starts crossing the portion of the threshold manifold "above" the fixed point, *i.e.*, that the stimulus becomes able to bring the state-point from the left branch of the v-nullcline to the portion of the threshold manifold along which responses with an appearance intermediate between that of a subthreshold response and that of an AP can be elicited (below the critical amplitude, only the portion of the threshold manifold "below" the fixed point is accessible from the left branch).

For all amplitudes above $I_0 = 0.135$ in Fig. 6.12, the PTC remains degree-0. Correspondingly, the PRC exhibits a discontinuity of size 1. As explained in Sec. 6.2.1.2, this gap reflects the fact that an additional AP can be grown in the v waveform of the FHN oscillator for $I_0 > I_{th}$.

6.2.2.2 Qualitative features of the phase-resetting map

Because the phase-resetting map is a simple vertical shift of the PTC, a few qualitative characteristics of the bifurcation diagrams for the 1D map can be deduced directly from

[14] This is because, under the approximation that the stimulus has a finite duration, the topological degree changes when the shifted cycle intersects the unstable fixed point (see Sec. 6.2.1.1).

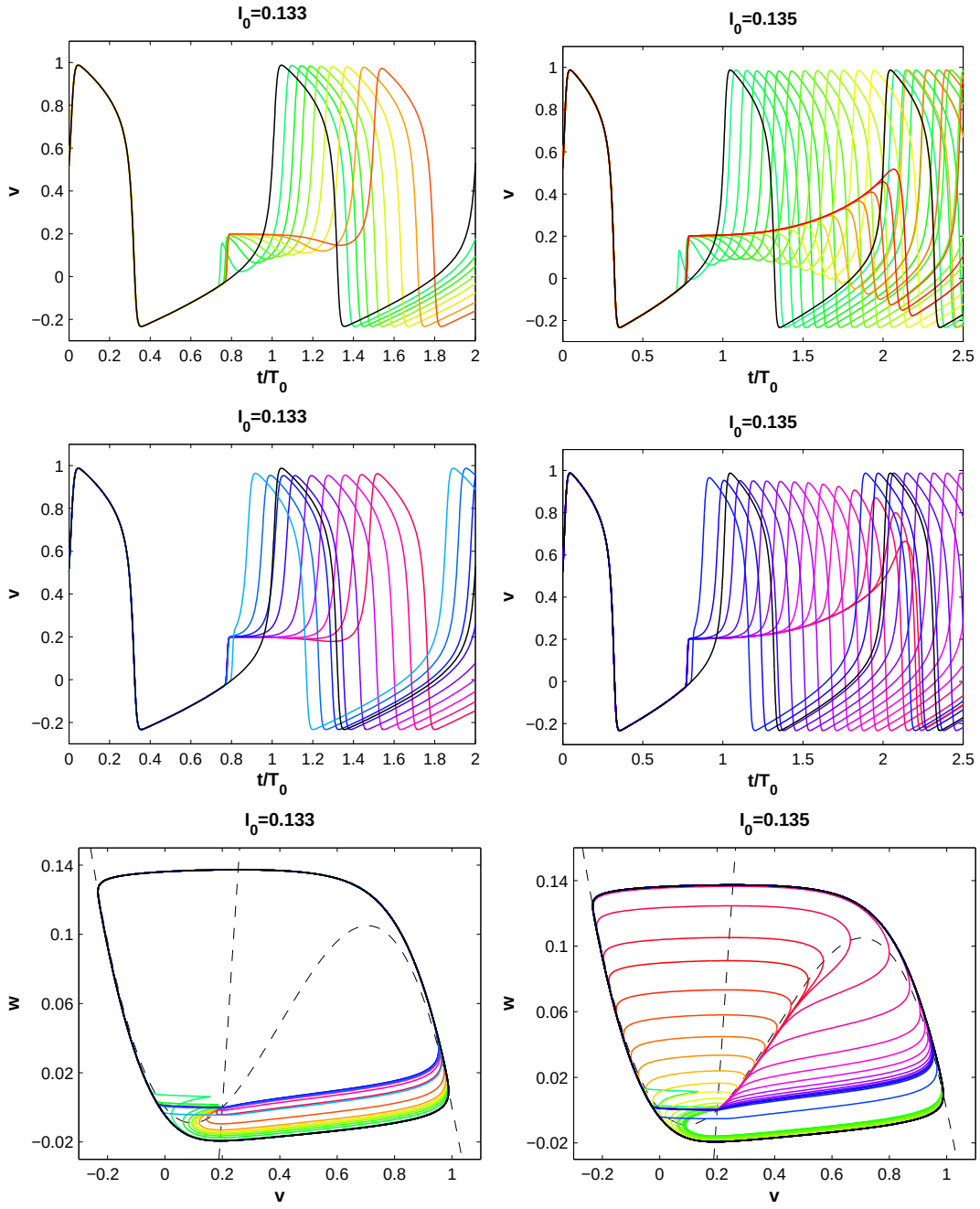

Figure 6.13. *Upper and middle panels: temporal evolution of the potential v for a sample of the trajectories used to make the animations provided in the supplementary material [epa]; lower panels: corresponding trajectories in the phase plane. In the upper panels, the phase at which the stimulus is given increases from green (through yellow) to red, and this increase in phase causes an increasing delay of the occurrence of the next AP; in the middle panels, the phase of stimulation continues to increase from red (through magenta) to blue, but the delay before the occurrence of the next AP is gradually resorbed. For $I_0 = 0.135$, the resorption of the delay occurs via the growth of a new AP, while no such additional AP is produced for $I_0 = 0.133$. The increase of the stimulation phase from one coloured curve to the next is invisible in most curves because it is very small; sometimes it is of an amount less than double numerical precision – this is why pseudo-arclength continuation was needed to obtain these trajectories.*

the appearance of the PTCs in Fig. 6.12.

For $I_0 = 0.1$, the PTC is monotonic, so that no iterate of the 1D map can exhibit PD points. This is consistent with the bifurcation diagram of the original ODE (Fig. 6.3), where none of the period-M loops exhibits PD points. In addition, the PTC exhibits two downwards deviations from the line of identity. This implies that there will bistability between period-1 fixed points in the map over a range of T/T_0 values (range over which the vertical shift of the PTC has four intersections with the line of identity). The corresponding range of $1:1$ self-bistability is found in the bifurcation diagram of the ODE (Fig. 6.3)[15].

For $I_0 = 0.133$, the PTC is no longer monotonic, exhibiting regions with slope ≤ -1. This implies that even the first iterate of the 1D map (the "period-1 map") will have PD points. This is consistent with the fact that even the period-1 loops exhibit PD points in Fig. 6.8.

From $I_0 = 0.2$ to $I_0 = 0.7$ in Fig. 6.12, the PTC gradually flattens out, so that the ranges of T/T_0 over which the fixed points of the map are unstable gradually shorten. This agrees with the fact that the period-1 branch becomes stable over increasingly large ranges of T/T_0 as I_0 increases in the ODE (Fig. 6.10).

6.2.2.3 Period-1 map: fixed points and their stability

In order to compare quantitatively the predictions of the phase-resetting map with the results obtained for the original ODE, one needs to compute the fixed points of the map as a function of the stimulation period T/T_0. In general, this requires solving a nonlinear algebraic equation for each value of the parameter, and the use of a continuation software is often helpful in that process. However, for the kind of map we consider in this work, where the parameter T/T_0 appears in an additive fashion only, no computation is needed to obtain the branch of fixed points for the period-1 map at a given value of I_0, as we show below.

From (6.6) and (6.7), the period-1 map is:

$$\phi_{i+1} = \phi_i + \Delta\phi(\phi_i) + T/T_0 \pmod 1,$$

so that its fixed points ϕ^* satisfy

$$\Delta\phi(\phi^*) + T/T_0 \pmod 1 = 0,$$

or

$$\phi^* = [\Delta\phi]^{-1}(-T/T_0 \pmod 1). \tag{6.10}$$

Of course, for some values of T/T_0, the inverse function $[\Delta\phi]^{-1}$ is not defined, or is multi-valued, but (6.10) still provides a simple graphical way to obtain ϕ^* as a function of T/T_0. Indeed, it implies that one simply needs to rotate the PRC by 90 degrees counterclockwise about the origin, and replicate the curve thus obtained at all distances equal to an integer along the T/T_0 axis (Fig. 6.14). Computations are needed only to locate the bifurcations along the branch of fixed points[16]. The result of these operations

[15] As mentioned earlier, another, tiny, range of $1:1$ self-bistability is present in the bifurcation diagram of Fig. 6.3. It is also accounted for by the presence of two deviations of the PTC from the line of identity, but one of these two (upward) deviations is so tiny that it is invisible in Fig. 6.12.

[16] These computations have consisted in: a) numerically estimating the derivative of the PTC from the points computed by the method described in Sec. 6.2.1.2; b) locateing the points at which two test functions defined to be zero resp. at a PD and at a SN change sign; c) using linear interpolation to improve the estimation of the locations of the bifurcations.

for the 6 values of I_0 from Fig. 6.12 are shown in the upper parts of the panels of Fig. 6.15. The lower parts of the panels show the corresponding bifurcation diagrams for the original ODE restricted to the period-1 solutions. Vertical dashed and dotted lines highlight respectively the locations of the SN and PD bifurcations for the ODE, in order to facilitate visual comparison with the bifurcations for the map (which are only indicated by the usual crosses and circles).

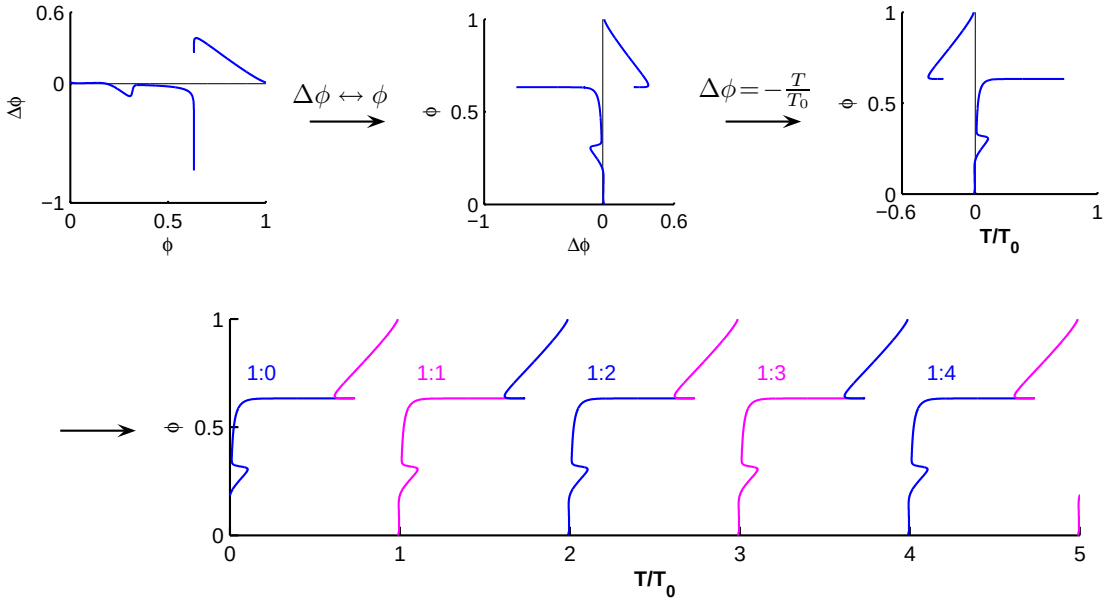

Figure 6.14. *Graphical operations needed to obtain the branch of period-1 fixed points. The bottom curve is defined in an implicit manner by* $\Delta\phi(\phi) = -T/T_0 + i$ *with* $i = 0, 1, \ldots, 5$ *for* $I_0 = 0.3$. *The rotation number is* $1/N$ *where, according to* (6.9), $N = F(\phi) - \phi = \Delta\phi(\phi) + T/T_0 = i$. *This implies that the rotation number changes at the same values of* T/T_0 *as those at which the branch changes colour.*

Quantitative comparison confirms that the phase-resetting map does an excellent job in accounting for the period-1 bifurcations occurring in the ODE until rather small T/T_0. For example, at $I_0 = 0.5$, the PD point occurring at $T/T_0 = 0.353777$ in the ODE coincides with that found in the map up to the first 6 digits. The phase-resetting map does not however account for the everywhere-unstable period-1 branch existing at small stimulation amplitudes (Figs. 6.3 and 6.8). This is because, for solutions belonging to this branch, the state-point never reaches the limit cycle of the unforced system (Fig. 6.6), so that the phase of stimulation is not even defined.

While the bifurcation diagrams in Fig. 6.15 allow a direct comparison between the two approaches insofar as the locations of the bifurcations are concerned, they do not allow comparison of all the solutions along the branches since the variables for the map and for the ODE are different. In order to make such a comparison, one would need to identify the phase of stimulation for the period-1 solutions of the ODE. The paradox is however that such an identification only makes sense when the map is a good approximation of the ODE, since phases are only defined for points belonging to the limit cycle of the unforced system. Nevertheless, one can always locate the point on the limit cycle

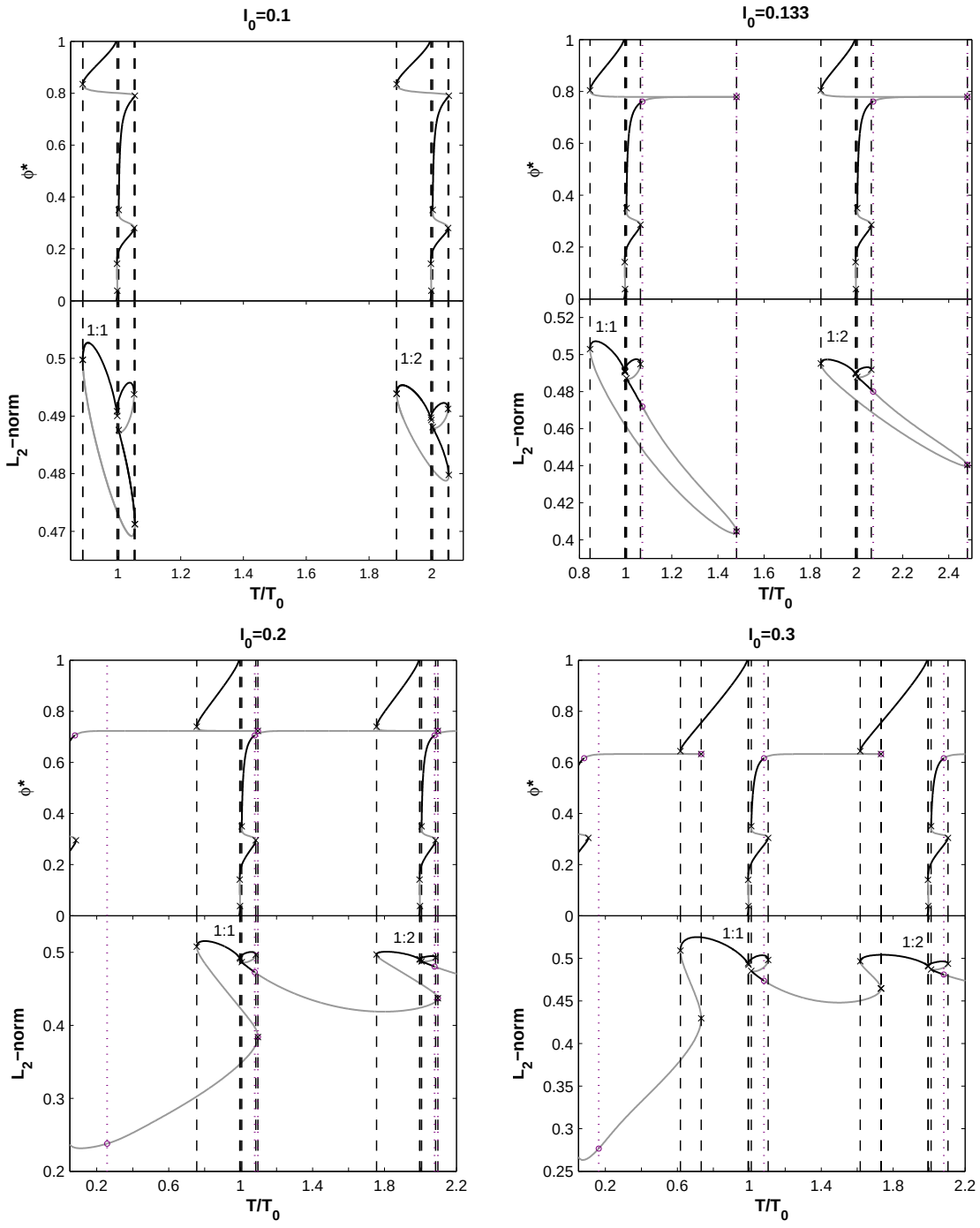

Figure 6.15. *Comparison of the period-1 solutions for the map and for the original ODE (resp. upper and lower sets of curves in each panel) for the values of I_0 used in Fig. 6.12. The locations of the bifurcations in the ODE are highlighted by vertical dashed (SN) or dotted (PD) lines. These lines look thick when two bifurcations occur for very close values of T/T_0.*

closest to the state-point at the moment when the stimulus is given, compute the phase corresponding to this point, and see how this phase compares with the phase predicted

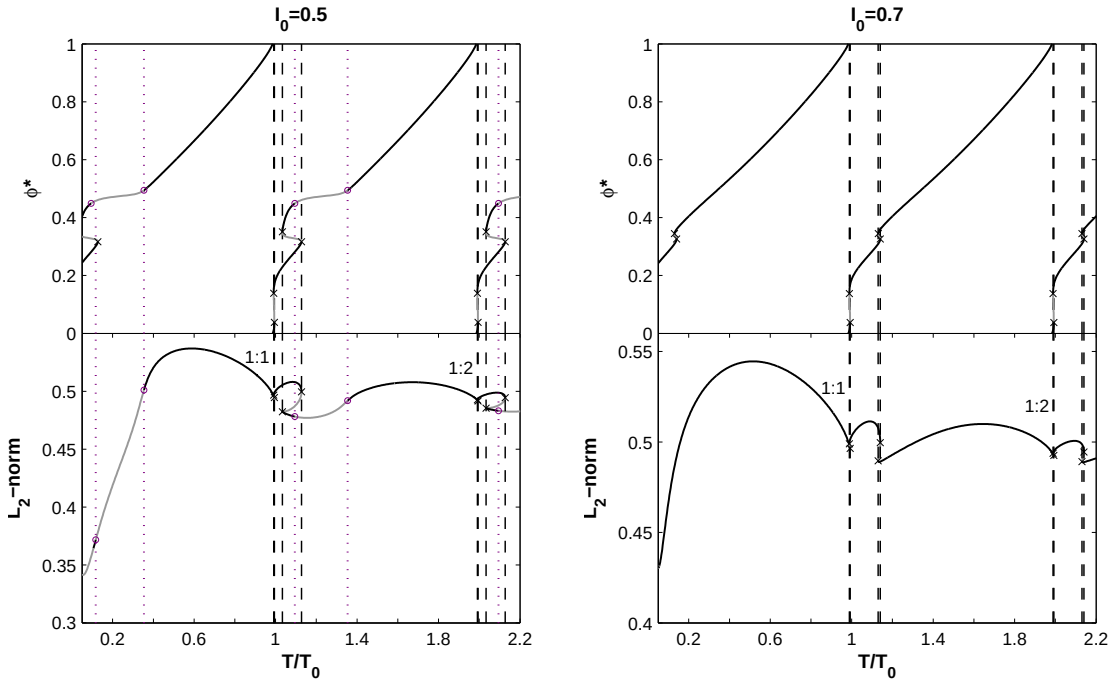

Figure 6.15. *(Continued)*

by the 1D map for the same stimulation period. Strictly speaking, this procedure does not yield a comparison between the two approaches (it is only a genuine comparison when the predictions of two approaches coincide, in which case it is pointless), but it does allow one to estimate the value of T/T_0 at which the 1D map approximation breaks down.

We have applied this procedure to a sample of the periodic solutions from the left part of the period-1 branch for $I_0 = 0.2$ ($T/T_0 < 1.1$ in Fig. 6.10, upper panel). The moment at which the stimulus starts is assumed to be $t_{m3} = t_{st} - 3\sigma$, where t_{st} is the time at which the gaussian-shaped stimulus goes through its maximum, since the effect of the stimulus can still be considered to be negligible before $t = t_{m3}$. The coordinates of the state-point at that moment are then compared to those of a stored array of points on the limit-cycle (obtained via a preliminary integration) to determine which of these points is the closest to the state-point. We use a weighted euclidean distance as our metric, with a 10 times larger weight for the w-variable since it varies over a range about 10 times smaller than the v-variable. The phase ϕ_{m3} of the closest point on the limit cycle is then identified (this identification is straightforward provided the preliminary integration of the equations has been carried out from the initial conditions corresponding to phase zero, and that time was stored at each step in addition to the coordinates of the points). We then compare the phase $\hat{\phi} = \phi_{m3} + 3\sigma/T_0 \pmod 1$ to the phase ϕ^* predicted by the map (indeed, the latter phase is defined considering the time at which the gaussian-shaped stimulus goes through its maximum, not the time at which the stimulus "starts"). The method just described has been used previously as an alternative to the method described in Sec. 6.2.1.2 to compute the PTC [GGMS83].

The left panel of Fig. 6.16 shows the projections onto the (v, w) phase-plane of the period-1 solutions of the ODE, labeled by a number that increases as T/T_0 decreases

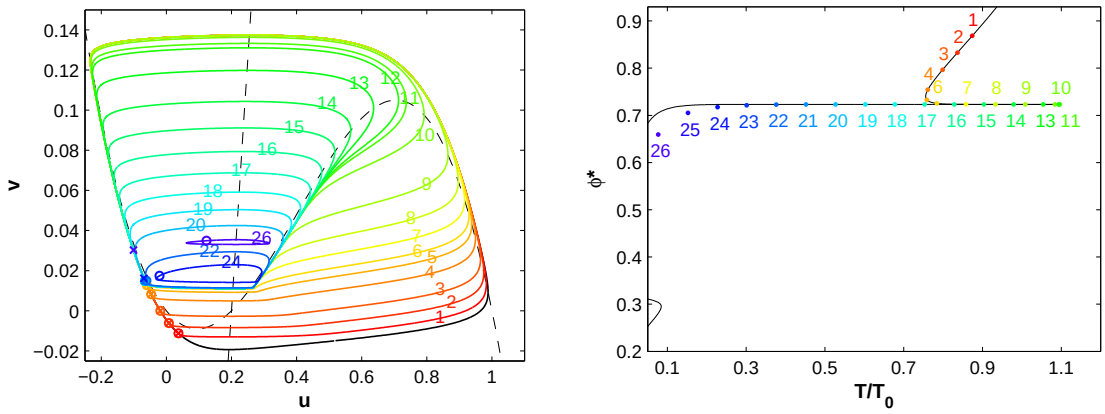

Figure 6.16. *Left: projections onto the phase-plane of a sample of period-1 solutions of the ODE for* $I_0 = 0.2$ *(*$0.05 < T/T_0 < 1.1$*). The unlabeled solid black curve is the limit cycle of the unforced system, the dashed curves are the nullclines, and the numbered coloured curves are the periodic solutions of the ODE. See text for details. Right: phases computed for the solutions shown in the left panel (numbered coloured dots) and phase predicted by the corresponding period-1 map (solid black curve).*

(the solutions numbered 21, 23, and 25 are not shown for the sake of clarity). The circle symbol on each trajectory represents the coordinates of the state-point at $t = t_{m3}$ and the corresponding cross represents the closest point on the limit cycle (the crosses (resp. circles) corresponding to the solutions numbered 7 to 22 appear superimposed in the figure because they correspond to very close stimulus phases, *cf.* right panel). The right panel shows the phases computed for the solutions in the left panel (numbered coloured dots), superimposed on the phases predicted by the map (solid black curve). The two sets of phases start to diverge around $T/T_0 = 0.3$. The discrepancy involves, as expected, the solutions with number 24 and above, since these are the solutions in the left panel for which the circles and crosses do not coincide, *i.e.*, solutions for which the assignment of a phase does not make sense. Also nicely illustrated in this figure is the canard-like behaviour of most of the unstable limit cycles along this branch (only the periodic solutions labeled 1 to 4, which are stable, and the periodic solution labeled 26, which is unstable, do not follow the threshold manifold along a part of their course).

6.2.2.4 Period-1 map: topology of solution branches

It is not a coincidence that the topological degree of the PTC changes at the same amplitude I_{th} as that at which the period-1 loops merge with the everywhere-unstable period-1 branch in the bifurcation diagram of the original ODE. Indeed, eqn. (6.10) implies that the fixed points of the period-1 map belong to isolated loops when the PTC is of degree 1 and to a unique branch when the PTC is of degree 0, as we explain now. Since $\Delta\phi = \phi' - \phi$, the mean slope of the PRC is obtained by subtracting one from the mean slope, or degree, of the PTC. Thus, when the PTC is of degree 1, the PRC has a mean slope equal to 0. Rotating the PRC by 90 degrees counterclockwise, to obtain the period-1 fixed points, gives a curve with infinite mean slope, that is a deformation of a vertical line. The ends of this curve, $\phi = 0$ and $\phi = 1$, thus have the same abscissa T/T_0. Because $\phi = 0$ is the same phase as $\phi = 1$, the curve is actually a closed loop. The bifurcation diagram for the period-1 map is thus made up of the replication of the

same loop every unit along the T/T_0 axis (e.g., upper curves in Fig. 6.15 for $I_0 = 0.1$ and $I_0 = 0.133$). In contrast, when the map is of degree 0, the PRC has a mean slope equal to -1, which implies that the curve of period-1 fixed points has a mean slope equal to 1. Its ends $\phi = 0$ and $\phi = 1$ thus span a distance of 1 along the T/T_0 axis, so that the replication of the curve every unit of T/T_0 gives in this case a unique continuous branch (e.g., upper curves in Fig. 6.15 for $I_0 \geq 0.2$). Hence, the bifurcation diagram of any circle map of the form (6.7) has its period-1 fixed points belonging to isolated loops when the topological degree of the map is one, while they belong to a unique branch when the degree is zero. To our knowledge, this topological property of circle maps had not been underscored before. As a consequence, if the 1D map is a good approximation of the original ODE, the change of topological degree in the map should occur at the same stimulation amplitude as that at which the period-1 loops in the bifurcation diagram of the original ODE merge with the everywhere-unstable period-1 branch, which indeed is what happens. However, it is important to remember that the 1D map does not account for the everywhere-unstable period-1 branch that exists at small stimulation amplitudes in the original ODE, whereas its presence is crucial to the merging phenomenon: from a topological point of view, the period-1 loops existing for $I_0 < I_{th}$ could not form an unbounded period-1 branch for $I_0 > I_{th}$ if they were not to collide with an unbounded period-1 branch at $I_0 = I_{th}$.

The important role of the everywhere-unstable period-1 branch in the main topological change of the bifurcation diagram of the ODE is not surprising to the extent that it reflects the existence of the unstable fixed point of the unforced system. Indeed, for planar oscillators described by a stable limit cycle surrounding a single unstable fixed point, the fixed point is crucially implicated in the change of topological degree of the PTC, since the change of degree occurs when the shifted cycle (see Sec. 6.2.1.1) intersects the unstable fixed point. Note however that the notion of shifted cycle is not rigorously defined for a stimulus with no clear-cut end such as the one we use in this work.

6.2.2.5 Period-M maps and translational symmetry of the bifurcation diagram

The translational symmetry that characterizes the bifurcation diagram for the fixed points of the period-1 map actually extends to the fixed points of all iterates (period-M maps), due to the additive dependence of the map on the bifurcation parameter T/T_0 (eqn (6.7)). Physically, this corresponds to the fact that stimulating the oscillator at time t or at time $t + T_0$ does not make any difference when the state-point lies on the limit cycle, since the phase reached by the state-point will be the same. More precisely, given a circle map of the form (6.7), if $\{\phi_1^*, ..., \phi_M^*\}$ is a period-M orbit for $T = T^*$ with rotation number $\rho = N/M$, then $\{\phi_1^*, ..., \phi_M^*\}$ is also a period-M orbit for $T = T^* + KT_0$, where K is any positive integer, and its rotation number is $\rho = (N + KM)/M$ [BG85, GG82].

As a consequence, and because we know that the phase-resetting map accounts almost perfectly for the solutions of the ODE at large stimulation periods, one way to evaluate how the map succeeds in approximating the original ODE at small stimulation periods is to determine to what extent the translational invariance is present in the bifurcation diagrams for the ODE. This indirect method is the only procedure we use in this work to compare the period-M orbits of the map to the period-M solutions of the ODE for $M > 1$, *i.e.* we do not explicitly compute fixed points of the period-M maps.

The translational invariance predicted by the map is well verified in the bifurcation

diagram of the ODE for $I_0 = 0.1$ (Fig. 6.7), since even the bifurcations on the $3:1$ loop coincide visually with those of the $3{:}4$ loop, when the later are shifted by -1 (the left SN is at $T/T_0 = 0.307797$ for the $3:1$ loop and at $T/T_0 = 0.307795$ for the $3:4$ loop, while the locations of the right SNs coincide up to 6 digits). For $I_0 = 0.133$ (Fig. 6.17) however, a large discrepancy is present at the right of the $3{:}1/3{:}4$ loops, whereas the left SNs still coincide up to 6 decimal digits. This might seem surprising, since one expects a priori the 1D map approximation to break down at the smallest stimulation periods, where the state-point gets the smallest amount of time to recover back to the limit cycle following a perturbation. However, at the right end of the $3:1$ loop, the stimulus falls at just the right phase to kick the state-point near to the fixed point of the unforced system, where the dynamics is very slow. Thus, even if there is more time to recover than at smaller stimulation periods, there is still not enough time to allow the state-point to return to the limit cycle before the next stimulus occurs – hence the 1D map approximation breaks down.

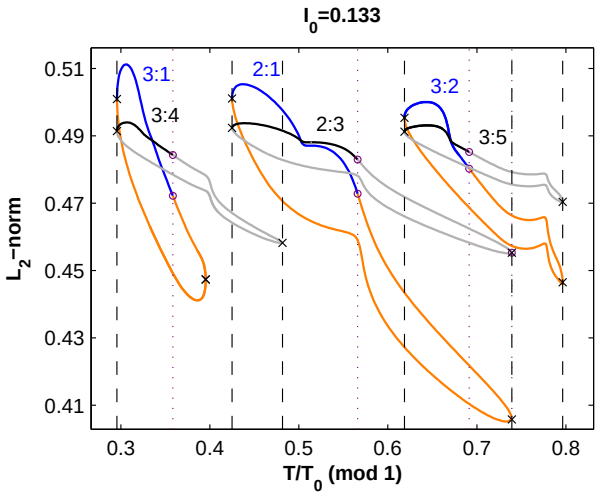

Figure 6.17. *Evaluation of the translational symmetry in the bifurcation diagram of the original ODE for $I_0 = 0.133$, using the procedure and conventions described in Fig. 6.7. Here, in addition, vertical dotted lines highlight the locations of the PD points for the shifted loops. The period-1 loops are not shown since their symmetry under translation can be deduced from the comparison with the fixed points of the period-1 map (Fig. 6.15).*

The picture for $I_0 = 0.135$ is even more striking (Fig. 6.18, upper panels), with the $3{:}4$ loop being completely different from the $3{:}1$ loop (left), and the $2{:}3$ having become a branch while the $2{:}1$ is still a loop (right). The phenomenon does not occur for $I_0 = 0.1$ (Fig. 6.7) because the stimulation amplitude is not large enough to kick the state-point from the limit cycle to near the fixed point, and it does not happen for $I_0 = 0.5$ (lower panels of Fig. 6.18) because the stimulation amplitude is too large to do so. For $I_0 = 0.2$ (middle panels of Fig. 6.18), a small discrepancy is still present at the right end of the period-3 loops, but it is much smaller than the discrepancy at the left end.

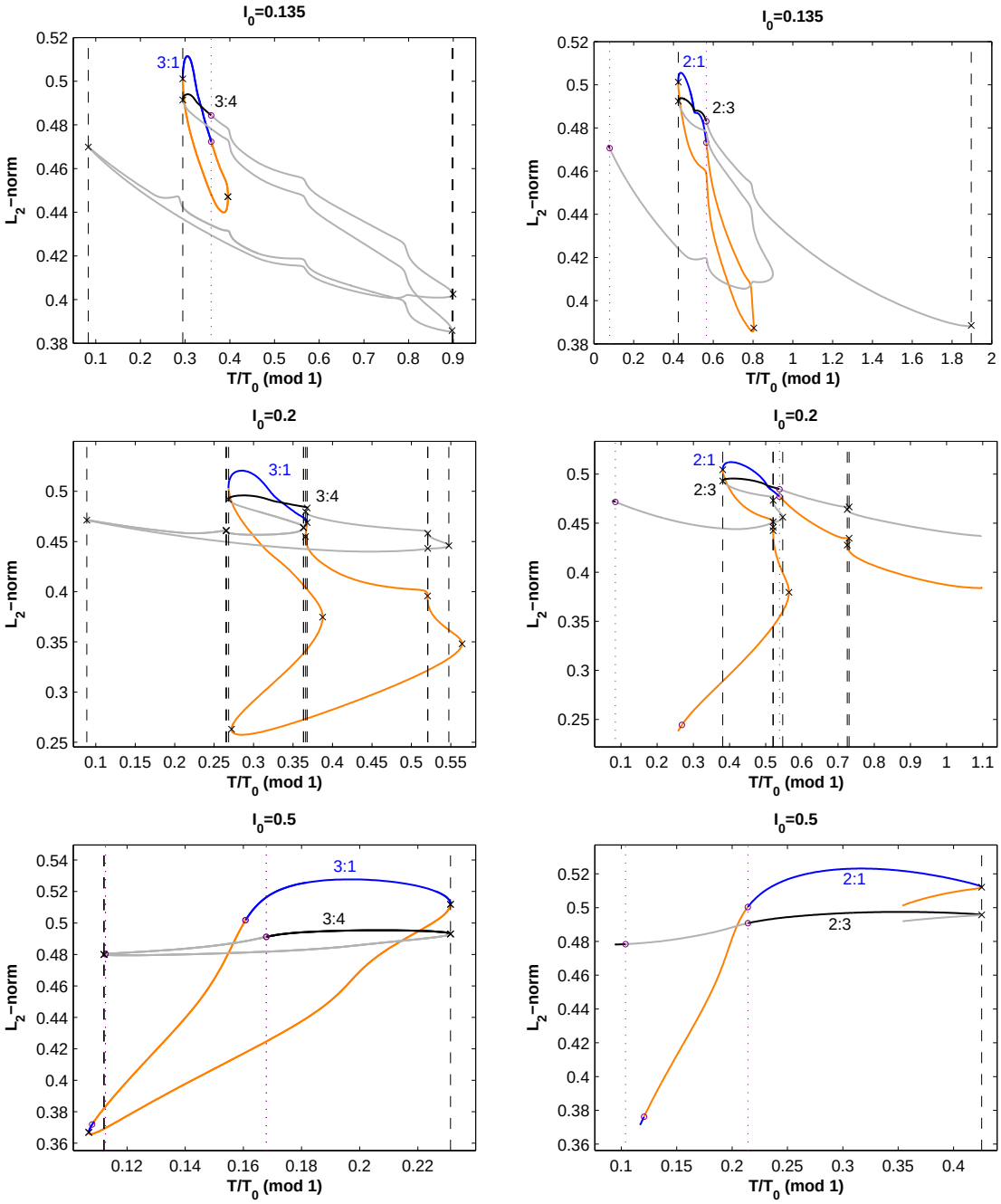

Figure 6.18. *Evaluation of the translational symmetry in the bifurcation diagram of the original ODE for* $I_0 = 0.135$, $I_0 = 0.2$, *and* $I_0 = 0.5$. *See Figs. 6.7 and 6.17 for the conventions. The* $3:1$ *and* $3:4$ *solutions (left panels) are plotted separately from the* $2:1$ *and* $2:3$ *solutions (right panels) to allow distinction of the different branches.*

6.3 Discussion

6.3.1 The topology of phase-resetting

As I_0 is increased, we find a transition from a degree-1 invertible PTC to a degree-1 noninvertible PTC to a degree-0 PTC (Fig. 6.12; see also [NSD$^+$94, CGG$^+$89]). All these three types of PTC have been reported previously in the FHN oscillator [Sco79, GGMS83, NSD$^+$93, YNPS99].

A simple continuity argument shows that at a sufficiently low stimulation amplitude, the PTC has to be of degree one and invertible, while at a sufficiently high stimulation amplitude, it has to be of degree zero[17][Win00]. A degree-1 curve can be invertible or not, while a degree-0 curve is, by definition, non-invertible. In models that are intrinsically discontinuous, as stimulation amplitude is increased, there can be a direct transition from a degree-1 invertible PTC to a degree-0 PTC (e.g., [GG82, GP84, KG84, Din87, GS94]). In continuous models, there is often a transition from a degree-1 invertible curve to a degree-1 non-invertible curve, and then to a degree-0 curve [Din88, GJ90, CGM$^+$93, NSD$^+$94]. There are also several other studies demonstrating parts of this sequence: e.g., the transition from invertibility to non-invertibility of a degree-1 PTC [GGBS84] or from a degree-1 non-invertible to a degree-0 PTC [Din87, DFSM89]. There have been very few systematic studies on non-invertible degree-1 PTCs. In one experimental study, the PTC was found to be non-invertible over about 50% of the range of amplitude over which it was of degree 1 [GGBS84], which is a larger range than we find above (at most 25%).

Even at the lowest I_0, there are three noticeable bumps in the PRC of our oscillator[18]. For example, at $I_0 = 0.1$ (top left of Fig. 6.12), the first bump (at $\phi = 0.2-0.3$) is caused by the stimulus extending the duration of the action potential (as can be seen, e.g., in the black trace in Fig. 6.4, left). The second bump, at $\phi = 0.7 - 0.8$ for $I_0 = 0.1$ (Fig. 6.12), is due to a prolongation of the "diastolic interval", which is the time between the end of the action potential and the start of the subsequent action potential (grey trace in Fig. 6.4, left). The third bump is at $\phi = 0.8 - 1.0$ and is caused by a shortening of the diastolic interval by the stimulus (grey trace in Fig. 6.11 shows this effect for $I_0 = 0.2$). While there are cases in experimental (e.g., [GGBS84, GSG86]) and modelling [GS87, GJ90, TZF$^+$07] work on cardiac oscillators where one can see all three of these bumps in the same PRC, the amplitude of the first bump is usually considerably less pronounced than in the FHN oscillator. As we discuss below, the amplitude of this bump has an important consequence in determining whether or not 1:1 self-bistability will be observable.

6.3.2 Discontinuities in the PTC

We have mentioned above (Sec. 6.2.1.2) that an artifactual discontinuity can arise in the PTC if the oscillator is not given enough time to recover from the stimulation before making the phase-resetting measurement [Kaw81, GJ90]. In experimental work on phase-resetting in electrophysiological systems, one often encouters a second type

[17]Indeed, on the one hand, in the limit of zero stimulation amplitude, the PTC must coincide with the line of identity; on the other hand, for very large stimulation amplitude, the shifted cycle can no longer contain the unstable fixed point enclosed by the limit cycle.

[18]As mentioned in Sec. 6.2.2.2, there are actually four bumps, but one is so tiny that it is not visible in Fig. 6.12.

of discontinuity in the PTC, with the sequence of transitions for increasing amplitude being: degree-1 invertible → degree-1 noninvertible → discontinuous → degree-0 [GGBS84, GSG86, KMGDG04]. The discontinuity is observed in the critical region of phases where the transition from phase-delay to phase-advance occurs, and is due to the "all-or-none" character of voltage depolarization in many excitable cells.

In 2D ODE models where the oscillation is described by a globally attracting limit cycle surrounding a single unstable fixed point, such as the FHN oscillator above, the PTC must be continuous except at the amplitude at which the topological degree changes [GW84]. This is a consequence of the fact that solutions of sufficiently smooth (Lipschitz continuous) vector fields depend continuously on the initial conditions. However, numerical integration at standard precision can fail to reveal the continuity of the PTC. We have found it necessary to apply a pseudo-arclength continuation method to resolve the apparent discontinuity in the FHN model (Sec. 6.2.2.1). While pseudo-arclength continuation has previously been used in an ionic model to reveal the continuity of the PTC [KMGDG04], this was done in an indirect way, in that the continuation parameter was not the phase of stimulation, but rather the value reached by the voltage immediately after the stimulus. This was done to allow continuation on the unforced equations, because the stimulus used (a rectangular pulse) was not smooth and thus not suitable for continuation. The method we employ in this work uses the phase of stimulation ϕ itself as the continuation parameter, and so allows a direct unambiguous demonstration of the continuity of the PTC. Oscillator models that are formulated in an inherently discontinuous fashion (e.g., "integrate-and-fire" models [GM79, GW84, Gla01]) exhibit unavoidable discontinuities in their PTCs.

6.3.3 1:1 self-bistability

Bistability and the resultant hysteresis have been well known in forced relaxation oscillators for a very long time (e.g., [vdPvdM27, Jac90]). We observe several forms of bistability in the forced FHN oscillator, among which are: $1:1 \leftrightarrow 1:1$ (Figs. 6.3 and 6.4: $I_0 = 0.1$; Fig. 6.10), $1:1 \leftrightarrow 2:1$ (Fig. 6.10: $I_0 = 0.5$), and $2:1 \leftrightarrow 3:1$ (Fig. 6.10: $I_0 = 0.5$). We shall restrict the present discussion to only one of these bistabilities: the $1:1 \leftrightarrow 1:1$ bistability, or 1:1 self-bistability.

In the forced FHN oscillator, the 1:1 self-bistability extends from zero amplitude all the way up to very high I_0 (Fig. 6.10). In the two-parameter plane, this self-bistability corresponds to the presence of 1:1 Arnol'd flames in addition to the main 1:1 SN curve (Fig. 6). The 1:1 self-bistability is accounted for by the phase-resetting map (Fig. 6.15), with the origin of the main range of bistability being traceable to the fact that there are two regions ("bumps") of phase-delay in the PRC (Fig. 6.12, left). At the lowest amplitudes at which this self-bistability is seen, the map is an invertible degree-1 circle map (e.g., $I_0 = 0.1$, top right in Fig. 6.12), which is in contrast to other forms of ("non-self-")bistability, which require non-invertibility: *i.e.*, either a non-invertible degree-1 or a degree-0 map (e.g., [PG82, GGBS84, KG84, BG85, Din87, NSD$^+$94, GAG08]). At the largest amplitudes at which we observed the 1:1 self-bistability, the phase-resetting map is a degree-0 circle map (e.g., $I_0 = 0.7$, bottom right in Fig. 6.12). Recent experimental and modelling work on a hydrodynamical relaxation oscillator [GAG08] also shows the occurrence of 1 : 1 self-bistability in the degree-0 regime of phase-resetting (it is not clear whether an earlier report on the FHN oscillator was for a degree-0 or a degree-1 non-invertible phase-resetting map (Fig. 5c of [NSD$^+$94])).

In most published diagrams of Arnol'd tongues from maps and ODEs, there is an amplitude below which no bistability is seen (e.g., Fig. 78 in [Arn83]; Fig. 5 in [GGBS84]; Fig. 8 in [NSD$^+$93]). This is rather surprising given that the presence of an Arnol'd flame in at least one of the N/M Arnol'd tongues has been shown to be a generic feature of invertible circle maps, and therefore also of periodically forced planar oscillators, at small forcing amplitude [MP96]. We see two possible reasons for which self-bistability has rarely been detected.

First, it could be that self-bistability is restricted to very small ranges of parameters. There are indications that this is the case, in particular, for the $1:1$ self-bistability. Indeed, in electrophysiological experimental [GGBS84, GSG86] and modelling [GS87, ADV$^+$91, GJ90, TZF$^+$07] work, one can see PTCs with two downward bumps, but the amplitude of the first bump is typically very small. This implies that the range of T/T_0 over which the $1{:}1$ self-bistability would be predicted to exist would be very narrow. In one study where a parametric fit was made to the PRC in order to obtain the phase-resetting map over a wide range of amplitude, this first bump was even completely ignored, and so $1:1$ self-bistability, had it been truly present, would not have been predicted to exist [GGBS84]. Thus, a very carefully targeted experimental search would have to be made to look for $1{:}1$ self-bistability, which might not be found in the presence of noise.

The second possible reason is that most of the forced oscillators that have been studied hitherto are nongeneric in the sense defined in [MP96], so that they cannot exhibit self-bistability. This is true, e.g., of the famous canonical "sine-map" model of Arnol'd [Arn83]. In addition, the majority of experimental and modelling studies on forced oscillators used forcing with a pure sine-wave, while the few works in which self-bistability has been reported employed a forcing waveform with higher harmonics [RVR84, RPE02, PK02]. This could reflect the fact that the first category of forced oscillators (the sinusoidally forced ones) is nongeneric.

6.3.4 The omnipresent period-1 solution in forced oscillators

In the bifurcation diagram of the ODE, there exists, at sufficiently small I_0, an everywhere-unstable period-1 branch (e.g., Figs. 6.3, 6.6, 6.8), corresponding to the persistence of the unstable period-1 solution enclosed by the invariant torus. The everywhere-unstable period-1 branch merges with the period-1 loops as the amplitude is raised, so that one then has alternating stable and unstable period-1 segments (e.g., Figs. 6.9, 6.10). This evolution of the bifurcation diagram for the period-1 solutions had been predicted analytically many decades ago for the sinusoidally forced van der Pol oscillator, but in the weakly nonlinear limit (see [vdP27] for the original result about the $1{:}1$ solution, and, e.g., [HSN60, Hay64] for the extension to other period-1 solutions). Numerical studies on non-relaxation oscillators have confirmed this prediction [KAS86, KSA86] and have shown that the collision of the two period-1 solutions corresponds to the breaking of the invariant torus for the corresponding values of (T, I_0). They have also shown that the collision of period-2 solutions, such as the one that is about to occur for the $2{:}1$ rhythm in the bifurcation diagram for $I_0 = 0.135$ (Fig. 6.9), implies the breaking of the invariant torus at the corresponding parameter values as well. Our numerical results indicate that the same collision scenarios occur in a relaxation oscillator.

The existence of a period-1 solution for all values of T and I_0 has been proven for the periodically forced FHN model [KRS04], as well as for a simple forced 2D oscillator (the

Poincaré oscillator) [GS94]. However, these two proofs say nothing about the stability of the period-1 solution and the possible co-existence of other period-1 solutions, whereas the analytical and numerical results discussed above shed light on these aspects.

6.4 Summary

We have compared the dynamics of a periodically forced relaxation oscillator to that of a one-dimensional discrete map of the circle derived from the phase-resetting curve of this oscillator. We have shown that the agreement between the two approaches is, for most stimulation amplitudes, very good until rather small stimulation periods. The discrepancies observed are easily explained in terms of the violation of the hypotheses underlying the derivation of the circle map. In addition, guided by the topological changes observed in the bifurcation diagram of the original ODE as the stimulation amplitude is raised, we have shown that the bifurcation diagram of any circle map where the bifurcation parameter appears only in an additive fashion is characterized by the the period-1 fixed points belonging to loops when the map is of topological degree one, and to a unique continuous branch when the topological degree is zero. To our knowledge, this is the first time this property of circle maps has been underscored.

Conclusions and perspectives

In this thesis, we have studied the response of the FitzHugh-Nagumo model of a slow-fast system to a periodic, pulsatile forcing. This model provides a qualitative description for both an excitable and a spontaneously beating cell submitted to a periodic train of electrical pulses, which is a configuration often studied in cardiac electrophysiology. Indeed, it provides a simplified model of the situation of a cardiac cell in the intact heart, where the cells undergo a periodic stimulation under the form of an electrical current propagating from the sinus node. We have used continuation methods to compute periodic-solution branches for this system, taking the stimulation period as bifurcation parameter and studying the evolution of the bifurcation diagram as the stimulation amplitude is raised. To our knowledge, this is the first time that continuation methods have been applied to the study of a pulse-forced slow-fast system.

In both the excitable and oscillatory regimes, we find that there exists a critical amplitude of stimulation below which the behaviour of the periodically forced slow-fast system is "trivial": in the excitable case, the bifurcation diagram consists of a single stable $1:0$ branch, and in the oscillatory case, all the stable $M:N$ rhythms belong to isolated loops. In addition to the isolated loops, an everywhere-unstable $1:0$ branch is present in the bifurcation diagram of the forced relaxation oscillator below the critical amplitude.

In both systems, the appearance of the bifurcation diagram changes very abruptly as the critical amplitude is crossed, while it re-simplifies much more softly beyond some other amplitude, to reduce finally to an everywhere-stable period-1 branch. We have explained that this asymmetry is related to the slow-fast nature of the system. In the excitable system, the critical amplitude is the amplitude at which a first pair of PD points appears on the period-1 branch, quickly followed by the development of a whole "tree" of period-doubled branches. The first of these period-doubled branches, the period-2 branch, exhibits a large stable $2:1$ segment. On both sides of this stable $2:1$ segment, isolated loops are present. They correspond to $N:1$ rhythms ($N > 2$) on the left of the stable $2:1$ segment, and to $N:N-1$ ($N > 2$) or Wenckebach rhythms on the right of the stable $2:1$ segment. In the relaxation oscillator, the critical amplitude is the amplitude at which the period-1 and period-2 loops, the $2:1$ loop excepted, merge with the everywhere-unstable period-1 branch. A pair of PD points also appears at the critical amplitude on the period-1 branch, on the left of the $1:1$ rhythm. The $2:1$ loop merges with the unstable period-2 branch born from this pair of PD points at slightly larger stimulation amplitude. As for the period-3 loops, they remain isolated.

If we make the approximation that the effect of our stimulus in the (v, w) phase-plane is a horizontal translation of the state-point to the right, then the critical amplitude appears to coincide with the amplitude necessary to bring the state-point:

- in the excitable case, from the *stable* fixed point of the unforced equations, located

on the left branch of the v-nullcline, to a point on the threshold manifold;

- in the oscillatory case, from a point on the left branch of the v-nullcline to the *unstable* fixed point of the unforced equations, located on the threshold manifold.

It follows that the critical amplitude coincides, in both cases, with the amplitude at which the stimulus becomes capable of eliciting an action potential along the portion of the threshold manifold located "above" the fixed point.

In the forced relaxation oscillator, the above observation is equivalent to stating that the critical amplitude is also the amplitude at which the shifted cycle intersects the unstable fixed point, *i.e.*, it is the amplitude at which phase-resetting changes type. We have explained this coincidence by the fact that the phase-resetting map, a circle map derived from the phase-resetting curve of the oscillator, constitutes a good approximation of the periodically forced oscillator. Indeed, we have shown that the bifurcation diagram of any such circle map, where the bifurcation parameter appears only in an additive fashion, is always characterized by the period-1 orbits belonging to isolated loops when the topological degree (the type) of the map is one, while these period-1 solutions belong to a unique branch when the topological degree is zero. Hence, if the phase-resetting map constitutes a good approximation of the differential equations, it must change topological degree at the same stimulation amplitude as that at which the merging of the period-1 solution branches occurs in the bifurcation diagram of the original differential equations, which is indeed what is observed.

Perspectives

For both the excitable system and the relaxation oscillator, it would be valuable to pursue the study of the bifurcation curves in the two-parameter plane, *i.e.*, to extend Figs. 5.2 and 6.5 to the loci of the other bifurcations encountered along the solution branches, and to analyse the resulting pictures in detail.

Another interesting extension of our work would be to study how the bifurcation diagrams and bifurcation curves evolve as the difference in time scale between the two variables of the slow-fast system is decreased. We expect[19], of course, some degenerate phenomena to disappear; for instance, the extreme proximity of some solutions branches and bifurcation points in several bifurcation diagrams (e.g., Figs. 5.5–5.7; Figs. 6.8–6.10), the simultaneous merging of all period-1 loops with the everywhere-unstable period-1 branch in the forced relaxation oscillator,... We also expect torus (Neimark-Sacker) bifurcations to develop along the branches, since the presence of a torus bifurcation curve in the two-parameter plane has been shown to be the rule for periodically forced planar oscillators [Pec90]. Their absence, or at least, their evanescence, in our system is very likely due to the fact that such bifurcations can appear only in three-dimensional systems, while a periodically forced slow-fast system is nearly two-dimensional (that is why a family of 1D maps can, to a great extent, provide an approximation to the system, as the Poincaré maps of a two-dimensional ODE are one-dimensional.). A three-parameter continuation analysis (with the third parameter being the time scale difference between the variables) of a periodically forced relaxation oscillator has already been carried out [MPL93], but for a symmetrical system, so that the study of a non-symmetrical pulse-forced relaxation oscillator might still reveal new phenomena.

[19] And we have already checked that this is the case in some instances, *cf.* Chap. 6.

The transition from the oscillatory regime to the excitable regime in a forced slow-fast system could also be interesting to investigate with continuation tools. This has already been done for a periodically forced non-slow-fast system [OK94], *i.e.*, a system in which, depending on the parameter values, the unforced equations have either a globally attracting fixed point, or a globally attracting limit cycle. Torus bifurcation curves were found to be involved in the transition. This transition has also been investigated in a slow-fast system [YNPS99], but without continuation methods, so that the nature of the bifurcations bounding the different stable regions in the two-parameter plane, and the way they interact during the transition, were not examined.

As we have reminded in Chap. 6, the standard notion of rotation number is defined for circle homeomorphisms, and therefore applies to periodically forced oscillators at small forcing amplitude only. We know that extensions of this notion have been proposed, to forced oscillators at large forcing amplitude on the one hand [PL86, Pec90], and to forced excitable systems on the other hand [ADO90]. It would be interesting to determine how these extensions relate to the physiological notion of an $M:N$ rhythm.

In the study of the periodically forced relaxation oscillator, we have examined a 1D map approximation of the ODE, which takes the form of a circle map. The aim was mainly to uncover the connections between the topological changes observed in the bifurcation diagram at a critical value of the stimulation amplitude and the topological property of circle maps known as the topological type or degree. We are not aware of the existence of an analogous property for maps of the interval, which are typically the kind of 1D maps the periodically forced excitable system could be reduced to. It might however still be interesting to compare, with continuation tools, the dynamics of the forced excitable ODE to a 1D map approximation of it, since the greater simplicity of the second model might provide more direct insight into some of the phenomena observed.

Finally, with respect to the pertinence of the results to cardiac electrophysiology, it would definitely be interesting to repeat the same kind of continuation analysis with a more realistic model of the heart electrical activity. We have actually started such an analysis, using the Luo-Rudy ionic model [LR91], but the very fast upstroke of the action potential in this model has given rise to numerical problems that we have not solved yet.

Appendix A

Singularly perturbed systems

A.1 Generalities

A *singularly perturbed* system is a system of ODE that can be written under the form:

$$\begin{cases} \dfrac{dx}{dt} = f(x,y) \\ \dfrac{dy}{dt} = \varepsilon g(x,y) \end{cases}, \tag{A.1}$$

where $x \in \mathbb{R}^m$, $y \in \mathbb{R}^n$, and ε is a small parameter (see, e.g., [Guc02, DKO08]). Because ε is small, the dynamics of the variables x is much faster than the dynamics of the variables y. Thus, the variables x are referred to as the *fast variables* and the variables y as the *slow variables*. For non-zero values of ε, (A.1) is equivalent to:

$$\begin{cases} \varepsilon\dfrac{dx}{d\tau} = f(x,y) \\ \dfrac{dy}{d\tau} = g(x,y) \end{cases}, \tag{A.2}$$

where $\tau = \varepsilon t$. The two systems (A.1) and (A.2) are no longer equivalent for $\varepsilon = 0$. Setting $\varepsilon = 0$ in (A.1) defines the *fast subsystem*, or *layer equations*:

$$\begin{cases} \dfrac{dx}{dt} = f(x,y) \\ \dfrac{dy}{dt} = 0 \end{cases}, \tag{A.3}$$

where the slow variables y are constant parameters in the vector field of the fast variables. Setting $\varepsilon = 0$ in (A.2) defines the *slow subsystem*, or *reduced system*:

$$\begin{cases} 0 = f(x,y) \\ \dfrac{dy}{d\tau} = g(x,y) \end{cases}, \tag{A.4}$$

which is a differential-algebraic system of equations.

The set of solutions of $f(x,y) = 0$ in $\mathbb{R}^{m+n}$ is called the *critical manifold* S of the singularly perturbed system. It is, in the same time, the set of equilibria (fixed points) of the fast subsystem in $\mathbb{R}^{m+n}$, and the phase space of the slow subsystem.

It follows from geometric singular perturbation theory that each subset of the critical manifold S on which the Jacobian f_x is nonsingular, *i.e.*, each subset of S containing no bifurcation point of the fast subsystem (BPFS), perturbs, for ε sufficiently small, as a collection of invariant manifolds, called *slow manifolds* (see, e.g., [Guc02, DKO08] and refs. therein). The flow on these slow manifolds is well approximated by the flow of (A.4). The slow manifolds in a given collection are, away from the BPFS, $\mathcal{O}(\varepsilon)$ close to the corresponding subset of the critical manifold and $\mathcal{O}(e^{-c/\varepsilon})$ (where c is a positive constant) close to each other (e.g., [Guc02] and refs. therein).

In singularly perturbed systems in which all the attractors of the fast subsystem are fixed points, trajectories approach an ε-neighbourhood of an attracting portion of the critical manifold on the fast time scale, and then move inside this neighbourhood (along an attracting slow manifold) on the slow time scale, until they come close to a BPFS[1]. At such a point, it is usually expected that the trajectory escapes from the critical manifold, and exhibits a second fast segment[2] (this is what happens, e.g., in the BVP-FHN model for the parameter values used in Sec. 2.2.1). But it can also happen that the trajectory remains in the vicinity of the critical manifold past the BPFS, and follows a repelling slow manifold close to a repelling portion of the critical manifold[3] (this is what happens, e.g., in the BVP-FHN model in tiny ranges of parameter values around the two values at which the fixed point coincides with a knee of the critical manifold, see next section). Such trajectories are called *canards* (e.g., [Wec05] and refs. therein – see also Fig. A.3 below).

Canards are restricted to exponentially small ranges of parameter values in singularly perturbed systems which contain only one slow variable and one fast variable (e.g., [Wec05]). An example of such a singularly perturbed system is given below with the (unforced) BVP-FHN model. On the other hand, canards are "generic" (*i.e.*, they persist for "large" variations of the parameters) in singularly perturbed systems which contain at least two slow variables and one fast variable, in which the critical manifold is at least two-dimensional. An example of such a system is studied in [GHW03, BEG$^+$03], under the form of a periodically forced VDP oscillator where the forcing varies on the slow time scale. In the periodically forced slow-fast system we study in this work (Eq. (4.1)–(4.2)), the forcing varies on a time scale which is intermediate between those of the slow and fast variables, so that the three-dimensional autonomous system obtained by defining an additional variable evolving like time is not a singularly perturbed system in the sense defined above, and therefore the associated notion of critical manifold is not defined. That is why we qualify only as "canard-like" the periodic solutions in Chaps. 5 and 6 which remain close to the unstable part of the critical manifold *of the unforced equations* along a part of their course. Note that these "canard-like" solutions are generic in our system in that they are found in rather large ranges of stimulation amplitudes and periods.

[1]The trajectory of course ends up before the BPFS if a fixed point of (A.1) is encountered along the way.

[2]By definition of an invariant manifold, this fast segment belongs to the same invariant manifold as the previous segment, but the invariant manifold no longer deserves to be qualified as "slow" along the fast portion of the trajectory.

[3]In which case the attracting and repelling slow manifolds coincide, *i.e.*, they are one and the same invariant manifold.

A.2 The BVP-FHN model

The BVP model (2.3) can be written under the form (A.1) or (A.2) by rescaling time respectively to $t' = \mu t$ or $t' = t/\mu$. The FHN model (2.5) is of the form (A.1). The critical manifold of the BVP-FHN model is the cubic v-nullcline $f(v, w) = 0$. The derivative f_v is singular at the two knees, which are saddle-node bifurcations for the fast subsystem. They divide the critical manifold into three pieces: two attracting branches (the external branches of the v-nullcline), which are the sets of stable fixed points of the fast subsystem, and one repelling branch (the middle branch of the v-nullcline), which is the set of unstable fixed points of the fast subsystem. By the result above, for ε sufficiently small, each of these three branches perturbs as a family of slow manifolds which are $\mathcal{O}(\varepsilon)$ close to the corresponding branch.

For most parameter values, all the trajectories in the BVP-FHN model which come close to a knee of the v-nullcline rush towards the opposite branch at that point. This is the case for the parameter values used in Chap. 2. However, for parameter values very close to those at which the fixed point coincides with one knee, canards occur, as is illustrated in Figs. A.1 and A.2. A possible origin of the "canard" terminology [Wec05] is illustrated in Fig. A.3.

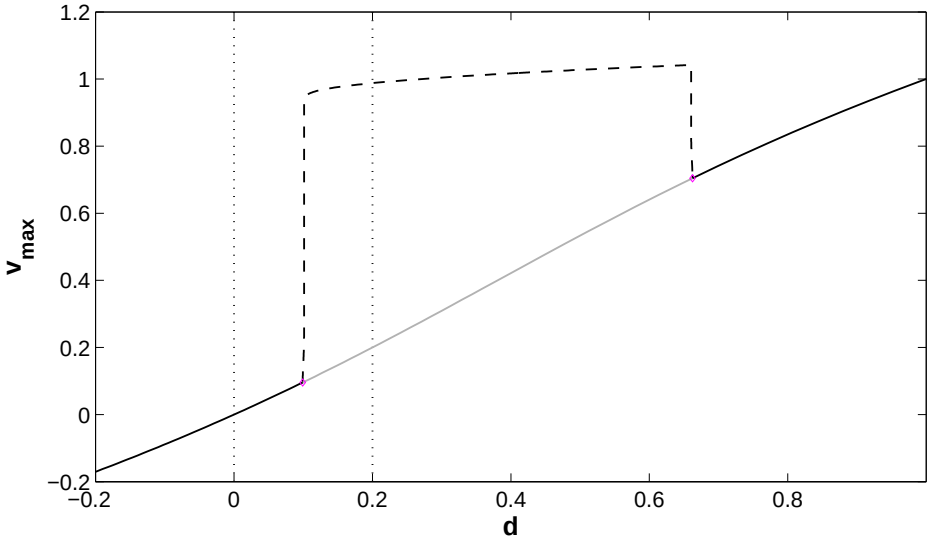

Figure A.1. *Bifurcation diagram for Eq.* (2.5) *with* $\varepsilon = 0.005$, d *being the bifurcation parameter. The solid curve is the branch of fixed points, for which the* v *coordinate is plotted as ordinate. The dashed curve is the branch of periodic solutions, for which the maximum value of* v *over one period is represented. The two branches are connected through Hopf bifurcations, represented by magenta diamonds. Stable solutions are shown in black, unstable solutions in grey. The vertical dotted lines indicate the two values of* d *used in this work (Chaps. 5 and 6). Along the two almost vertical portions of the periodic solution branch, canards occur, as is illustrated in Fig. A.2.*

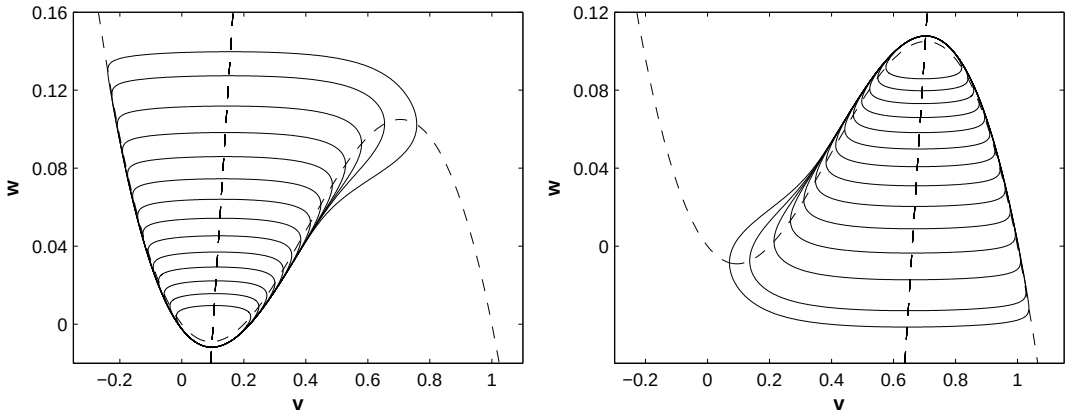

Figure A.2. *Left (resp. right) panel: periodic solutions belonging to the almost vertical left (resp. right) portion of the periodic solution branch in the bifurcation diagram of Fig. A.1. These solutions are canards since they follow an attracting slow manifold close to the left (resp. right) branch of the v-nullcline, pass close to the left (resp. right) knee, and then follow a repelling slow manifold close to the middle branch of the v-nullcline (trajectories are traveled counter-clockwise). These solutions occur for values of d very close to those two at which the fixed point of* (2.5) *coincides with one knee of the v-nullcline, as show the nullclines (there are actually as many w-nullclines as they are canards, but the different w-nullclines in a given panel are indistinguishable due to the very close values of d they correspond to).*

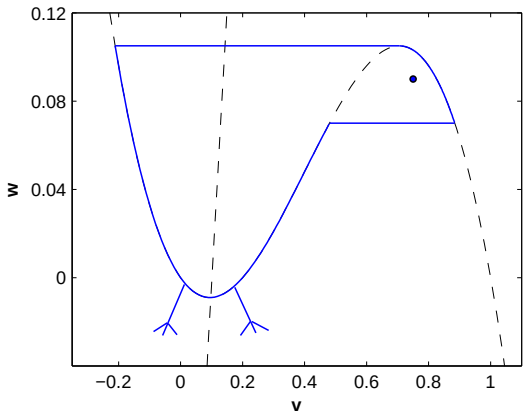

Figure A.3. *A canard in the FHN model* (2.5) *in the limit $\varepsilon \to 0$.*

Bibliography

[ADO90] J. C. Alexander, E. S. Doedel, and H. G. Othmer, *On the resonance structure in a forced excitable system*, SIAM J. Appl. Math. **50** (1990), 1373–1418.

[ADV+91] J. M. Anumonwo, M. Delmar, A. Vinet, D. C. Michaels, and J. Jalife, *Phase resetting and entrainment of pacemaker activity in single sinus nodal cells*, Circ. Res. **68** (1991), 1138–1153.

[AFH94] J. Argyris, G. Faust, and M. Haase, *An exploration of chaos*, Elsevier Science, 1994.

[ALG02] H. Arce, A. López, and M. R. Guevara, *Triggered alternans in an ionic model of ischemic cardiac ventricular muscle*, Chaos **12** (2002), 807–818.

[Arn83] V. I. Arnold, *Geometrical methods in the theory of ordinary differential equations*, Springer, New-York, 1983.

[AS82] R. H. Abraham and C. D. Shaw, *Dynamics – The geometry of behavior. Part one: periodic behavior*, Aerial Press, Santa Cruz, CA, 1982.

[BCD+02] W. J. Beyn, A. Champneys, E. J. Doedel, W. Govaerts, Y. A. Kuznetsov, and B. Sandstede, *Numerical continuation and computation of normal forms*, Handbook of Dynamical Systems, Vol. 2 (B. Fiedler, ed.), Elsevier Science, 2002, pp. 149–219.

[BEG+03] K. Bold, C. Edwards, J. Guckenheimer, S. Guharay, K. Hoffman, J. Hubbard, R. Oliva, and W. Weckesser, *The forced van der Pol equation II: canards in the reduced system*, SIAM J. Appl. Dyn. Syst. **2** (2003), 570–608.

[BG85] J. Bélair and L. Glass, *Universality and self-similarity in the bifurcations of circle maps*, Physica D **16** (1985), 143–154.

[Bon48] K. F. Bonhoeffer, *Activation of passive iron as a model for the excitation of nerve*, J. Gen. Physiol. **32** (1948), 69–91.

[BR77] G. W. Beeler and H. Reuter, *Reconstruction of the action potential of ventricular myocardial fibres*, J. Physiol. **268** (1977), 177–210.

[BSB+04] V. E. Bondarenko, G. P. Szigeti, G. C. L. Bett, S.-J. Kim, and R. L. Rasmusson, *Computer model of action potential of mouse ventricular myocytes*, Am. J. Physiol. Heart Circ. Physiol. **287** (2004), H1378–1403.

[CD07] H. Croisier and P. C. Dauby, *Continuation and bifurcation analysis of a periodically forced excitable system*, J. Theor. Biol. **246** (2007), 430–448.

[CGD09] H. Croisier, M. R. Guevara, and P. C. Dauby, *Bifurcation analysis of a periodically forced relaxation oscillator: Differential model versus phase-resetting map*, Phys. Rev. E. **79** (2009), 016209.

[CGG+89] A. Campbell, A. Gonzalez, D. L. Gonzalez, O. Piro, and H. A. Larrondo, *Isochrones and the dynamics of kicked oscillators*, Physica A **155** (1989), 565–584.

[CGM+93] G. A. Cecchi, D. L. Gonzalez, M. O. Magnasco, G. B. Mindlin, O. Piro, and A. J. Santillan, *Periodically kicked hard oscillators*, Chaos **3** (1993), 51–62.

[CMJ90] D. R. Chialvo, D. C. Michaels, and J. Jalife, *Supernormal excitability as a mechanism of chaotic dynamics of activation in cardiac Purkinje fibers*, Circ. Res. **66** (1990), 525–545.

[CO00] S. Coombes and A. H. Osbaldestin, *Period-adding bifurcations and chaos in a periodically stimulated excitable neural relaxation oscillator*, Phys. Rev. E **62** (2000), 4057–4066.

[Cyt04] E. N. Cytrynbaum, *Periodic stimulus and the single cardiac cell - getting more out of 1D maps*, J. Theor. Biol. **229** (2004), 69–83.

[DCF+98] E. J. Doedel, A. R. Champneys, T. F. Fairgrieve, Y. A. Kuznetsov, B. Sandstede, and X. Wang, *Auto97: Continuation and bifurcation software for ordinary differential equations*, 1998, `http://cmvl.cs.concordia.ca/publications/auto97.ps.gz`.

[DFSM89] M. Dolník, J. Finkeová, I. Schreiber, and M. Marek, *Dynamics of forced excitable and oscillatory chemical reaction systems*, J. Phys. Chem. **93** (1989), 2764–2774.

[DGK03] A Dhooge, W Govaerts, and Y. A. Kuznetsov, *MATCONT: A MATLAB package for numerical bifurcation analysis of ODEs*, ACM Transactions On Mathematical Software **29** (2003), 141–164.

[Din87] E. J. Ding, *Analytic treatment of a driven oscillator with a limit cycle*, Phys. Rev. A **35** (1987), 2669–2683.

[Din88] ———, *Structure of the parameter space for the van der Pol oscillator*, Physica Scripta **38** (1988), 9–16.

[DKK91a] E. J. Doedel, H. B. Keller, and J. P. Kernevez, *Numerical analysis and control of bifurcation problems: (I) Bifurcation in finite dimensions*, Int. J. Bifurc. Chaos **1** (1991), 493–520.

[DKK91b] ———, *Numerical analysis and control of bifurcation problems: (II) Bifurcation in infinite dimensions*, Int. J. Bifurc. Chaos **1** (1991), 745–772.

[DKO08] M. Desroches, B. Krauskopf, and H. M. Osinga, *Geometry of slow manifolds near folded nodes*, SIAM J. Appl. Dyn. Syst. **7** (2008), 1131–1162.

[DMJ89] M. Delmar, D. C. Michaels, and J. Jalife, *Slow recovery of excitability and the Wenckebach phenomenon in the single guinea pig ventricular myocyte*, Circ. Res. **65** (1989), 761–774.

[DN85] D. DiFrancesco and D. Noble, *A model of cardiac electrical activity incorporating ionic pumps and concentration changes*, Philos Trans R Soc Lond B Biol Sci **307** (1985), 353–98.

[Doe97] E. J. Doedel, *Lecture notes on numerical analysis of bifurcation problems*, Summer School on Nonlinear Equations, Technical University of Hamburg, 1997, `http://cmvl.cs.concordia.ca/publications/hamburg1997.ps.gz`.

[Doe00] ———, *Lecture notes on numerical analysis of bifurcation problems*, Summer School on Nonlinear Dynamics in Physiology and Medicine, McGill University, Montreal, 2000, `http://cmvl.cs.concordia.ca/publications/montreal2000.ps.gz`.

[DS95] S. Doi and S. Sato, *The global bifurcation structure of the BVP neuronal model driven by periodic pulse trains*, Math. Biosci. **125** (1995), 229–250.

[epa] See EPAPS Document No. E-PLEEE8-78-102812 for the movies "phiI0133tu.avi", "phiI0135tu.avi", "phiI0133uv.avi" and "phiI0135uv.avi". This document can be accessed from `ftp://ftp.aip.org/epaps/phys_rev_e/E-PLEEE8-78-102812/`. For more information on EPAPS, see `http://www.aip.org/pubservs/epaps.html`.

[Fen71] N. Fenichel, *Persistence and smoothness of invariant manifolds for flows*, Ind. Univ. Math. J. **21** (1971), 193–226.

[FGPV88] M. Feingold, D. L. Gonzalez, O. Piro, and H. Viturro, *Phase locking, period-doubling, and chaotic phenomena in externally driven excitable systems*, Phys. Rev. A **37** (1988), 4060–4063.

[FH78] J.E. Flaherty and F.C. Hoppensteadt, *Frequency entrainment of a forced Van der Pol oscillator*, Stud. Appl. Math. **58** (1978), 5–15.

[Fit61] R. FitzHugh, *Impulses and physiological states in theoretical models of nerve membrane*, Biophys. J. **1** (1961), 445–466.

[GAG08] H. Gonzalez, H. Arce, and M. R. Guevara, *Phase resetting, phase locking, and bistability in the periodically driven saline oscillator: experiment and model*, Phys. Rev. E. **78** (2008), 036217.

[GAJvG89] M. R. Guevara, F. Alonso, D. Jeandupeux, and A. C. G. van Ginneken, *Alternans in periodically stimulated isolated ventricular myocytes: Experiment and model*, Cell to cell signaling: from experiments to theoretical models (A. Goldbeter, ed.), Harcourt Brace Jovanovich, London, 1989, pp. 551–563.

[GB86] L. Glass and J. Bélair, *Continuation of Arnold tongues in mathematical models of periodically forced biological oscillators*, Nonlinear Oscillations in Biology and Chemistry, Lectures Notes in Biomathematics No. 66 (H. Othmer, ed.), Springer-Verlag, 1986, pp. 232–243.

[GFJ80] R. Guttman, L. Feldman, and E. Jakbsson, *Frequency entrainment of squid axon membrane*, J. Membrane Biol. **56** (1980), 9–18.

[GG82] M. R. Guevara and L. Glass, *Phase locking, period doubling bifurcations and chaos in a mathematical model of a periodically driven oscillator: a theory for the entrainment of biological oscillators and the generation of cardiac dysrhythmias*, J. Math. Biol. **14** (1982), 1–23.

[GGBS84] L. Glass, M. R. Guevara, J. Belair, and A. Shrier, *Global bifurcations of a periodically forced biological oscillator*, Phys. Rev. A **29** (1984), 1348–1357.

[GGMS83] M. R. Guevara, L. Glass, M. C. Mackey, and A. Shrier, *Chaos in neurobiology*, IEEE Trans. Syst. Man Cybern. **13** (1983), 790–798.

[GGS81] M. R. Guevara, L. Glass, and A. Shrier, *Phase locking, period-doubling bifurcations, and irregular dynamics in periodically stimulated cardiac cells*, Science **214** (1981), 1350–1353.

[GHW03] J. Guckenheimer, K. Hoffman, and W. Weckesser, *The forced van der Pol equation I: the slow flow and its bifurcations*, SIAM J. Appl. Dyn. Syst. **2** (2003), 1–35.

[GJ90] M. R. Guevara and H. J. Jongsma, *Phase resetting in a model of sinoatrial nodal membrane: ionic and topological aspects*, Am. J. Physiol. **258** (1990), H734–H747.

[GJAM89] M. R. Guevara, D. Jeandupeux, F. Alonso, and N. Morissette, *Wenckebach rhythms in isolated ventricular heart cells*, International conference on singular behavior and nonlinear dynamics, vol. 2 (T. Bountis St. Pnevmatikos and Sp. Pnevmatikos, eds.), World Scientific, Singapore, 1989, pp. 629–642.

[Gla01] L. Glass, *Synchronization and rhythmic processes in physiology*, Nature **410** (2001), 277–284.

[GM79] L. Glass and M. C. Mackey, *A simple model for phase locking of biological oscillators*, J. Math. Biol. **7** (1979), 339–352.

[GOW97] R. F. Gilmour Jr., N. F. Otani, and M. A. Watanabe, *Memory and complex dynamics in cardiac Purkinje fibers*, Am J. Physiol. **272** (1997), H1826–H1832.

[GP82] L. Glass and R. Perez, *Fine structure of phase locking*, Phys. Rev. Lett. **48** (1982), 1772–1775.

[GP83] D. L. Gonzalez and O. Piro, *Chaos in a nonlinear driven oscillator with exact solution*, Phys. Rev. Lett. **50** (1983), 870–872.

[GP84] ———, *One-dimensional Poincaré map for a non-linear driven oscillator: analytical derivation and geometrical properties*, Phys. Lett. A **101** (1984), 455–458.

[Gra87] J. Grasman, *Asymptotic methods for relaxation oscillations and applications*, Springer–Verlag, New-York, 1987.

[GS87] M. R. Guevara and A. Shrier, *Phase resetting in a model of cardiac Purkinje fiber*, Biophys. J. **52** (1987), 165–175.

[GS90] ———, *Rhythms produced by high-amplitude periodic stimulation of spontaneously beating aggregates of embryonic chick ventricular myocytes*, Ann. N. Y. Acad. Sci. **591** (1990), 11–22.

[GS94] L. Glass and J. Sun, *Periodic forcing of a limit-cycle oscillator: fixed points, Arnold tongues, and the global organization of bifurcations*, Phys. Rev. E **50** (1994), 5077–5084.

[GSG86] M. R. Guevara, A. Shrier, and L. Glass, *Phase resetting of spontaneously beating embryonic ventricular heart cells aggregates*, Am. J. Physiol. **251** (1986), H1298–H1305.

[GSG88] ———, *Phase-locked rhythms in periodically stimulated heart cells aggregates*, Am. J. Physiol. **254** (1988), H1–H10.

[GSG90] ———, *Chaotic and complex cardiac rhythms*, Cardiac Electrophysiology: From Cell to Bedside, First Edition (D. P. Zipes and J. Jalife, eds.), Saunders, Philadelphia, 1990, pp. 192–201.

[Guc02] J. Guckenheimer, *Bifurcation and degenerate decomposition in multiple time scale dynamical systems*, Nonlinear Dynamics and Chaos: where do we go from here? (J. Hogan, A. Champneys, B. Krauskopf, M. di Bernardo, E. Wilson, H. Osinga, and M. Homer, eds.), IOP Press, Bristol, 2002, pp. 1–21.

[Gue03] M. R. Guevara, *Dynamics of excitable cells*, Nonlinear Dynamics in Physiology and Medicine (A. Beuter, L. Glass, M. C. Mackey, and M. S. Titcombe, eds.), Springer-Verlag, 2003, pp. 87–121.

[GW84] L. Glass and A. T. Winfree, *Discontinuities in phase-resetting experiments*, Am. J. Physiol. **246** (1984), R251–R258.

[GX01] P. L. Gong and J. X. Xu, *Global dynamics and stochastic resonance of the forced FitzHugh-Nagumo neuron model*, Phys. rev. E **63** (2001), 031906.

[HADJ90] K. Hoshino, J. Anumonwo, M. Delmar, and J. Jalife, *Wenckebach periodicity in single atrioventricular nodal cells from the rabbit heart*, Circ. Res. **82** (1990), 2201–2216.

[Hal84] G. R. Hall, *Resonance zones in two-parameter families of circle homeomorphisms*, SIAM J. Math. Anal. **15** (1984), 1075–1081.

[HAM99] B. Hille, C. M. Armstrong, and R. MacKinnon, *Ion channels: from idea to reality*, Nature Medicine **5** (1999), 1105–1109.

[Hay64] C. Hayashi, *Nonlinear oscillations in physical systems*, McGraw–Hill, New York, 1964.

[HBG99] G. M. Hall, S. Bahar, and D. J. Gauthier, *Prevalence of rate-dependent behaviors in cardiac muscle*, Phys. Rev. Lett. **82** (1999), 2995–2998.

[HH52] A. Hodgkin and A. Huxley, *A quantitative description of membrane current and its application to conduction and excitation in nerve*, J. Physiol. **177** (1952), 500–544.

[HS89] J. Hescheler and R. Speicher, *Regular and chaotic behaviour of cardiac cells stimulated at frequencies between 2 and 20 Hz*, Eur. Biophys. J. **17** (1989), 273–280.

[HSN60] C. Hayashi, H. Shibayama, and Y. Nishikawa, *Frequency entrainment in a self-oscillatory system with external force*, IRE Trans. Circ. Theory **CT-7** (1960), 413–422.

[Hux02] A. Huxley, *From overshoot to voltage clamp*, Trends in Neuroscience **25** (2002), 553–558.

[IAJ98] N. Ichinose, K. Aihara, and K. Judd, *Extending the concept of isochrons from oscillatory to excitable systems for modelling an excitable neuron*, Int. J. Bifurc. Chaos **8** (1998), 2375–2385.

[Jac90] E. A. Jackson, *Perspectives of nonlinear dynamics, Vol. 1*, Cambridge University Press, Cambridge, 1990.

[Kan07] T. Kanamaru, *van der Pol oscillator*, Scholarpedia **2** (2007), 2202.

[KAS86] I. G. Kevrekidis, R. Aris, and L. D. Schmidt, *Forcing an entire bifurcation diagram: case studies in chemical oscillators*, Physica D **23** (1986), 391–395.

[Kaw81] M. Kawato, *Transient and steady state phase response curves of limit cycle oscillators*, J. Math. Biol. **12** (1981), 13–30.

[KCM+96] D. T. Kaplan, J. R. Clay, T. Manning, L. Glass, M. R. Guevara, and A. Shrier, *Subthreshold dynamics in periodically stimulated squid giant axons*, Phys. Rev. Lett. **76** (1996), 4074–4077.

[Kee08] J. P. Keener, *Invariant manifold reductions for Markovian ion channel dynamics*, J. Math. Biol. **NIL** (2008), NIL.

[KG84] J. P. Keener and L. Glass, *Global bifurcations of a periodically forced nonlinear oscillator*, J. Math Biol. **21** (1984), 175–190.

[KMGDG04] T. Krogh-Madsen, L. Glass, E. J. Doedel, and M. R. Guevara, *Apparent discontinuities in the phase-resetting response of cardiac pacemakers*, J. Theor. Biol. **230** (2004), 499–519.

[KOD+05] B. Krauskopf, H. M. Osinga, E. J. Doedel, M. E. Henderson, J. Guckenheimer, A. Vladimirsky, M. Dellnitz, and O. Junge, *A survey of methods for computing (un)stable manifolds of vector fields*, Int. J. Bifurc. Chaos **15** (2005), 763–791.

[KRS04] T. Kostova, R. Ravindran, and M. Schonbek, *FitzHugh-Nagumo revisited: types of bifurcations, periodical forcing and stability regions by a Lyapunov functional*, Int. J. Bifurc. Chaos **14** (2004), 913–925.

[KS98] J. Keener and J. Sneyd, *Mathematical physiology*, Springer-Verlag, New-York, 1998.

[KSA86] I. G. Kevrekidis, L. D. Schmidt, and R. Aris, *Some common features of periodically forced reacting systems*, Chem. Engng. Sci. **41** (1986), 1263–1276.

[KST91] C. Knudsen, J. Sturis, and J. S. Thomsen, *Generic bifurcation structures of Arnol'd tongues in forced oscillators*, Phys. Rev. A **44** (1991), 3503–3510.

[LDD+91] P. Lorente, C. Delgado, M. Delmar, D. Henzel, and J. Jalife, *Hysteresis in the excitability of isolated guinea pig ventricular myocytes*, Circ. Res. **69** (1991), 1301–1315.

[LG90] T. J. Lewis and M. R. Guevara, *Chaotic dynamics in an ionic model of the propagated cardiac action potential*, J. Theor. Biol. **146** (1990), 407–432.

[LR91] C. H. Luo and Y. Rudy, *A model of the ventricular cardiac action potential. Depolarization, repolarization, and their interaction*, Circ. Res. **68** (1991), 1501–1526.

[MNT75] R. E. McAllister, D. Noble, and R. W. Tsien, *Reconstruction of the electrical activity of cardiac Purkinje fibres*, J. Physiol. **251** (1975), 1–59.

[MP95] J. Malmivuo and R. Plonsey, *Bioelectromagnetism - principles and applications of bioelectric and biomagnetic fields*, Oxford University Press, New-York, 1995, `http://butler.cc.tut.fi/~malmivuo/bem/bembook/`.

[MP96] R. P. McGehee and B. B. Peckham, *Arnold flames and resonance surface folds*, Int. J. Bifurc. Chaos **6** (1996), 315–336.

[MPL93] R. Mettin, U. Parlitz, and W. Lauterborn, *Bifurcation structure of the driven van der Pol oscillator*, Int. J. Bifurc. Chaos **3** (1993), 1529–1555.

[MS02] C. Meunier and I. Segev, *Playing the Devil's advocate: is the Hodgkin-Huxley model useful?*, Trends in Neuroscience **25** (2002), 558–563.

[NAY62] J. Nagumo, S. Arimoto, and S. Yoshizawa, *An active pulse transmission line simulating nerve axon*, Proc. IRE **50** (1962), 2061–2070.

[Nob62] D. Noble, *A modification of the Hodgkin–Huxley equations applicable to Purkinje fibre action and pacemaker potentials.*, J. Physiol. **160** (1962), 317–352.

[Nob02] ———, *Modelling the heart: insights, failures and progress*, Bioessays **24** (2002), 1155–1163.

[NSD+93] T. Nomura, S. Sato, S. Doi, J. P. Segundo, and M. D. Stiber, *A Bonhoeffer-van der Pol oscillator model of locked and non-locked behaviors of living pacemaker neurons.*, Biol. Cybern. **69** (1993), 429–437.

[NSD+94] ———, *Global bifurcation structure of a Bonhoeffer-van der Pol oscillator driven by periodic pulse trains*, Biol. Cybern. **72** (1994), 55–67.

[OK94] M. W. Olesen and C. Knudsen, *Destruction of dominant Arnol'd tongues in forced oscillators*, Int. J. Bifurc. Chaos **4** (1994), 737–739.

[OX99] H. G. Othmer and M. Xie, *Subharmonic resonance and chaos in forced excitable systems*, J. Math. Biol. **39** (1999), 139–171.

[Pec90] B. B. Peckham, *The necessity of the Hopf bifurcation for periodically forced oscillators*, Nonlinearity **3** (1990), 261–280.

[PG82] R. Perez and L. Glass, *Bistability, period doubling bifurcations and chaos in a periodically forced oscillator*, Phys. Lett. A **90** (1982), 441–443.

[PK02] B. B. Peckham and I. G. Kevrekidis, *Lighting Arnold flames: resonance in doubly forced periodic oscillators*, Nonlinearity **15** (2002), 405–428.

[PL86] U. Parlitz and W. Lauterborn, *Resonances and torsion numbers of driven dissipative nonlinear oscillators*, Z. Naturforsch. **41a** (1986), 605–614.

[PSB+64] D. H. Perkel, J. H. Schulman, T. H. Bullock, G. P. Moore, and J. P. Segundo, *Pacemaker neurons: effects of regularly spaced synaptic input*, Science **145** (1964), 61–63.

[RF06] A. Rabinovitch and M. Friedman, *Fixed points of two-dimensional maps obtained under rapid stimulations*, Phys. Lett. A **355** (2006), 319–325.

[RL88] S. Rajasekar and M. Lakshmanan, *Period doubling route to chaos for a BVP oscillator with periodic external force*, J. Theor. Biol. **133** (1988), 473–477.

[RL95] D. S. Rubinstein and S. L. Lipsius, *Premature beats elicit a phase reversal of mechanoelectrical alternans in cat ventricular myocytes*, Circulation **91** (1995), 201–214.

[RPE02] M. Rivera, P. Parmananda, and M. Eiswirth, *Birhythmicity induced by perturbing an oscillating electrochemical system*, Phys. Rev. E **65** (2002), 025201(R).

[RS06] Y. Rudy and J. R. Silva, *Computational biology in the study of cardiac ion channels and cell electrophysiology*, Q. Rev. Biophys. **39** (2006), 57–116.

[RTF94] A. Rabinovitch, R. Thieberger, and M. Friedman, *Forced Bonhoeffer–van der Pol oscillator in its excited mode*, Phys. Rev. E **50** (1994), 1572–1578.

[RVR84] P. Rehmus, W. Vance, and J. Ross, *Generation of multiple attractors and nonequilibrium phase transitions*, J. Chem. Phys. **80** (1984), 3373–3380.

[Sch74] J. C. Schelleng, *The physics of the bowed string*, Sci. Am. **230** (1974), 87.

[Sco79] S. Scott, *Stimulation simulations of young yet cultured beating hearts*, Ph.D. thesis, State University of New York, Buffalo, New York, 1979.

[SD92] S. Sato and S. Doi, *Response characteristics of the BVP neuron model to periodic pulse inputs*, Math. Biosci. **112** (1992), 243–259.

[SDCM88] I. Schreiber, M. Dolník, P. Choc, and M. Marek, *Resonance behavior in two-parameter families of periodically forced oscillators*, Phys. Lett. A **128** (1988), 66–70.

[Sey88] R. Seydel, *From equilibrium to chaos : Practical bifurcation and stability analysis*, Elsevier Science, 1988.

[SRG+89] G. V. Savino, L. Romanelli, D. L. González, O. Piro, and M. E. Valentinuzzi, *Evidence for chaotic behavior in driven ventricles*, Biophys. J. **56** (1989), 273–280.

[Str00] S. H. Strogatz, *Nonlinear dynamics and chaos*, Perseus Books, Cambridge, 2000.

[THM+90] N. Takahashi, Y. Hanyu, T. Musha, R. Kubo, and G. Matsumoto, *Global bifurcation structure in periodically stimulated giant axons of squid*, Physica D **43** (1990), 318–334.

[TK79] K. Tomita and T. Kai, *Chaotic response of a limit cycle*, J. Stat. Phys. **21** (1979), 65–86.

[TZF+07] D. G. Tsalikakis, H. G. Zhang, D. I. Fotiadis, G. P. Kremmydas, and L. K. Michalis, *Phase response characteristics of sinoatrial node cells*, Comput. Biol. Med. **37** (2007), 8–20.

[VCMJ90] A. Vinet, D. R. Chialvo, D. C. Michaels, and J. Jalife, *Nonlinear dynamics of rate-dependent activation in models of single cardiac cells*, Circ. Res. **67** (1990), 1510–1524.

[vdP26] B. van der Pol, *On relaxation oscillations*, Phil. Mag. **2** (1926), 978.

[vdP27] ———, *Forced oscillations in a circuit with non-linear resistance. (Reception with reactive triode.)*, Phil. Mag. **3** (1927), 65–80.

[vdPvdM27] B. van der Pol and J. van der Mark, *Frequency demultiplication*, Nature **120** (1927), 363–364.

[vdPvdM28] ———, *The heartbeat considered as a relaxation oscillation, and an electrical model of the heart*, Phil. Mag. **6** (1928), 763–775.

[VR89] W. Vance and J. Ross, *A detailed study of a forced chemical oscillator: Arnol'd tongues and bifurcation sets*, J. Chem. Phys. **91** (1989), 7654–7670.

[VR94] A. Vinet and F. A. Roberge, *Analysis of an iterative difference equation model of the cardiac cell membrane*, J. Theor. Biol. **170** (1994), 201–214.

[Wal77] J. Walker, *The salt fountain and other curiosities based on the different density of fluids*, Sci. Am. **237** (1977), 142.

[Wec05] M. Wechselberger, *Existence and bifurcation of canards in* $\mathbb{R}^3$ *in the case of a folded node*, SIAM J. Appl. Dyn. Syst. **4** (2005), 101–139.

[Wig90] S. Wiggins, *Introduction to applied nonlinear dynamical systems and chaos*, Springer-Verlag, New-York, 1990.

[Wig94] ———, *Normally hyperbolic invariant manifolds in dynamical systems*, Springer-Verlag, New-York, 1994.

[Win00] A. T. Winfree, *The geometry of biological time*, second ed., Springer, New-York, 2000.

[XCKA08] Y. Xie, L. Chen, Y. M. Kang, and K. Aihara, *Controlling the onset of Hopf bifurcation in the Hodgkin-Huxley model*, Phys. Rev.E **77** (2008), 061921.

[XOW96] M. Xie, H. G. Othmer, and M. Watanabe, *Resonance in excitable systems under step-function forcing: II. subharmonic solutions and persistence*, Physica D **98** (1996), 75–110.

[YJAG99] A. R. Yehia, D. Jeandupeux, F. Alonso, and M. R. Guevara, *Hysteresis and bistability in the direct transition from 1:1 to 2:1 rhythm in periodically driven single ventricular cells*, Chaos **9** (1999), 916–931.

[YNPS99] K. Yoshino, T. Nomura, K. Pakdaman, and S. Sato, *Synthetic analysis of periodically stimulated excitable and oscillatory membrane models*, Phys. Rev. E **59** (1999), 956–969.

[YR03] E. Yellin and A. Rabinovitch, *Properties and features of asymmetric partial devil's staircases deduced from piecewise linear maps*, Phys. rev. E **67** (2003), 016202.

[YSLG97] A. R. Yehia, A. Shrier, K. C. L. Lo, and M. R. Guevara, *Transient outward current contributes to Wenckebach-like rhythms in isolated rabbit ventricular cells*, Am. J. Physiol. **273** (1997), H1–H11.